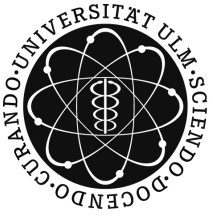

ulm university universität
uulm

Single spins in diamond for nanoscale sensing and microscopy

Von der Fakultät für Naturwissenschaften der Universität Ulm zur Erlangung der Würde eines Doktors der Naturwissenschaften (Dr. rer. nat.) genehmigte Abhandlung

Vorgelegt von

Anna Ermakova
aus Novopolotsk, Belarus

Institut für Quantenoptik der Universität Ulm

2016

Amtierender Dekan: Prof. Dr. Peter Dürre

Erstgutachter: Prof. Dr. Fedor Jelezko

Zweitgutachter: PD Dr. Boris Naydenov

Tag der mündlichen Prüfung: 09.11.2016

version of 08th December 2016

©2016, Anna Ermakova

Summary

This thesis is dedicated to the demonstration of using single spins in diamond for nanoscale sensing and microscopy for biological applications. The most popular defect in diamond is the nitrogen-vacancy (NV) complex. This center consists of substitutional nitrogen atom next to a vacancy and can be in one of two charge states: neutral and negative. They both are optically stable. The emission wavelength of zero phonon line (ZPL) for NV^0 is equal to 575 nm, and 637 nm for NV^-. At room temperature ZPL emission gives only 4 % of total fluorescence of the color center. The rest light is related to the phonon sideband. The maximum of the phonon wing is around 700 nm. This opens for NV center a broad area of medical and biological *in vivo* applications, because the transmission of tissue is higher for red shifted fluorescence. For optical markers it does not matter, which charge state the color center has. However, NV^- defect with electron spin $S = 1$ can be used for the detection of constant and fluctuating magnetic fields including nuclear magnetic resonance spectroscopy. NV^- center can be stabilized even in small nanodiamonds with the size down to 5 nm. Diamond is a highly biocompatible material, which is non-toxic and can be utilized *in vivo*. Thus, nanodiamonds with the color centers can be used as optical labels and as magnetic detectors with high sensitivity and nanoscale resolution.

The first part of this thesis describes experiments, which show opportunities to use nanodiamonds with color centers as optical labels. Presented results were obtained on diamond nanocrystals with NV centers. The first problem, which should be solved in this subject, is stabilization of the hydrodynamic properties of the nanodiamonds and protection of them from aggregation. Acid treated nanodiamonds were coated with modified Human Serum Albumin (HSA) proteins, which were labeled with Rhodamine molecules for visualization. Hydrodynamical properties of coated nanocrystals were characterized by Fluorescence Correlation Spectroscopy (FCS) measurements in four different buffers with pH levels 2, 4, 6, and 8. The diffusion curves exhibited double exponential decay. One component is related to movement of free proteins. The second

exponent describes the diffusion of coated nanodiamonds. All samples show similar values for the diffusion times. The FCS data does not show the presence of the nanodiamonds' clusters, which is an important feature for potential *in vivo* applications of such nanocrystals. The coated nanodiamonds with color centers were proven to be a good drug delivery system. For that, Doxorubicin molecules were bound to the modified HSA proteins. The attachment was done by pH sensitive bonds, that release the drug at pH level less than 5.5. Many cancer cells have acidic pH level in contrast to healthy tissue. Such pH sensitive bonds present a good opportunity to deliver chemotherapy drug. The release in buffer was measured by FCS technique. It demonstrates that after 24 hours at pH level 5 around 70 % of drug is released from the coated nanodiamonds. The prepared drug delivery system was tested inside HeLa cells. The observed data shows that the nanocrystals with the attached drug pass through the cell membrane into the cytoplasm. Then after the release Doxorubicin molecules penetrate into the cell nucleus, which is necessary for the medical effect. Whereas, the coated nanodiamonds stay inside the cytoplasm. Preclinical test shows that for system drug-nanodiamond the medical efficiency is higher than for free Doxorubicin molecules. Also the absorption of the drug for this complex in healthy tissues is much less while keeping higher concentration in the tumor. It is very promising results for further use of nanodiamonds for drug delivery, because a chemotherapy is always a competition between healthy and tumor tissues. Another interesting application can be found for nanodiamonds with two different color centers, for example, nitrogen-vacancy and silicon-vacancy (SiV) defects. SiV centers have ZPL at 738 nm, which makes it more preferable for biological applications. The principle of the creation of diamond nanocrystals with two type of lattice defects simultaneously was demonstrated. For these nanodiamonds seeds, milled from HPHT bulk crystal with high concentration of nitrogen impurities, were grown in CVD reactor with silicon doping. During the growth the number of NV centers does not increase much, but the concentration of SiV defects within first 90 s in CVD reactor rises slowly and linearly and after that rapidly and non-linearly.

In the second part, nanodiamonds with NV centers are used as magnetic detectors for sensing of metallo-proteins. For such experiments only NV^- centers can be used. In case of nanodiamonds or shallow implanted color centers the diamond's surface strongly affects NV's charge. To stabilized it in the negative state, the surface should be terminated with oxygen.

This can be done by acid treatment, which removes graphite residues and protects diamond's surface by carboxyl groups. These groups were used for the attachment of metallo-proteins to nanodiamonds. Ferritin was chosen for the detection. It is a globular molecule, which consists of protein shell and iron core. Ferritin keeps iron atoms in non-toxic for living organisms form, where in a normal situation one molecule can contain around 4500 atoms of metal. Iron atoms are mostly in Fe^{3+} state. Ferritin does not have a constant magnetic moment at room temperature, but spin flip-flops create a fluctuating magnetic field, which can be detected. Many diseases are related to the changes in ferritin core. For example, less number of iron atoms leads to anemia, and presence of another metals can result in Alzheimer's or Parkinson's diseases. The detection of the real concentration can give many advantages in medical diagnosis. NV center in diamond can be a good sensor to investigate structure of ferritin core. In our case nanodiamonds were bound with 10 ± 2 ferritin molecules per one nanocrystals. For magnetic detection the relaxation times were measured. All measurements were carried out on nanodiamonds with single color center inside, which was proven by antibunching. T_1 and T_2 times were observed for 32 nanodiamonds without and with ferritin molecules. The obtained data shows that in the presence of metallo-proteins T_1 is 7 times shorter than for free nanodiamonds. T_2 time decreases about 9 times. A theoretical model was developed for the investigated system. The numerical simulations demonstrated good agreement with the experiments. In our case the position of NV center and relative position of ferritin molecules are unknown. It means that the distance between the color center and metallo-proteins varies from nanocrystal to nanocrystal, similarly to the real number of ferritin per one nanodiamond. However, if the distance would be controllable, presented theoretical model might be used for the calculation of iron atoms per one molecule. It can be potentially done by combination of confocal and atomic-force microscopes. To realize this the experimental setup should have high stability and control.

f

Zusammenfassung

Diese Arbeit soll den Nachweis von Detektion mit Nanoauflösung und Mikroskopie für biologische Anwendungen mit Hilfe von einzelnen Spins in Diamant erbringen. Der meistuntersuchte Defekt in Diamant ist das Stickstoff-Fehlstellen-Zentrum (NV). Diese Fehlstehle besteht aus einem Kohlenstoff ersetzendem Stickstoff Atom und einer angrenzenden Fehlstelle. Es kann in zwei Ladungszuständen gefunden werden: neutral und negativ. Beide sind optisch stabil. Die Zero Phonon Line (ZPL) des NV^0 liegt bei 575 nm, die des NV^- bei 637 nm. Bei Raumtemperatur werden nur 4 % der gesamten Fluoreszenz der Fehlstelle in die ZPL emittiert. Der Rest der Fluoreszenz kommt aus dem Phononen Seitenband. Das Maximum des Phononenseitenbandes befindet sich bei 700 nm. Dies eröffnet dem NV Zentrum einen breiten Bereich der medizinischen und biologischen Anwendungen, da die Transmission von Gewebe bei Rot verschobener Fluoreszenz höher ist. Für optische Markierungen ist es unwichtig, in welchem Ladungszustand sich das NV befindet. Das NV^- Zentrum mit Elektronen Spin $S = 1$ kann jedoch für die Detektion von konstanten und fluktuierenden Magnetfeldern, einschlielich der Kernspinrensonanzspektroskopie, genutzt werden. Das NV^- kann sogar bei kleinen Nanodiamanten bis zu 5 nm Gröe stabilisiert werden. Diamant ist höchst biokompatibles Material, welches nicht toxisch und *in vivo* eingesetzt werden kann. Deshalb können Nanodiamanten mit Farbzentren als optische Marker und magnetische Detektoren mit hoher Sensitivität und Nanometer Auflösung eingesetzt werden.

Der erste Teil dieser Arbeit beschreibt das Experiment, welches die Möglichkeiten Nanodiamanten mit Farbzentren als optische Marker zu verwenden, aufzeigt. Die gezeigten Ergebnisse wurden mit Nanodiamantkristallen mit NV Zentren gewonnen. Das erste Problem, welches in diesem Zusammenhang gelöst werden sollte, ist die Stabilisierung er hydrodynamischen Eigenschaften und der Schutz vor Verklumpung der Nanodiamanten. Säure behandelte Nanodiamanten wurden mit einem modifiziertem Human Serum Albumin (HSA) Protein umhüllt, welches für die Visualisierung mit Rhodamin Molekülen kenntlich gemacht wur-

de. Die hydrodynamischen Eigenschaften der umhüllten Nanodiamanten wurde für 4 verschiedene Puffer mit pH Leveln von 2, 4, 6 und 8 mit Hilfe von Fluoreszenz Korrelations Spektroskopie (FCS) überprüft. Die Diffusionskurven zeigten einen doppelt exponentiellen Zerfall. Eine Komponente rührt aus der Bewegung der freien Proteine. Der zweite Exponent beschreibt die Diffusion der Nanodiamanten. Alle Proben zeigen ähnliche Diffusionszeit Werte. Mit den FCS Daten lässt sich keine Verklumpung von Nanodiamanten nachweisen, welches eine wichtige Eigenschaft für potentielle Anwendung von solchen Nanodiamanten *in vivo* ist. Es wurde gezeigt, dass die umhüllten Nanodiamanten mit Farbzentren gut als drug delivery system geeignet sind. Dafür wurde Doxorubicin an HSA Proteine gebunden. Die Befestigung wurde mit Hilfe von pH sensitive Bindungen vorgenommen, welche das Medikament bei pH-Werten geringer als 5.5 freigeben. Im Gegensatz zu gesundem Gewebe haben viele Krebszellen einen sauren pH-Wert. Solch pH sensitiven Bindungen bieten eine gute Möglichkeit der Zuführung von Chemotherapeutika. Die Freisetzung in Pufferlösung wurde mit Hilfe von FCS vermessen. Es lässt sich nachweisen, dass nach 24 Stunden bei einem pH-Wert von 5 um die 70 % des Medikaments von den Nanodiamanten freigesetzt wurden. Das präparierte drug delivery system wurde in HeLa Zellen getestet. Die beobachteten Daten zeigen, dass Nanokristalle mit gebundenem Medikament durch die Zellwand in das Zytoplasma vordringen. Nach der darauffolgenden Freisetzung dringen die Doxorubicin Moleküle in den Zellkern ein, welches entscheidend für den medizinischen Effekt ist. Im Gegensatz dazu bleiben die umhüllten Nanodiamanten im Zytoplasma. Vorklinische Studien zeigen, dass für Medikament-Nanodiamant Systeme die medizinische Effizienz höher ist als für freie Doxorubicin Moleküle. Zusätzlich ist die Absorption des Komplexes in gesundem Gewebe wesentlich geringer während es eine höhere Konzentration im Tumor hält. Dies ist ein sehr viel versprechendes Ergebnis für die weitere Verwendung von Nanodiamanten für drug delivery, da es sich bei einem Chemotherapeutikum immer um einen Wettbewerb zwischen gesundem und tumorösen Gewebe handelt. Eine andere interessante Anwendung kann für Nanodiamanten mit zwei verschiedenen Farbzentren, z.B. Stickstoff- uns Silizium Fehlstellen (SiV), gefunden werden. SiV Zentren haben ihre ZPL bei 738 nm, welches es wünschenswert für biologische Anwendungen macht. Das Herstellungsprinzip von Diamant Nanokristallen mit je zwei Arten von Kristalldefekten konnte nachgewiesen werden. Dafür wurden HPHT Einkristalle mit hoher Konzentration von Stickstoff Fremdatomen zu Nanodiamanten gemahlen und in einem CVD Reaktor mit Silizium Dotierung überwachsen. Während

des Wachstumsprozesses steigt die Anzahl an NV Zentren nicht beachtlich an, aber die Konzentration von SiV Fehlstellen in den ersten 90 Sekunden im CVD Reaktor wächst langsam und linear, danach schnell und nicht linear.

Im zweiten Teil werden Nanodiamanten mit NV Zentren als Detektoren für Metallo-Proteine benutzt. Für solche Experimente kann man nur NV^- Zentren benutzen. Im Falle von Nanodiamanten oder nahe der Oberfläche implantierten Farbzentren wird die Ladung des NVs stark von der Diamantoberfläche beeinflusst. Um den negativ geladenen Zustand zu stabilisieren sollte die Oberfläche mit Sauerstoff terminiert werden. Dies kann mit einer Säurebehandlung getan werden, welche die Graphit Rückstände beseitigt und die Diamantoberfläche mit Carboxyl Gruppen schützt. Diese Gruppen werden genutzt um Metallo-Proteine an Nanodiamanten zu binden. Zur Detektion wurde Ferritin gewählt. Es ist ein kugelförmiges Protein, welches aus einer Proteinhülle und einem Eisenkern besteht. Ferritin sorgt dafür, dass Eisen nicht toxisch für lebend Organismen ist, wobei sich in einer normalen Situation bis zu 4500 Metall Atome in einem Molekül befinden können. Eisen Atome befinden sich hauptsächlich im Fe^{3+} Zustand. Ferritin hat kein konstantes magnetisches Feld bei Raumtemperatur, sondern ein durch Spin Flip-Flops erzeugtes fluktuierendes Feld, welches gemessen werden kann. Viele Krankheiten stehen in Verbindung mit Veränderungen im Ferritin-Kern. So führt zum Beispiel ein geringerer Wert an Eisenatomen zur Anämie, und die Gegenwart eines anderen Metalls kann zu Alzheimer oder Parkinson führen. Die Feststellung der tatsächlichen Konzentration kann zu vielen Vorteilen in der medizinischen Diagnose führen. NV Zentren in Diamant können gute Sensoren zur Untersuchung der Ferritin Kerns sein. In unserem Fall wurden 10 ± 2 Ferritin Moleküle an einen Nanodiamanten gebunden. Zur Magentfelddetektion wurden die Relaxationszeiten gemessen. Durch Antibunching wurde gezeigt, dass alle Messungen an Nanodiamanten mit einem einzigen Farbzentrum vorgenommen wurden. T_1 und T_2 wurden für 32 Nanodiamanten mit und ohne Ferritin Moleküle gemessen. In Gegenwart der Metallo-Proteine zeigt sich, dass die T_1 um das 7fache verkürzt ist im Verhältnis zu freien Nanodiamanten, während sich die T_2 Zeit um das 9fache verringerte. Für das untersuchte System wurde ein theoretisches Model entwickelt. Dessen numerischen Simulationen stimmen gut mit dem Experiment überein. In unserem Fall sind die Position des NV Zentrums und die relative Position des Ferritin Moleküls unbekannt. Dies bedeutet, dass die Distanz zwischen dem Farbzentrum und dem

Metallo-Protein von Nanokristall zu Nanokristall variiert, ähnlich wie die tatsächlich Anzahl an Ferritin pro Nanodiamant. Falls die Distanz jedoch kontrollierbar wäre, könnte das präsentierte theoretischen Model für die Berechnung der Anzahl von Eisenatomen pro Molekül benutzt werden. Dies kann möglicherweise durch eine Kombination von Konfokal und Rasterkraft Mikroskopie gesehen. Für eine Realisierung sollte der experimentelle Aufbau eine hohe Stabilität und eine exakte Kontrolle der Experimentierparameter haben.

Contents

Titel a

Summary c

Zusammenfassung g

Contents k

Abbreviations o

1. Introduction 1

2. Theoretical background 5
2.1. Diamond: creation and properties 5
2.1.1. Carbon and diamond 5
2.1.2. Physical properties of diamond 7
2.2. Nitrogen-vacancy center in diamond 8
2.2.1. Creation of NV centers 9
2.2.2. Structure of the nitrogen-vacancy center 10
2.2.3. Ground state of the nitrogen-vacancy center 13
2.2.4. Electron spin initialization and readout 15
2.2.5. Electron spin manipulation 17
2.2.6. Charge stability of NV center 25
2.3. Silicon-vacancy center in diamond 26
2.4. Nanodiamonds: creation and functionalization 28
2.4.1. Creation of nanodiamonds 28
2.4.2. Nanodiamonds with color centers 30
2.4.3. Surface functionalization of nanodiamonds 31

3. Experimental background 33
3.1. Optical markers 33
3.1.1. Organic fluorescent particles 33
3.1.2. Quantum dots 34

3.1.3. Metallic nanoparticles . . . 35
3.1.4. Nanodiamonds with color centers . . . 35
3.1.5. Drug delivery . . . 36
3.2. NV center as magnetic detector . . . 37
3.2.1. Detection of DC field by NV center . . . 37
3.2.2. Detection of AC field by NV center . . . 40
3.2.3. Nuclear magnetic resonance by NV center . . . 40

4. Experimental setups **43**
4.1. Optical measurements . . . 43
4.1.1. Confocal microscopy . . . 43
4.1.2. Fluorescence correlation spectroscopy . . . 45
4.2. Size and structure measurement . . . 48
4.2.1. Atomic-force microscopy . . . 48
4.2.2. Electron microscopy . . . 50

5. Optical markers based on nanodiamonds **51**
5.1. Introduction . . . 51
5.2. Functionalization of nanodiamonds . . . 52
5.2.1. Protein modification . . . 52
5.3. Colocalization of nanodiamonds and protein . . . 55
5.3.1. pH stability . . . 55
5.3.2. Cell stability . . . 57
5.4. Drug delivery by nanodiamonds . . . 59
5.4.1. Doxorubicin . . . 59
5.4.2. Nanodiamonds with Doxorubicin . . . 59
5.4.3. Buffer measurements . . . 60
5.4.4. Cell measurements . . . 63
5.4.5. Pre-clinical test . . . 66
5.5. Nanodiamonds with two color centers . . . 69
5.5.1. Sample preparation . . . 69
5.5.2. Size measurements . . . 69
5.5.3. Fluorescence measurements . . . 71
5.6. Conclusion . . . 74

6. Magnetic sensors based on NV center **77**
6.1. Introduction . . . 77
6.2. Ferritin . . . 78
6.3. Sample preparation . . . 79
6.4. Coherence time measurements . . . 80
6.4.1. T_1 time measurements . . . 82

6.4.2. T_2 time measurements 83
6.4.3. Theoretical model 86
6.5. Further experiments 88
6.5.1. Single protein sensing 88
6.6. Conclusion 93

A. Appendix **A**
A.1. Membrane transport . . . . . A
A.1.1. Cell membrane . . . . . A
A.1.2. Passive membrane transport . . . . . A
A.1.3. Active membrane transport C

B. Bibliography **I**

List of Figures **XXXIII**

Acknowledgement **XXXV**

Curriculum Vitae **XXXVII**

List of publications **XXXIX**

Erklärung **XLI**

Abbreviations

AFM	Atomic-force microscope
AC	Alternating current
BSA	Bovine serum albumin
CAM	Chorioallantoic membrane model
CVD	Chemical vapor deposition
DC	Direct current
DNA	Deoxyribonucleic acid
DOX	Doxorubicin molecule
EDC	1-Ethyl-3-(3-dimethylaminopropyl)carbodiimide
EPR	Electron paramagnetic resonance
FCS	Fluorescence correlation spectroscopy
HPHT	High pressure high temperature
NMR	Nuclear magnetic resonance
NV	Nitrogen-vacancy center
ODMR	Optically detected magnetic resonance
PBS	Phosphate-buffered saline
PALM	Photo-activated localization microscopy
PEG	Polyethylene glycol
RNA	Ribonucleic acid
SiV	Silicon-vacancy center
STED	Stimulated emission depletion microscopy
STORM	Stochastic optical reconstruction microscopy
ZPL	Zero-phonon line

1. Introduction

The XX century were the golden ages of physics. It had strong development in fundamental and applied science. The creation of theory of relativity and the formation of quantum mechanics have a special place in this progress. One of the important aspects of social development in the last century is the integration of pure science, technology, and industry. This interaction leads to the abrupt decrease of time for technical realization of discovery in real industry. But it brings us to new limits. For example, microelectronics, which started with transistor discovery in 1947 [1], already encounters the limit of modern implantation process. Gordon Moore predicted in 1975 that every two years the number of transistors in an integrated circuit would be doubled. Now the size of the single transistor reaches the limit, when the quantum effects start to play big role in the production of semiconductor devices. The solution of such problems can take some time and be very expensive. However, the smoothly running physical methods can be applied for investigations in another academic disciplines, especially in biology and medicine, where there are a lot of important unanswered questions.

Interdisciplinary sciences take more and more place in modern time. The application of physical methods leads to the creation of many new interdisciplines, for example, geophysics, biophysics, medical physics, and others. The quantum mechanics made possible to look in a new way at chemistry and gave new life of physical chemistry and chemical physics. The term of biophysics was introduced by Karl Pearson in 1892 in his book "The Grammar of Science" [2]. However, the fast development of that direction was started only few tens of years ago. In biology and medicine many physical methods can find productive applications, for example, fluorescent, X-ray, and neutron spectroscopies, electron and atomic-force microscopies, and others.

One of the optical methods, which has already broad applications in biology and medicine, is the confocal microscopy. This technique gives a high-contrast image of a narrow slice of sample by blocking the "out of focus" light. Principle of scanning confocal microscope was patented in 1957 by M. Minsky [3]. The resolution of confocal microscope is lim-

ited by the wavelength of excitation light and the parameters of optical system. It can be improved by using, for example, STORM (stochastic optical reconstruction microscopy) [4], PALM (photoactivated localization microscopy) [5], or STED (stimulated emission depletion) [6] techniques. Confocal imaging finds a lot of applications in visualization of human and animal tissues *in vivo* and *in vitro*. Many cells emit autofluorescence light, which can be detected in confocal measurements. Also cells can be selectively marked with optical labels, such as fluorescent molecules or proteins, quantum dots, or others. It is possible to label drug molecules, proteins, cell membranes or any cell parts. For *in vivo* experiments these markers should satisfy special conditions, for example, be non-toxic, optically stable, easily functionalized, et cetera. One of the good candidates to be used as an optical label are nanodiamonds with color centers, for example, nitrogen-vacancy (NV) [7] or silicon-vacancy (SiV) [8] centers.

In the first part of this thesis it is demonstrated that coated nanodiamonds with NV centers can be used as optical markers and as a drug delivery system [9]. Nanodiamonds were coated with modified BSA proteins, which stabilize the hydrodynamic properties of particles. Drug molecules were attached to proteins by pH sensitive bonds, the release happens at pH level less than 5.5. It shows also the principle and first results of the creation of diamond nanocrystals with two different types of color centers (NV and SiV) simultaneously [10]. For that milled nanodiamonds (from high-pressure and high-temperature crystals) were grown by chemical vapor deposition with silicon doping. Such nanocrystals can find many application in biology and medicine, when the red shifted fluorescence is more preferable [11].

An nitrogen-vacancy center has not only optical properties. In a negative charge state it has electron spin $S = 1$, which can be optically read out and controlled. Spin properties of NV defect potentially can be used as a qubit for a quantum computer equally with cold atoms [12], Josephson junction [13], quantum dots [14] or other spin centers in crystals [15, 16]. However, the spin of that color center might be also used as a magnetic detector with high sensitivity and nanoscale resolution [17]. The sensitivity of NV centers depends on the coherence time and on distance between color center and measured spin system. It was shown that NV defect can be used for detecting the field from a single electron or a single proton [17, 18]. Nuclear magnetic resonance can also be done by this color center, but for this the distance to detected spins should be smaller than 10 nm [19, 20]. Color centers in nanodiamonds have shorter coherence times than defects in pure bulk crystal. This is a result of the large surface of nanocrystals

in respect to their volume. Different molecules and chemicals groups are adsorbed on the diamond's surface, and they shorten the relaxation times. However, nanodiamonds can be chemically attached to interesting spin systems, such as molecules or proteins. It gives the possibility to have a short distance between NV center and investigated object, and also to place that magnetic detector *in vivo* organisms.

The second part of this thesis shows that nanodiamonds with NV centers can be used as a magnetic detector of metallo-proteins [21]. To demonstrate it ferritin molecules were chosen. It is a globular protein, which stores iron atoms in a living organisms in a non-toxic state. Problems with the substance of ferritin core can lead to many diseases. The investigation of core's components can facilitate the medical diagnosis.

2. Theoretical background

2.1. Diamond: creation and properties

2.1.1. Carbon and diamond

Carbon is one of the most interesting and important atoms in nature, it is part of all organic molecules and as a result part of all proteins, cells and living organisms, which we know. The carbon atom has six electrons, which configuration is $1s^2\ 2s^2\ 2p^2$. Two or four of them might be valence depending on the bonding elements. According to that carbon can make up to four chemical bonds with other atoms. Possible orbital hybridizations of carbon are sp^1, sp^2 and sp^3. Interesting point of carbon is that it can be not only part of different molecules and compounds with other atoms, but carbon also shows properties of allotropy. For example, carbon itself can form graphite and graphene, where atoms have sp^2 hybridized orbitals, and diamond, which consists of sp^3 hybridized atoms. sp^1 hybridization can only occur in linear compounds, where carbon is usually combined with other atoms.

A formation of natural diamond takes long time under the high temperature together with high pressure in the deep layer of Earth's crust [22, 23]. Diamonds start to grow from a liquid phase. This is solution with high concentration of carbon (fig. 2.1), metals as catalysts and other elements which are situated around. Depending on the compounds of diamond impurities they can be separated in two main types, each of them also includes subtypes. Firstly, two types of classification of diamonds were proposed by Sir Robert Robertson in 1934 [24, 25]. He and his colleagues compared physical properties (such as infra-red absorption, ultra-violet spectroscopy, photoconductivity and other) of different diamonds. They recognized that all samples can be sorted in two groups (type I and II), but they did not know the physical reason behind this separation. It was found only twenty years late in 1959 [26], when W. Kaiser and W. L. Bond showed in their research that a major impurity in diamonds of type I is nitrogen. They concluded that diamonds of the type I have high concentration of nitrogen in different forms, and the type II has significantly lower concentration or

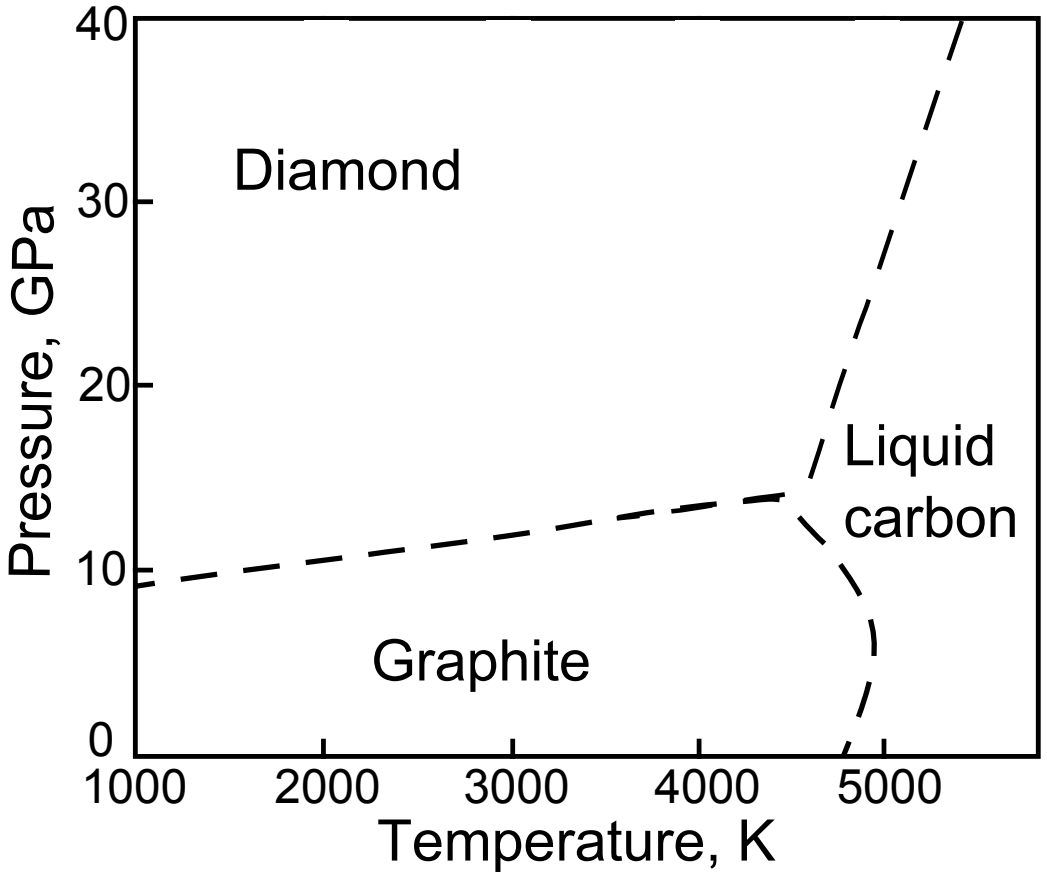

Figure 2.1.: Phase diagram of the equilibrium between diamond, graphite and liquid carbon.

does not have nitrogen at all. Subdivision of the I type is based on the concentration and forms of nitrogen impurities [27]. Two main subtypes of the I type are Ib with the concentration of nitrogen impurities around 500 ppm and Ia with higher concentration app. 3000 ppm.

With natural diamonds we can not exactly know the impurities structure of the crystal, which is important for many productions based on a diamond. The synthetic diamond can be a good solution for such problem. First steps to grow diamonds were done a long time before people really understood all unique properties of diamond. First successful result in diamond's growth was made in 1955 [28]. In this work the method of the growth, which is called "high pressure, high temperature" (HPHT), was used for the first time. The idea of it is simple and reminiscence to the natural process which occurs in Earth's crust, but requires significantly shorter time. The growth of the HPHT diamonds is going from the liquid

phase with a high concentration of carbon atoms. Temperature, pressure and time of growth affect the crystal size and its quality. The typical parameters for diamond growth are $P = 5 - 6$ GPa and $T = 1300 - 1600$ ^{o}C for time more than 100 hours [29]. Right conditions might be created in different apparatuses, for example, belt type [30] or BARS type (press-free high-pressure setup "split sphere") [31]. Metals are used as catalytic agents in this process. All metals are usually contaminated with nitrogen, which easily incorporates in a diamond crystal lattice. It means that by this method we can produce mainly Ib crystals with high concentration of nitrogen impurities. To overcome the purity problem of diamonds the growing method based on chemical vapor deposition (CVD) was proposed [32]. In this case the growth occurs from the gas phase (CH_4 mixed with H_2), and we have a better controllable system for the impurities. Diamond grows on the substrate inside CVD plasma chamber. It might be, for example, silicon or diamond plate. A substrate gives the position of carbon atoms for crystal growth. If the interatomic distance of the substrate is different than in diamond, it causes many defects in the crystal structure. It is better to use thin diamond plate as a substrate for the growth. CVD process is simultaneous combination of growth and etching, enabling to get diamond with less number of crystal defects. CVD diamonds have higher quality than HPHT crystals, but on the other hand they are more expensive and take longer time for creation. CVD diamonds are more needed in the areas where purity of crystals plays important role such as spectroscopy, electronic devices or spin physics. In case of using only mechanical properties of diamonds, HPHT crystals are cheaper and easier object to be used.

2.1.2. Physical properties of diamond

Diamond has a face-centered cubic lattice structure, when one cube is shifted compared to another by $1/4^{th}$ length of the space diagonal (fig. 2.2). The distance between carbon atoms is approximately 0.154 nm, which is smaller compared with other semiconductors (for example, silicon, with the same crystal lattice, has 0.234 nm). The refractive index of diamond is equal to 2.417. The covalent bonds between carbon atoms in diamond are very strong. The bonding energy is up to 711 kJ/mol [33]. Such crystals have high hardness and high temperature of melting. The diamond is a one of the hardest material. At Mohs scale diamond has highest hardness, which is equal to 10 [33]. That is exactly the diamond hardness made it so popular in ancient times.

The crystal structure of diamond leads to a high Debye temperature, which is 2200 K. This results in high thermal conductivity (app. 146.5 W/(m·K) [33]). Diamond is an indirect wide-band-gap semiconductor with the band gap energy is equal to 5.4 eV [34, 35]. This makes diamond an isolator at room temperature, since the thermal energy at temperature 300 K is around 0.025 eV. High Debey temperature and large band-gap make the effect from phonons at room temperature extremely small. This gives us an opportunity to work with single defects in diamond at room temperature without special cooling.

2.2. Nitrogen-vacancy center in diamond

There are a lot of different crystal defects in diamond from single substitutional as vacancies or different impurity atoms to more complicated complexes [36]. Some of these defects are optically, electrically or magnetically active. Alexander Zaitzev in his book "Optical properties of diamond" [37] collects the information about all known optical center in diamond. Among numerous color centers in diamond we can select the nitrogen-vacancy (NV) defect. The NV center consists of a substitutional nitrogen atom next to a vacancy (fig. 2.2). This is an optically active and paramagnetic defect [15]. First observation of electron paramagnetic resonance (EPR) related to NV centers in illuminated samples was demonstrated in the paper by J. H. N. Loubser and J. A. van Wyk [38]. The signal of NV centers in a dark sample was presented later in [39].

First optical observation of the ensemble of NV centers in diamond was done by G. Davies and M. F. Hamer in 1976 [40]. They found absorption and luminescent spectra of color center and unambiguously correlated zero phonon line (ZPL) at 1.945 eV with NV defect. The investigation and operation of a single NV center became possible with the revolution in single molecule detection [41]. And first application of this technique to NV was done in 1997 by A. Gruber et al. [15]. By confocal microscopy they resolved at room temperature single optical diamond defects, which were produced by electron irradiation. The first obtained fluorescence spectrum was done using excitation at 514 nm. In the same paper they demonstrated optically detected magnetic resonance (ODMR) of an NV center.

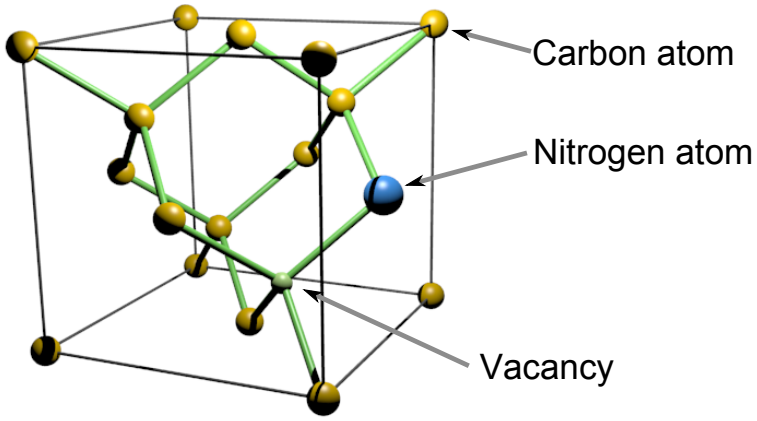

Figure 2.2.: The nitrogen-vacancy center inside the diamond lattice structure. Yellow - carbon atoms, blue - nitrogen atom, green - vacancy.

2.2.1. Creation of NV centers

The major impurity in diamond is nitrogen [24–26]. It can make be a constituting atom in numerous crystal defects [37]. It might be single impurity centers, double nitrogen centers or their clusters with vacancies. One of these centers is nitrogen vacancy (NV) defect. In natural crystals NV centers are placed chaotically and can be close to each other or to other paramagnetic centers. Different applications of color centers require different conditions. For example, the creation of qubits for quantum computing needs a system of closely located color centers [42]. High sensitive NMR measurements of molecules at diamond surface require single shallow NV centers [19, 20]. Imaging of big magnetic system such as neurons can be done with a layer of shallow defects [43]. For all these measurements the coherence time of NV centers should be as long as possible. It can be achieved in highly pure diamond. That brings our attention to the creation of NV centers in diamond in right order for unique experiments.

Nitrogen impurities in a diamond can be created during the growth process or later by ion implantation. In the CVD method there is a possibility to add nitrogen gas in the chamber and to create a layer of controlled amount of impurities. In case of HPHT diamond growth the opportunity to place impurities is missing. To create a single NV center the implantation method is more popular [44]. In the implantation it is possible to control not only the concentration of the impurities, but also its depths below the surface. Molecular implantation allows to make nitrogen defects

very close one to another, that is useful for the creation of strongly coupled spin qubits in diamond [42, 45, 46]. Negative point of the implantation is that high energy atoms or molecules break the crystal lattice and create many other defects, such as single or complexes of vacancies and interstitial defects. It also damages the upper diamond layer and graphitizes it. The thickness of the graphite layer depends on the implantation energy and dose. The annealing at high temperature repairs broken lattice, but it would never be as perfect as before the implantation. Sometimes it is better to polish out graphitized and reconstructed layer or to etch it off in plasma.

Secondly vacancies should be created in diamond lattice. Originally diamond contains some number of vacancies, but concentration of them is small and not enough to have a high yield of NV centers. Vacancies are formed during the nitrogen implantation too. However, the maximum of the implantation profiles for nitrogen atoms and vacancies are shifted and located at different depths [47]. This makes the yield of NV centers during annealing not high enough. New vacancies with right localization can be created by carbon implantation [45] or by electron irradiation [48, 49].

After nitrogen implantation and carbon implantation or electron irradiation diamond containing single nitrogen impurities and vacancies needs to be annealed to form NV centers and to reconstruct the damaged crystal lattice. The annealing occurs in the atmosphere of inert gases at temperature from 600 ^{o}C to 800 ^{o}C, at which vacancies start to move and can find nitrogen defects to create a complex together. Without high temperature and high pressure only small part of the graphitized layer will convert to diamond, the rest has to be removed by acid treatment. To remove the graphite layer from the diamond surface, the crystal is treated in three acid mixture of HNO_3, H_2SO_4 and $HClO_4$ in concentration $\{1:1:1\}$ and at the temperature of the acid boiling. This cleans the diamond and terminates the diamond surface with oxygen and carboxil groups. The importance of the surface treatment specially for NV centers will be discussed in chapter 2.4.3.

2.2.2. Structure of the nitrogen-vacancy center

An nitrogen atom and a vacancy occupy adjacent sites in the diamond lattice forming a new defect – nitrogen-vacancy. Its principal axis lies along $\langle 111 \rangle$ direction. The diamond lattice imposes C_{3v} symmetry onto the defect. Dangling bonds originated from sp^3 orbitals of carbon atoms and nitrogen form molecular orbitals of the defect (fig. 2.3, (a, d)). Using

group theory approach, one obtains two orbitals (a_1', a_1) which transforms as A_1 irreducible representation and one degenerated orbital (e_x, e_y) which transforms as E irreducible representation. Density functional theory calculation shows [50] that lowest a_1' orbital is situated in the valance band and therefore always occupied. The a_1 and $e_{x,y}$ orbitals lie in the band gap. The doubly degenerated orbital $e_{x,y}$ is the highest in energy. Further description of the color center's level structure requires to include electrons. Total wave functions are formed when orbital wave function is combined with a spin wave function resulting in states with their own symmetries.

It is known that the defect can exist at least in two charge states, namely neutral and negative. The first one requires five electrons: three electrons from carbon atoms and two from substitutional nitrogen atom. The ground state of the neutral NV is obtained when four electrons occupy a_1' and a_1 orbitals and one is placed onto $e_{x,y}$ (shortly it can be written as $a_1'^2 a_1^2 e_{x,y}^1$) (fig. 2.3, (a, b)). The symmetry of this state is ${}^2E$. The excited state is formed when one electron from a_1 orbital is promoted to the $e_{x,y}$ ($a_1'^2 a_1^1 e_{x,y}^2$). However, this configuration results in several possible states: ${}^4A_2$, ${}^2A_2$, ${}^2E$ and ${}^2A_1$, which order was recently assigned [51]. In the same work they have also shown that ZPL transition at 575 nm occurs between ${}^2E$ and ${}^2A_2$ states (fig. 2.3, (c)). The neutral NV center is not so extensively studied as its negatively charged counterpart and since it does not possess much interest for current work further discussions are omitted.

The negatively charged defect should acquire an addition electron from elsewhere in the lattice. This results in two unpaired electrons occupying e_x and e_y orbitals (fig. 2.3, (d)). Since the number of electrons is even, the total spin is integer, equal to $S = 1$. The $a_1'^2 a_1^2 e_{x,y}^2$ configuration forms the ground state of the defect. Combination of the spin degree of freedom with the spacial leads to formation of the six total states: three corresponding to the triplet state, usually denoted as ${}^3A_2$, and three singlets, denoted as ${}^1E_{1,2}$, and ${}^1A_1$ (fig. 2.3, (e)). Hund's rule suggests that the triplet state ${}^3A_2$ is the lowest. By analyzing the Coulomb interaction [52] it can be found that ${}^1A_1$ singlet lies higher in energy than ${}^1E_{1,2}$. The first excited state is formed by promoting an electron from a_1 orbital to one of the e ($a_1'^2 a_1^1 e_{x,y}^3$). The resulting states are double triplet ${}^3E$ and double singlet ${}^1E_{x,y}$. The axial part of spin-orbit interaction separates the ${}^3E$ manifolds into $A_{1,2}$, $E_{x,y}$, and $E_{1,2}$ states, whereas spin-spin interaction provides shifts of these levels and in addition lifts up the degeneracy of A_1 and A_2. Moreover, spin-spin interaction is responsible for mixing states with different spin projections. However, it was found that the fine structure of the excited state is temperature dependent [53], whereas at room temperature the structure of ${}^3E$

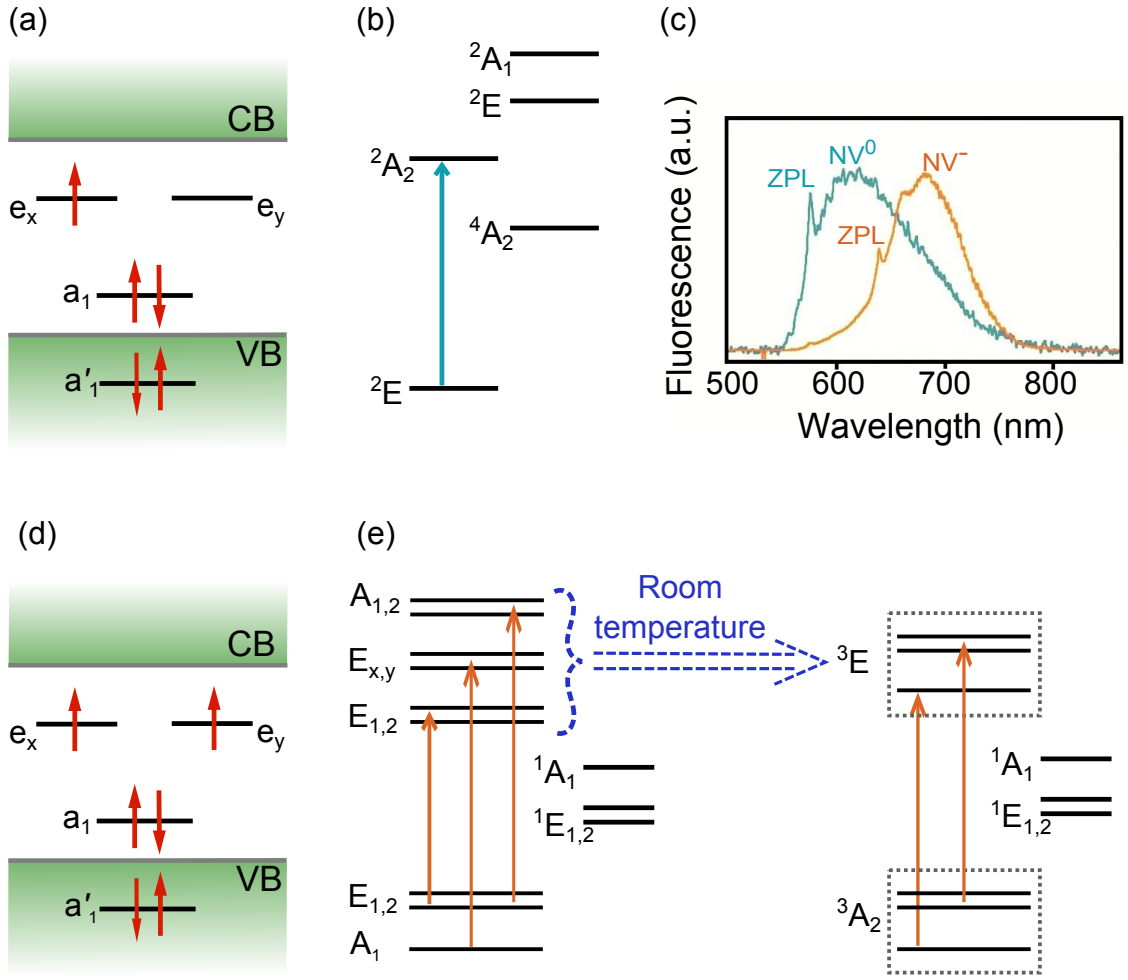

Figure 2.3.: The energy levels of a neutral (a) and negative (d) charge states of NV center. The electron structure of NV^0 (b) and NV^- (e) center. The fluorescent spectra (c) of NV^0 (blue line) and NV^- (orange line) center.

state is reminiscent of the ground state [54, 55]. This change was attributed to the phonon mediated averaging of the excited state orbital branches [56]. It is believed that phonons mix population between different levels of the same spin projection through the spin conserving phonon process with the rate faster than the radiative lifetime. Such averaging leads to effective quenching of the spin-orbit splitting of the $A_{1,2}$, $E_{x,y}$, and $E_{1,2}$ levels as well as the spin-spin splitting of the A_1 and A_2 states. Therefore, room temperature excited state is only influenced by spin-spin interaction which separates z and x, y spin projections by 1.42 GHz. Since all experiments presented in this thesis were performed at room temperature, only the "orbital averaged" excited state was used.

2.2.3. Ground state of the nitrogen-vacancy center

The ground state of NV center is used as a magnetometer, and therefore we should discussed it in more detail. As it was pointed out the ground state consists of the spin triplet ${}^3A_2$ and three singlets ${}^1E_{1,2}$ and ${}^1A_1$ (fig. 2.3, (e)). Since singlets are not important for the description of magnetic properties of the defect, they are omitted in this section. The full Hamiltonian can be written as following:

$$\hat{H} = \hat{H}_{so} + \hat{H}_{ss} + \hat{H}_{hf}, \tag{2.1}$$

where $\hat{H}_{so}$ is spin-orbit coupling, $\hat{H}_{ss}$ is spin-spin coupling, and $\hat{H}_{hf}$ is a hyperfine coupling term. Since ground state is represented by A_2 orbital symmetry, to a first approximation it does not have orbital magnetic moment. Hence, the ground state Hamiltonian is mainly governed by the spin-spin interaction. For the spin triplet system the spin-spin Hamiltonian along principal axis can be written in a form of:

$$\hat{H} = D_x\hat{\mathbf{S}}_x^2 + D_y\hat{\mathbf{S}}_y^2 + D_z\hat{\mathbf{S}}_z^2 \tag{2.2}$$

where $D_{x,y,z}$ are components of zero-field splitting tensor, which components are averaged over spatial wave functions. For spin $S = 1$ system, it is convenient to express this Hamiltonian in the basis $|+1\rangle$, $|0\rangle$, $|-1\rangle$:

$$\hat{H}_{ss} = \begin{pmatrix} \frac{1}{3}D & 0 & E \\ 0 & -\frac{2}{3}D & 0 \\ E & 0 & \frac{1}{3}D \end{pmatrix} \tag{2.3}$$

where it is taken into account that the $Trace[\mathbf{D}] = 0$, and notations $D/3 = D_z + (D_x + D_y)/2$ and $E = (D_x - D_y)/2$ are introduced. If the

symmetry of the defect is not distorted, $D_x = D_y$ and therefore E is zero. Value of D is known from EPR and ODMR experiments [15, 38, 39] and equal to 2870 MHz, whereas for most of the bulk diamonds E is close to zero (or absent).

The next term in the ground state Hamiltonian (2.1) describes coupling between electron and nuclear spins. There are several sources of nuclear spins, which can interact with the electron spin of NV center. First of all it is nitrogen, which can be not just a constituting part of the color center, but also nearby substitutional nitrogen defect. Nitrogen has two isotopes: ^{14}N with spin $I = 1$ and ^{15}N with spin $I = 1/2$, which natural abundances are 99.6 % and 0.4 %, correspondingly. Second source of nuclear spin is carbon, which forms the crystal lattice. However, only one isotope of carbon, namely ^{13}C has nuclear spin $I = 1/2$. But only 1.07 % of carbon is ^{13}C, then in most of the cases it should not be considered at all. The hyperfine interaction can be written as:

$$\hat{H}_{hf} = \hat{S}\mathbf{A}\hat{I} \tag{2.4}$$

where $\mathbf{A}$ is a hyperfine coupling tensor. It consists of two parts

$$\mathbf{A} = a_{iso}\mathbf{1} + \mathbf{A}_{aniso} \tag{2.5}$$

The first one a_{iso} is isotropic Fermi contact interaction which is proportional to the electron density at the nucleus location. This term has noticeable contribution only for those nuclei which are close to the NV defect, where electron spin density is high. The $\mathbf{A}_{aniso}$ is anisotropic part describing electron-nuclear magnetic dipole-dipole interaction. This term is valid for a longer range than the isotropic one, although it also decays fast as one over the cube of the distance. The splitting induced by hyperfine interaction is in the order of few megahertz which is significantly smaller with respect to D and can be neglected for all experiments discussed in this thesis.

In presence of magnetic field the Hamiltonian 2.1 acquires a Zeeman term

$$\hat{H}_{enZ} = g_e\mu_B\mathbf{B}\hat{\mathbf{S}} - g_n\mu_n\mathbf{B}\hat{\mathbf{I}} \tag{2.6}$$

where $\mathbf{B}$ is a magnetic field, g_e and g_n are the electron and nuclear g-factors, μ_B and μ_n are the Bohr and nuclear magnetons. Nuclear term in equation 2.6 is smaller than electron by at least three orders of magnitude, due to the magnetons ratio, so that we neglect it in further discussion. As it was mentioned earlier, the orbital magnetic moment of the ground state is small, therefore electron g-factor is almost isotropic and close to

$g = 2.023$. Written in the basis of $m_s = |+1\rangle, |0\rangle, |-1\rangle$ electron Zeeman term is

$$\hat{H}_Z = \begin{pmatrix} g_e\mu_B B_Z & g_e\mu_B \frac{B_x - iB_y}{\sqrt{2}} & 0 \\ g_e\mu_B \frac{B_x + iB_y}{\sqrt{2}} & 0 & g_e\mu_B \frac{B_x - iB_y}{\sqrt{2}} \\ 0 & g_e\mu_B \frac{B_x + iB_y}{\sqrt{2}} & -g_e\mu_B B_Z \end{pmatrix} \tag{2.7}$$

where $B_{x,y,z}$ are projections of magnetic field and z-direction is chosen as before along the principal axis of the defect. Combining matrices 2.3 and 2.7 one can see that if $E = 0$ and if the magnetic field is aligned along the principal axis or absent, the matrix has a diagonal form and $m_s = |+1\rangle, |0\rangle, |-1\rangle$ are eigenvectors. Distortion of the defect symmetry by crystal strain results in non-zero E parameter, and m_s is not a good quantum numbers anymore. The same is held if the magnetic field is tilted with respect to z-direction. This has an important issue for the ODMR contrast discussed in the next section.

2.2.4. Electron spin initialization and readout

Pure electronic transition occurs between the ground state $^3A_2$ and the excited state ^3E triplets which correspond to ZPL at 637 nm. However, optical excitation and relaxation processes are accompanied by displacement of the atomic cores which results in excitation of phonon modes. This coupling to phonons leads to significant broadening of the emission and absorption spectra. It enables the use of non-resonant excitation of the defect which is usually done at 532 nm by a frequency-doubled Nd:YAG laser. Obviously, such excitation cannot address separately different levels, which in any case is not possible at room temperature due to broadening of the ZPL. However, NV center's structure allows for optical spin polarization and readout even by non-resonant light.

Transitions between ground and excited states are spin conserving, i.e. selection rules by spin is $\Delta m_s = 0$ (fig. 2.4, (a)). Being excited to the ^3E triplet, system radiatively relaxes to the ground state but lifetimes for the $m_s = |0\rangle$ and $m_s = |\pm 1\rangle$ are different and found to be 12 and 7.8 ns, correspondingly [54, 57]. At the same time, number of photons emitted from the sublevels with spin projection $m_s = |\pm 1\rangle$ is less than for the transition with $m_s = |0\rangle$. The decrease of radiative lifetime is a result of inter-system crossing. The transverse part of spin-orbit interaction couples triplet and singlet states [58]. Thus, coupling assists non-radiative decay of the ^3E sublevels with non-zero spin projection to the metastable

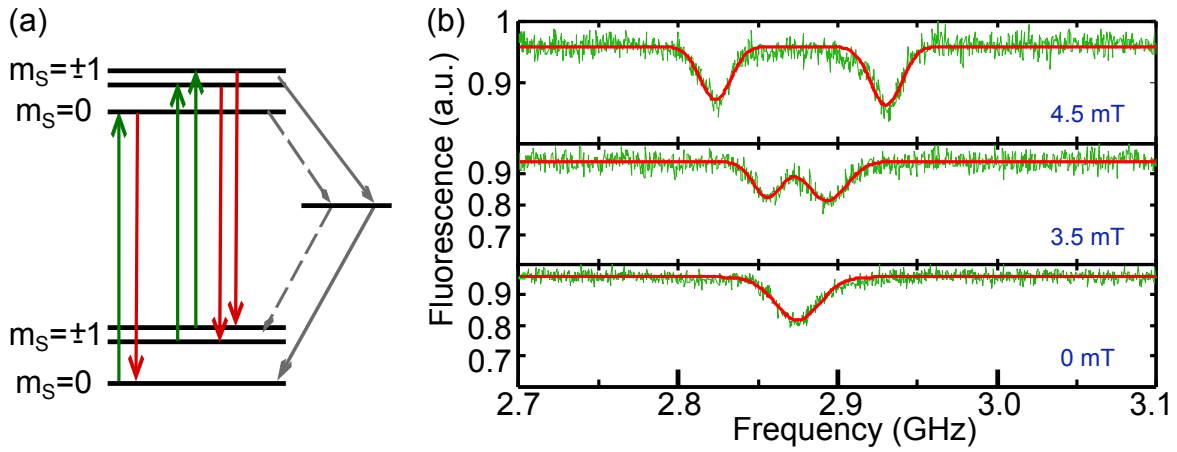

Figure 2.4.: (a) - The level structure of NV center, which represents the relaxation from the excited to the ground state. (b) - Typical ODMR spectra for NV center in different magnetic fields.

singlets $^1A_1$ and $^1E_{1,2}$. The latter are linked to the $^3A_2$ ground state by the same non-radiative spin-orbit mediated process. This additional relaxation channel for $m_s \neq |0\rangle$ leads to the effect of spin polarization. Let us consider this mechanism in more detail. Assume, that NV center is in the ground state. Since the zero-filed splitting is approximately 0.14 K all $^3A_2$ sublevels are populated equivalently. When laser excites the system, relaxation for $m_s = 0$ projection occurs predominantly over radiative channel preserving the spin, hence leaving NV center polarized. If after excitation system is in the sublevels with $m_s = |\pm 1\rangle$ projection, then it either decays radiatively back and excitation cycle is repeated to the same sublevel or non-radiative passage to the metastable states occurs from where it relaxes preferentially to the $m_s = |0\rangle$ state [59], leading to the polarization of NV center regardless of the initial state.

Spin dependent inter-system crossing has another important consequence. It allows to readout the spin state optically. If the NV center is prepared in $m_s = |0\rangle$ state, constant laser illumination does not change the spin projection and NV center continuously emits photons. However, if the initial state is $m_s = |\pm 1\rangle$, after excitation it has higher probability to decay over the metastable states, where population is trapped for about 250 ns [60], before repolarization into $m_s = |0\rangle$ state. Hence, $m_s = |\pm 1\rangle$ state amounts less number of photons. It is important to mention that only first few photons carry the information about spin state, since long illumination results in spin polarization destroying the information. These $|0\rangle$ and $|\pm 1\rangle$ states are sometimes referred as a “brigth” and “dark”. The

fluorescence difference for these two states is about 30% which is easily detectable. This property is used for example to observe electron paramagnetic resonance of a single NV center. In the ground state zero-field splitting separates the levels with zero and non-zero spin projections by 2.87 GHz. They are linked by the magnetic dipole transition with the selection rule $|\Delta m_s| = 1$. Therefore, if NV center is subjected to the microwave field at the frequency of zero-field splitting, the population oscillates between $m_s = |0\rangle$ and $m_s = |\pm 1\rangle$ states. Under constant laser illumination system becomes polarized in $m_s = |0\rangle$ state resulting in high fluorescence level. However, when resonant microwave field is applied population is redistributed between all levels in the ground state. This leads to decrease of the fluorescence due to high branching ratio into meta stable state from the excited state levels with non-zero spin projections. Such optical observation method of electron spin resonance signal is called optically detected magnetic resonance (ODMR). For the first time, ODMR on single NV defect was observed in 1997 by Gruber et al. [15]. As mentioned in the previous section, when symmetry of the defect in not disturbed, $m_s = |+1\rangle$ and $|-1\rangle$ levels are degenerated ($E = 0$) and only one resonance is observed. However, the presence of strain in crystal or external electric field distorts the symmetry of the defect resulting in $E \neq 0$ indicated by appearance of two dips in ODMR spectrum. Such splitting is very common for NV centers embedded in nanocrystals where strain has usually high value. Magnetic field also lifts up degeneracy of $m_s = |\pm 1\rangle$ as described by equation 2.7. Maximum contrast of ODMR is about 30 %, but it is influenced by the orientation and strength of the magnetic field. As it is seen from equations 2.3 and 2.7 application of the magnetic field along the principle axis of NV center does not change the diagonal form of the Hamiltonian (parameter E is assumed to be almost zero). At the same time, any deviation from z-direction result in mixing of the states with different spin projections, and $|+1\rangle$, $|0\rangle$, and $|-1\rangle$ are not good quantum numbers anymore. State $|0\rangle$ acquires admixture of non-zero components which reduces the fluorescence level due to shelving into metastable state. Therefore, with increase of the misaligned magnetic field strength the contrast of ODMR drops because the eigenvalues deviate from the initial $|+1\rangle$, $|0\rangle$, and $|-1\rangle$ basis.

2.2.5. Electron spin manipulation

Long spin relaxation times of NV center together with optical initialization, and ODMR technique open a way for manipulation of the spin in a con-

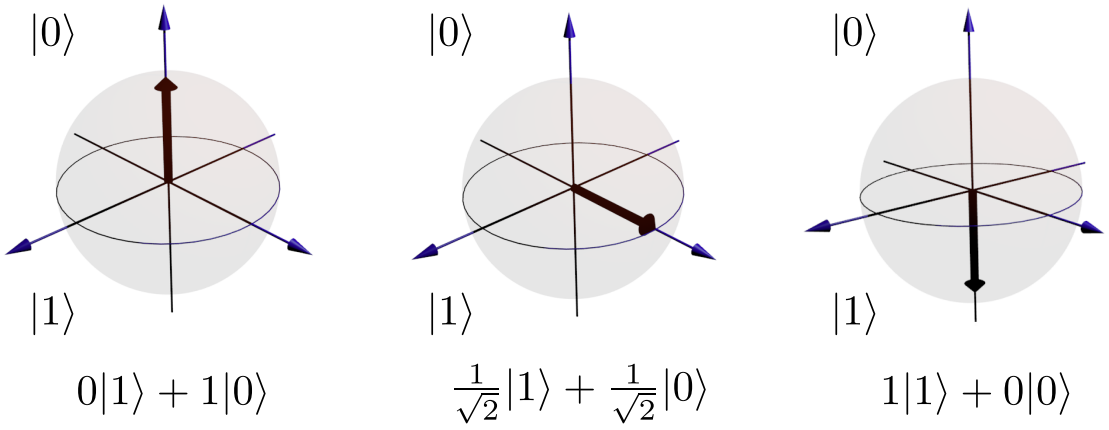

Figure 2.5.: The representation of bases states $|1\rangle$ and $|0\rangle$ and their superposition by Bloch vector.

trollable manner. That is why NV center is extensively studied as one of the solid state candidate for quantum computing. On the other hand these properties can be used for another important application in magnetometry and imaging. The ability to interact with external spins makes the NV center an atomic scale magnetic sensor, which is extremely important for life sciences. Fluctuating magnetic fields produced by either nuclear or electron spins of closely spaced atoms or molecules alter the relaxation times of NV defect which can be revealed by pulsed ODMR technique discussed in this section. Convenient way to describe dynamics of the spin system is to use Bloch sphere. This pictorial representation of the two-level system's state on a Riemann sphere was proposed by the Nobel Prize-winner Felix Bloch named after him. Poles of the sphere correspond to two basis vectors of the system whereas the end of an arbitrary unit vector points out any possible superposition of those two basis states (fig. 2.5). Although, ground state of the NV center is not a two-level system in most of the cases we are interested just in two states, for example $|0\rangle$ and $|+1\rangle$ (or $|-1\rangle$) when levels are split in magnetic field or $|0\rangle$ and $|\pm 1\rangle$ when states are degenerated.

Rabi oscillation

Although, ODMR technique under continuously applied microwave field is already to a certain extend a spin state manipulation, only pulsed ODMR can provide full control over the spin state. The problem of oscillatory field

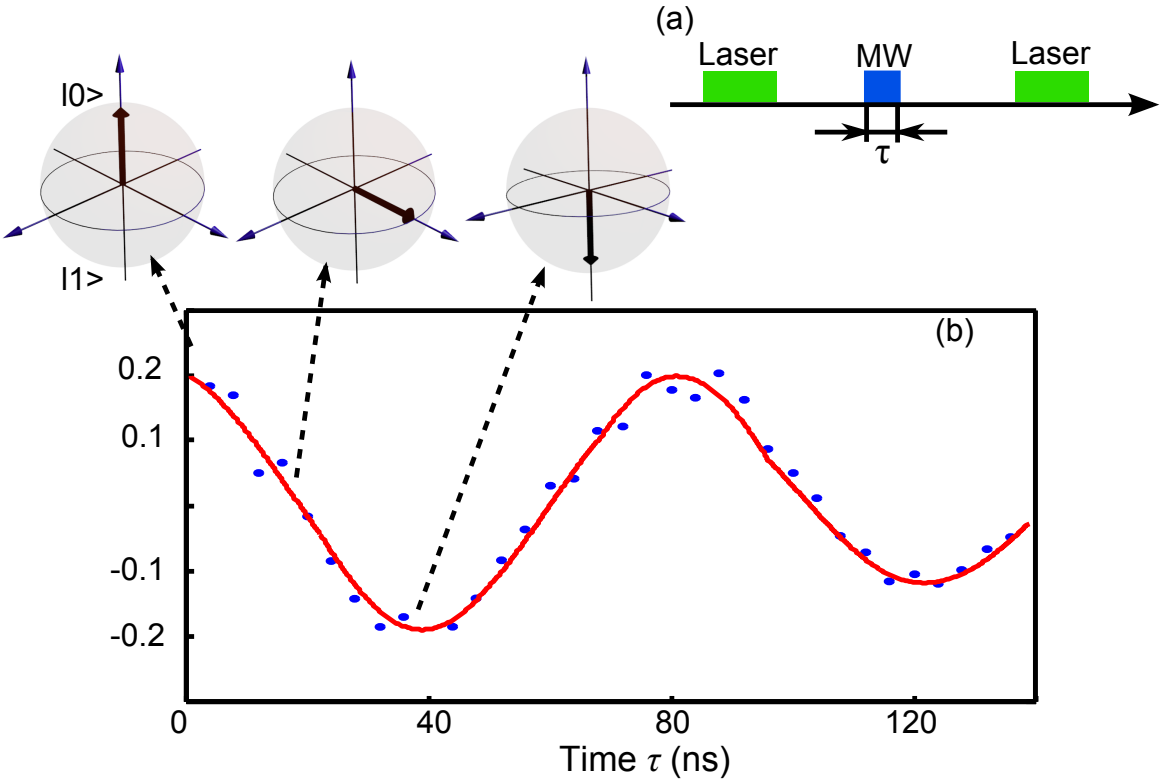

Figure 2.6.: (a) - The sequence for the measurement of the Rabi oscillation. First laser pulse converts the NV spin to state $|0\rangle$. The MW pulse changes the state of the spin depanding on its length. The second laser pulse reads out the NV spin state. (b) - Typical measurement of the Rabi oscillations.

interacting with a two-level system was described by I. I. Rabi in 1937 [61]. He showed that resonant field induces oscillation of the population between the ground and excited states with a frequency proportional to the product of the transition dipole moment with amplitude of the driving field. Such behavior allows to prepare the system in any arbitrary superposition state. Since probability to find the system in the excited state is periodic, it depends on time how long the system is subjected to the driving field:

$$\vartheta(t) = \frac{1}{\hbar} \int_{-\infty}^{t} \mathbf{d}\,\mathbf{E}(t')\,\mathrm{d}t' \tag{2.8}$$

where $\mathbf{d}$ is the transition electric (magnetic) dipole moment and $\mathbf{E}$ is the driving electric (magnetic) field. The equation 2.8 suggests that the same desirable state can be prepared either by changing the strength of the driving field at constant pulse length or by varying the pulse duration at constant field strength. Practically, both ways are used. However, in many cases it is easier to vary the pulse area by change of pulse duration. Especially important cases are achieved when pulse area becomes equal to $\pi/2$, π, $3\pi/2$ etc. The value of $\vartheta(t) = \pi$ correspond to entire transfer of population from the ground state to the excited state, whereas $\vartheta(t) = \pi/2$ results in preparation of a superposition state with equal probability to find the system either in ground or excited states.

In case of NV center, magnetic dipole transitions in the ground state $^3A_2$ are induced by an oscillatory magnetic component of microwave field. A typical pulse sequence is depicted in figure 2.6, (a). First, laser pulse of about 3 μs is applied to polarize the system in $|0\rangle$ state. Second, resonant microwave pulse creates a superposition $\alpha|0\rangle + \beta|\pm 1\rangle$, where the probabilities $|\alpha|^2$ and $|\beta|^2$ depend on the pulse duration. It is followed by a readout laser pulse which induces spin-dependent fluorescence and at the same time reinitializes the system into $|0\rangle$ state preparing for the next cycle. In each cycle microwave pulse area is varied resulting in a typical Rabi oscillation picture 2.6, (b). Besides pure demonstration of coherent manipulation of the electron spin, this measurements gives the duration of the $\pi/2$-, π-, and $3\pi/2$-pulses for a given field strength, which knowledge is important for spin relaxation times measurements.

Relaxation times

Once the desired state is prepared it does not remain forever. Relaxation processes bring the system to thermodynamic equilibrium with the environment. Relaxation is mainly characterized by two times: longitudinal (T_1) and transversal (T_2). Longitudinal relaxation time is responsible for population relaxation. Ground state levels of NV center are separated by approximately 0.14 K, thus at room temperature their are equally populated. Optical polarization of the spin results in an non-equilibrium state which exchanges energy with the lattice coming back to equilibrium. This is why it is also called spin-lattice relaxation. Since energy separation by zero-field splitting is low, the relaxation due to spontaneous emission proportional to the cube of frequency is negligible in contrast to optical transitions. Therefore the main source of relaxation is phonon scattering. Another reason for longitudinal relaxation is interaction of the spin with fluctuating local magnetic fields, which can originate either from surrounding electron or nuclear spins in the lattice or from external spins placed close to the NV center. The latter is more important for this thesis since measurements of spin-lattice relaxation time is utilized to observe presence of a magnetic particle in the vicinity of an NV center. Thermal motion forces spins to fluctuate. If this fluctuating field has effective frequency close to the Larmor frequency of NV center then it can cause a spin flip. It should be noticed that only xy-components of the fluctuating field induce spin flip exactly in the same way how it happens in EPR. However, in contrast to magnetic resonance technique, local field produces random "microwave pulses" defined by thermal motion and thus brings system into thermodynamic equilibrium with the reservoir.

The most straightforward way to measure T_1 time is to polarize the system in one of the basis state and then check how fast it decays. The typical sequence is depicted in figure 2.7, (a). First, the NV center is polarized by laser pulse with duration of about 3 μs in $|0\rangle$ state. Then after some time τ next laser pulse is applied which reads the degree of remaining polarization. By varying the waiting time τ between these two laser pulses, the decay curve is obtained. The time at which amplitude of the curve decreases by a factor of e defines T_1. The sequence discussed above can be slightly modified by additional microwave π-pulse, which is applied immediately after the polarizing laser pulse. So that, system is prepared in state $|1\rangle$. Usually, it is useful to measure T_1 time by both sequences, which allows to define precisely the fluorescence level corresponding to thermal equilibrium. Common relaxation curve is shown in

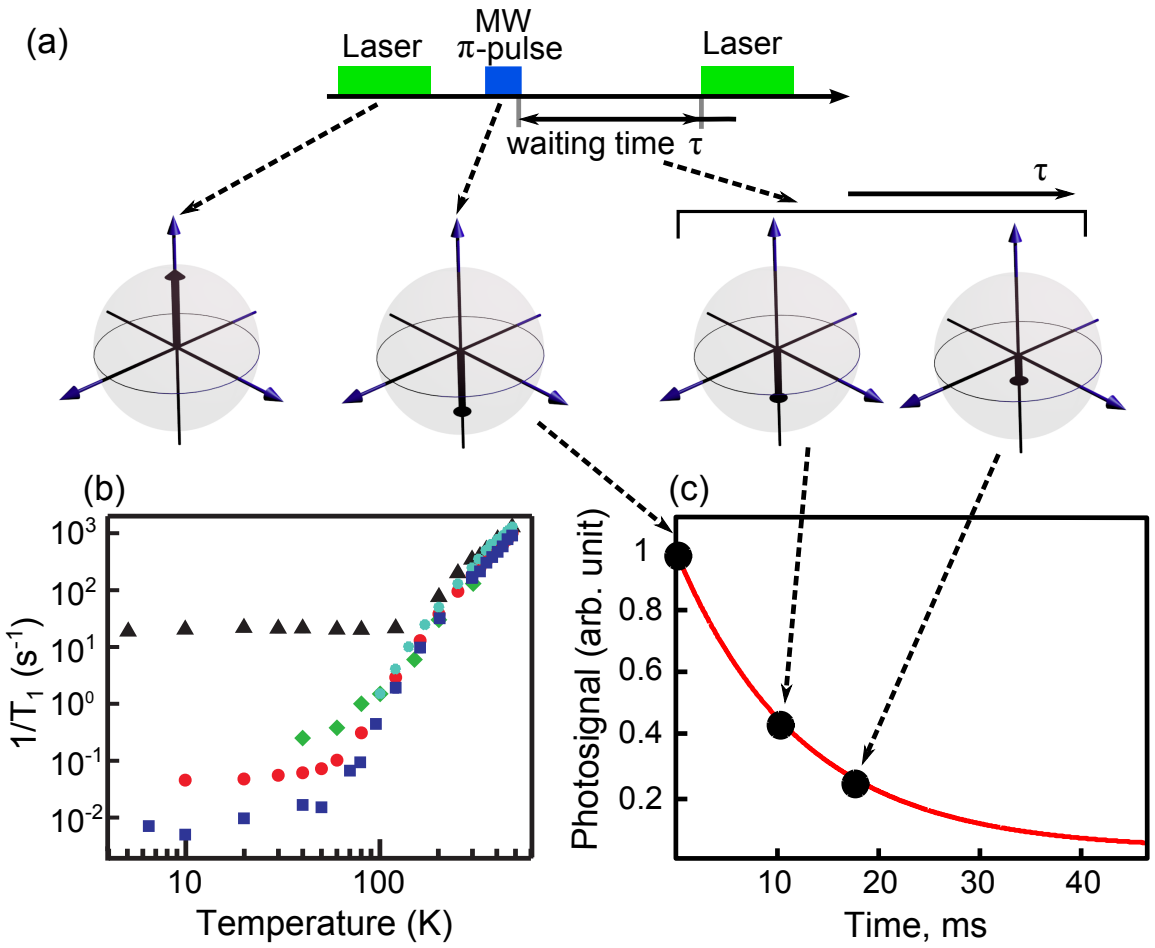

Figure 2.7.: The sequence for the measurement of the T_1 time (a). First laser pulse is for the state polarization, second pulse is for the readout of the NV state. Typical view of the T_1 time curve (c). The dependence T_1 time on the temperature (b), where different color show different diamond crystals (Adopted from [62]).

figure 2.7, (c). The longitudinal relaxation time depends on the particular crystal, but typically T_1 time for the spin of NV center is in the order of few milliseconds. T_1 is temperature dependent and it grows upon cooling the crystal down. Figure 2.7, (b) shows spin-lattice relaxation times of NV centers as a function of temperature in different diamond crystals.

While T_1 time determines the population relaxation rate, T_2 time defines loss of coherence. If a superposition between two basis states is created the phase is preserved until any random process destroys it. The time which characterizes irreversible loss of phase is called transversal or spin-spin relaxation time. To simplify further discussions we should point out that measurements of any parameter on a single spin require to carry out the experiment many times. According to the ergodic theorem multiple measurements on a single system are equivalent to one measurement on an ensemble. So the system will be considered as an ensemble, but it just implies that measurements are averaged over many repetitions on a single system. Assume, that the spins are initialized in one of the basis state $|0\rangle$ or $|1\rangle$ and then flipped to the equatorial plane by $\pi/2$-pulse. Thus, coherent superposition $|0\rangle/\sqrt{2} + |1\rangle/\sqrt{2}$ is created. At the beginning they all point in one direction producing non-zero magnetization in the xy-plane. Then the spins start to precess but owing to some inhomogeneity of the field the precession speed is slightly different for each spin. Therefore phase accumulation is also unique for each of them. If the time of free precession is long enough, magnetization in the xy-plane is lost, since spins are equally distributed in the equatorial plane. This time is called pure dephasing time and is denoted as T_2^*. However, the loss of transverse magnetization is reversible if phase accumulation is compensated. To do so, spins have to be inverted that they effectively see the same inhomogeneous field but in opposite direction. Thus, spins are refocused after time equal to the free precession time before inversion. Practically, refocusing is achieved by a microwave π-pulse. The phenomenon is called spin-echo, which was observed for the first time by E. L. Hahn in 1950 [63, 64]. Such recovery of the transverse magnetization is only possible if the field causing precession stays constant. However, the local field produced by surrounding spins in the crystal lattice undergoes random fluctuation due to thermal motion. This imprints as a random jump of the phase of the superposition state and therefore cannot be compensated. This results in a decrease of the echo signal with increasing the free precession time. The free evolution time at which the echo signal is reduced by factor of e is known as transversal relaxation (T_2) or coherence time. As it was pointed out local field is produced by neighboring magnetic dipoles which

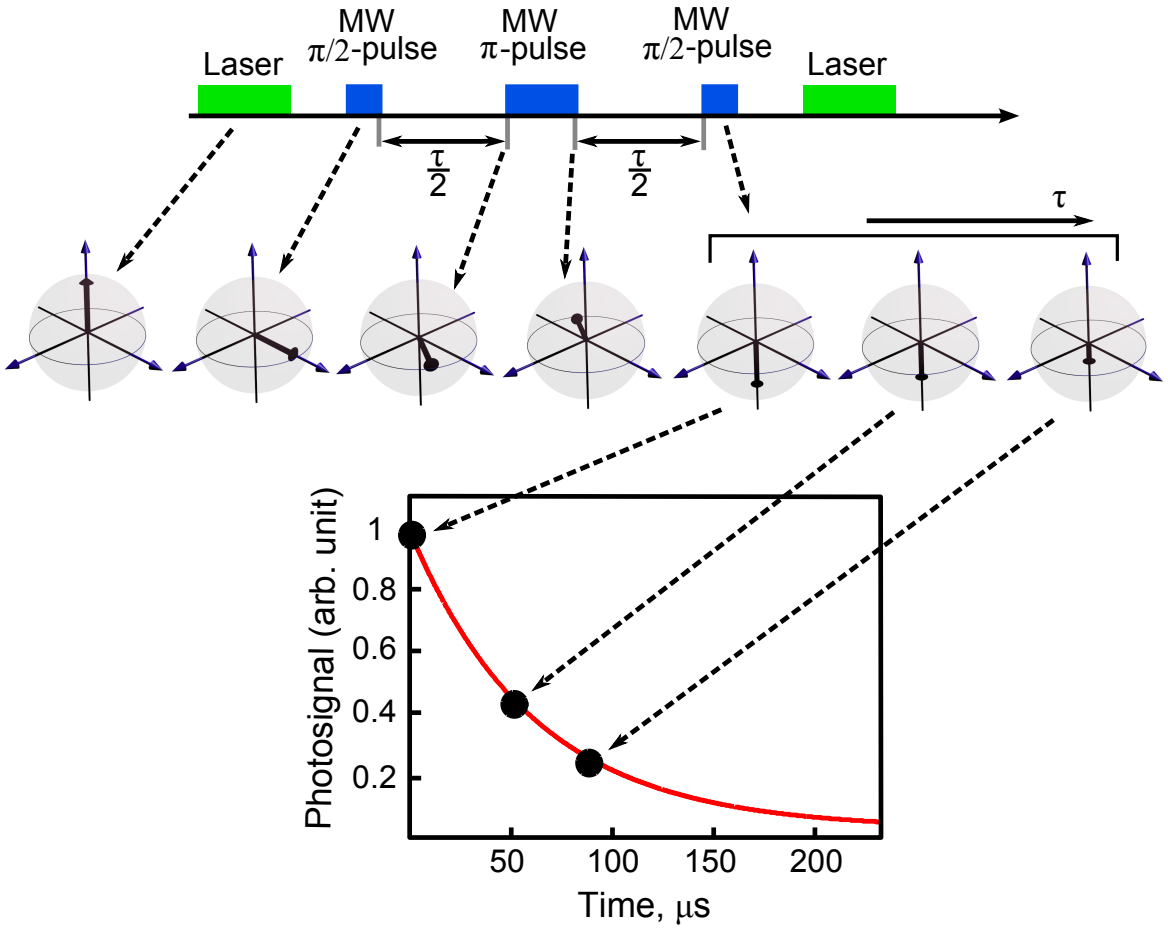

Figure 2.8.: The sequence for the measurement of the T_2 relaxation time. Typical view of the T_2 time curve.

are either nuclear or electron spins. This is why this type of relaxation is also called spin-spin relaxation. It should be mentioned that since the local field changes phase without energy transfer to the lattice only z-component of this field is responsible for this process.

Described above spin-echo experiment suggests a straightforward method for T_2 time measurement. The sequence is depicted in figure 2.8, (a). Laser pulse initializes the spin of NV center into state $|0\rangle$. Then a microwave $\pi/2$-pulse creates a superposition state $|0\rangle/\sqrt{2}+|1\rangle/\sqrt{2}$ which starts to evolve freely for time $\tau/2$. Microwave π-pulse rotates the spins by 180° and after the same time $\tau/2$ magnetization is restored. To readout this optically transverse magnetization has to be converted to population, which is achieved by an additional $\pi/2$ microwave pulse followed by laser. By varying $\tau/2$, the decay of the echo amplitude is measured which defines spin-spin relaxation time. The typical coherence

time of NV center obtained by this method is in the order of up to tens of microseconds for shallow implanted NV center (fig. 2.8, (b)). However, it can be prolonged by applying many refocusing pulses [65, 66].

2.2.6. Charge stability of NV center

An NV center is a single photon emitter and is photostable in its negative and neutral charge states [67, 68]. But there is a state of the NV defect, in which it does not emit light. This state is known as positively charged NV^+ from [69]. It means that the optical stability of NV depends on its charge stability. If the NV center is isolated from acceptors, which can take an electron from it, then the fluorescence of the color center is absolutely stable in time. This positively distinguishes NV center from other emitters as quantum dots, fluorescent molecules or proteins, which are quickly bleached and blinked off [70, 71]. Charge state of NV defect can be optically controlled and switched [72, 73]. The stability of a NV center is determined by environment conditions, such as crystal strains or another crystal defects.

The main and biggest lattice defect, which exist in all crystals, is its surface. The diamond surface gives an opportunity to control the charge state of NV centers, which are close to it. Inside the diamond crystal all carbons have sp^3 hybridization, but at the surface one carbon atom of four is missing, and without it the carbon bounds at the surface are converted to sp^2 hybridization, as in graphite. The graphite layer at the diamond surface takes an electron from NV center and quenches it [74]. Chemical treatment can close the free bond with external atom and transform the surface hybridization into sp^3. Different atoms at the diamond surface will give different results. For example, when NV centers are near the surface, which is treated with hydrogen, they lose electrons and thus are converted to the dark state (fig. 2.9, (a, b)) [75, 76]. To keep color centers in the negative charge state the diamond surface should be treated with oxygen (fig. 2.9, (c)) [75] or fluorine [77]. This is specially important for the shallow implanted NV centers or for centers inside nanodiamonds. Surface modification can be done by acid boiling or by etching in plasma. For nanodiamonds the surface treatment will be discussed in more details in chapter 2.4.3.

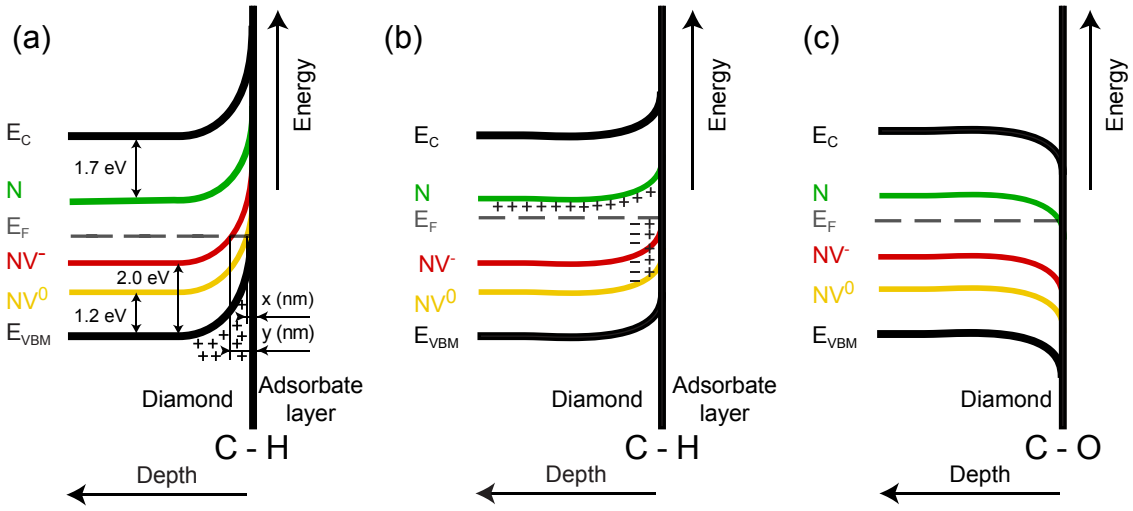

Figure 2.9.: NV levels in the band gap with hydrogen terminated diamond surface with (a) low concentration of nitrogen and (b) high concentration of nitrogen. (c) NV levels for oxidized diamond surface. (Adopted from [76])

2.3. Silicon-vacancy center in diamond

Another interesting but not yet well-known color center in diamond is the silicon-vacancy (SiV) defect. This color center consists of a single impurity silicon atom next to a single vacancy. The size of the silicon atom is larger than carbon atom. This leads to a shift of the silicon atom along the selected [111] trigonal axis (fig. 2.10, (a)) [78, 79]. SiV defects can be created during CVD growth, when diamond is grown on a silicon substrate, [80] or can be implanted [81].

The luminescence from the SiV centers was first observed in 1980 by Vavilov et al. in CVD diamonds [83]. The zero-phonon line of color center is located at 738 nm (1.68 eV) (fig. 2.10, (b)). Due to phonon wing the excitation of SiV can be done with a shorter wavelength. SiV center can be in neutral [84] or negative [82] charge states. The level structure of SiV^- center is shown in figure 2.10, (c). The observed luminescence is related to the transition between ^2E_u and ^2E_g levels. The fluorescence spectrum of SiV^- center at room temperature is presented in figure 2.10, (b). ZPL of SiV^- center splits into four lines at liquid helium temperature [85]. The four-line fine structure is related to the Jahn-Teller effect [86]. Each of these lines will have spin splitting in external magnetic field in two levels (fig. 2.10, (d)) [82]. The relaxation time of SiV is shorter than for

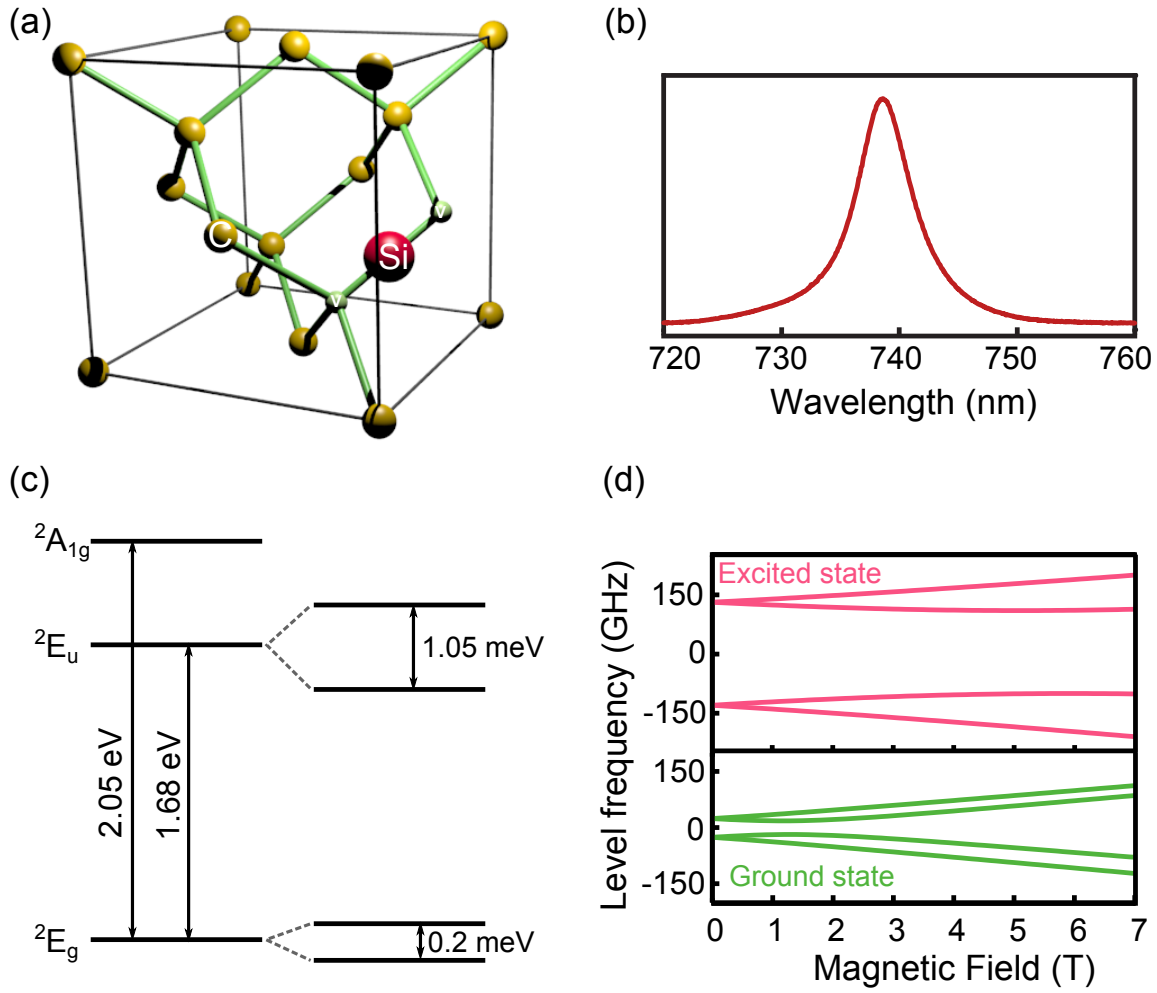

Figure 2.10.: (a) - The silicon-vacancy center inside the diamond lattice structure. (b) - Fluorescence spectrum of the SiV center at room temperature. (c) - Electronic structure of SiV^- center. The $^2E_u \leftrightarrow ^2 E_g$ transition gives ZPL at 738 nm. (d) - The splitting of the ground and excited levels of SiV in external magnetic field (Adopted from [82]).

NV center and can be up to 2 μs [16, 87]. It makes SiV defect not a good candidate for magnetic measurements as NV is. However, the ZPL of SiV located in the near infrared region making this center useful for medical applications, since the absorption of biological tissues in this spectral window is ten times smaller than for blue light [88].

2.4. Nanodiamonds: creation and functionalization

The first observation of nanodiamonds was done in 1987 in a meteorite sample [89]. The size of the found crystals was up to 10 nm. But first diamonds from meteorites were discovered more than one hundred years before. In 1888 Jerofejeff and Latschinoff have reported, that crystal formed from carbon atoms was detected in the Nowo-Urei meteorite [90]. That nanodiamond samples were created in meteorites by a shock, at some moment temperature and pressure were high enough to form diamonds from graphite [91]. Later this process came to be the basis to produce synthetic nanodiamonds. The nanocrystals, which were created by this method, are called detonation nanodiamonds. In that technique it is hard to control their properties. The milling production of nanodiamonds [92] permits to improve the quality of nanocrystals.

2.4.1. Creation of nanodiamonds

First nanodiamonds' growing process, which was realized in the laboratory, was based on the detonation technique [93]. However, first experiments did not provide stable results, and the method for mass production of detonation nanodiamonds was made only in 1988 [94–96].

Detonation synthesis of nanodiamonds occurs in a closed metallic chamber. Inside this chamber blast waves create high temperature together with high pressure, which are sufficient for diamonds formation (see point 1 at the figure 2.11(a)). Stable form of diamond can be reached by a negative oxygen balance, otherwise nanodiamonds are burned to graphite [97]. For example, to produce detonation diamond nanocrystals a mixture of 60 $wt\%$ trinitrotoluene ($C_6H_2(NO_2)_3CH_3$) and 40 $wt\%$ hexagon ($C_3H_6N_6O_6$) can be used [98]. In figure 2.11, (a) the red line shows how temperature-pressure balance evolves inside the chamber. Nanodiamonds might be transformed to graphite without fast cooling generated at the

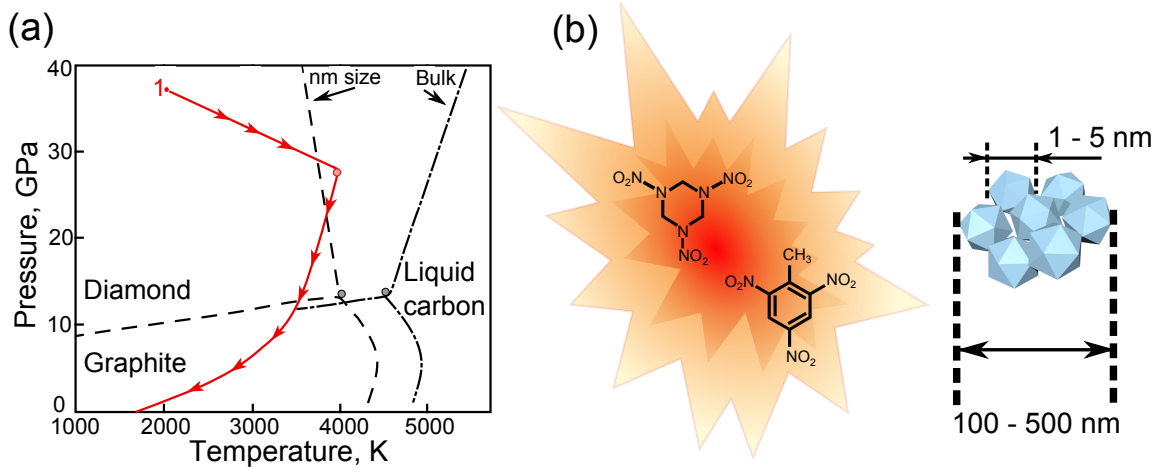

Figure 2.11.: (a) Phase diagram of the equilibrium between diamond, graphite and liquid carbon for nanocarbon materials and bulk together with detonation process of diamond growth. (b) Reaction inside the chamber for detonation nanodiamonds creation and form of detonation nanodiamonds.

moment of explosion. To prevent destruction of diamonds the reaction should go in an atmosphere of Ar, N_2, CO_2 and liquid or solid H_2O. The stability of nanodiamonds depends on the thickness of the water layer around nanocrystals [97]. Created by detonation synthesis nanodiamonds are very small (around a few nanometers), but during the generation process they form clusters, which are sintered with graphite (fig. 2.11, (b)).

Another possible method to grow nanodiamonds is based on the CVD method. The process is the same as for bulk diamonds, only the growing time should be much shorter [99]. In this technique it is possible to control the size of nanodiamonds and to dope them with elements in the right concentration.Thus CVD growth of nanodiamonds is a good method to make a new type of nanocrystal [10], but at the same time it is not very useful for mass production. The nanodiamond growth can be done only at a special substance such as another diamond or silicon plate. It also limits the area of the applications of such nanocrystals. For example, in case of *in vivo* experiments nanodiamonds should be placed inside the living cells or attached to proteins. It means that nanocrystals should be removed from the substrate. For example, in case of silicon plate it can be done by acid treatment. However, the efficiency of such method is not high. The best way for mass production of nanodiamonds is a milling process of HPHT bulk diamonds.

Milling of diamonds includes several steps [92]. The first one is to prepare microdiamonds with sizes around hundreds of micrometers. It could be done by crashing big diamonds to smaller pieces, as diamond is sufficiently fragile. Then big microdiamonds are milled to the size in the order of few micrometers. To do so nitrogen jet milling autogeneous micronization can be used [100]. The last step of the nanodiamonds preparation is a ball milling, which can be realized in argon atmosphere by using a planetary ball mill [101]. Now a lot of commercial milled nanodiamonds with different properties are available [102]. Milled nanodiamonds give more freedom to choose the size of nanocrystals, than the detonation method. The size separation can be done by centrifugation of solvent nanocrystals. Such method would not give narrow size distribution. However, it is not very critical, because nanodiamonds have non spherical form but are more elongated in one direction.

2.4.2. Nanodiamonds with color centers

Fluorescence of nanodiamonds is related to crystal defects inside them. For example, it can be nitrogen-vacancy (NV) or silicon-vacancy (SiV) centers.

Creation of fluorescent nanodiamonds with NV centers can be done in two ways. Firstly bulk diamond with high concentration of color centers can be milled to nanodiamonds. The second possibility is to create nanocrystals from *Ib* diamond and then irradiate them with electrons and anneal [103, 104]. In case of other impurities, doped nanodiamonds can be made from bulk crystals with right components by milling.

Nanodiamonds have large surface compare to the volume of nanocrystals. Color centers in this case are usually close to the surface. The latter can have graphite parts or absorb some molecules and chemical groups, which affect the color center inside. Thus the stability of the fluorescence of NV center inside nanodiamonds depends on the size of nanocrystals and the surface treatment (fig. 2.9) [76, 105, 106]. The smallest size of nanodiamonds reported to have stable fluorescence is 5 nm [7]. SiV defects have stable luminescence inside nanocrystals down to $1,6$ nm [8].

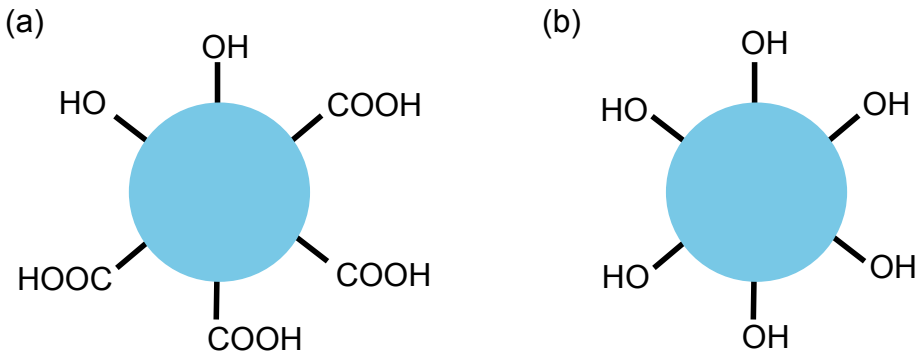

Figure 2.12.: Nanodiamod surface after (a) oxidation and (b) reduction.

2.4.3. Surface functionalization of nanodiamonds

The nanodiamond's surface is a big problem for color centers, but at the same time it gives great opportunities to use nanodiamonds for biological applications. Nanocrystals can be attached to any molecules or proteins to mark them or to investigate their magnetic properties, for example. The small nanodiamonds can be placed inside cells or can be attached to some part of it. For chemical bonding it is easy to use OH or $COOH$ groups at the surface. To have such treated nanodiamonds, they have to be oxidized. It can be realized by the same way as for bulk diamond.

Nanodiamonds' surface can be treated by boiling in three acid mixture (HNO_3, H_2SO_4 and $HClO_4$, $\{1:1:1\}$) for 24 hours or even longer. It is necessary to remove all graphite from the nanodiamonds surface, because it can quench the NV center. During this process the nanodiamond surface is covered with different functional groups such as carboxyl, hydroxyl, lactone, ketone and sometimes alkyl groups (fig. 2.12(a)) [107]. Reduction (with $BH_3 - THF$ or $LiAlH_4$) can help to increase the number of the hydroxy groups on the nanodiamond surface (fig. 2.12(b)) [107]. Exactly hydroxyl and carboxyl groups make nanodiamonds good candidates for functionalization for biological applications. Oxidized nanodiamonds can be also functionalized with amino groups [108]. This makes possible the further modification of nanodiamonds with biologically active molecules or proteins. The way of attachment is similar as for quantum dots [109] or gold nanoparticles [110]. Big advantage to use nanodiamonds for biological application is that diamond nanocrystals are highly biocompatible and even with size down to 2 nm are non toxic [111] compared to quantum dots [112] or gold nanoparticles [113].

Nanodiamonds' surface can be also modified during plasma etching. It

gives more varied and highly controlled results. However, for that nanodiamonds have to be spincoated on a substrate (such as glass or diamond plate). Then nanodiamonds can be used only on this substrate. Any acid removing as for CVD grown nanodiamonds will change their surface. It limits the areas of applications of nanodiamonds.

3. Experimental background

3.1. Optical markers

In biology there are many questions, which are related to the visualization of nanoscale objects, such as molecules or proteins, which do not have autofluorescence. It might be, for example, the study of the dynamics of some drugs inside living organisms, their absorption in different types of cells and so on. In that kind of investigation different parts of the cells or proteins should be marked. At the same time it might be necessary to visualized the labels separately. Also room temperature is a necessary condition to work with living organisms. *In vivo* imaging makes a lot of problems for scientists. And first of them is what is the best fluorescent object for labeling. There are a few possibilities: organic particles (as dye molecules or fluorescent proteins), quantum dots, metallic nanoparticles (as gold or silver nanoparticles) or nanodiamonds with color centers.

3.1.1. Organic fluorescent particles

First fluorescent tags were of course dictated by nature. In 1962 Osamu Shimomura published a work about the separation of green fluorescent proteins (GFP) from the jellyfish *Aequorea victoria* [114]. For that discovery and development of GFP O. Shimomura, M. Chalfie and R. Y. Tsien won the Nobel Price in chemistry in 2008. GFP gave a lot of advantages for the progress in biological research [115, 116]. After the discovery of GFP many other fluorescent protein were discovered [70, 117]. They cover a broad spectral region. The excitation and emission spectra of some of them are presented in figure 3.1.

Organic fluorophores have a lot of different possible types of attachment [118–121]. But one type of the bonding of GFP (and other organic fluorescent proteins) positively selects it from other optical markers. It is genetic labeling, which is realized by changing deoxyribonucleic acid (DNA) [118, 122]. For example, this method is very useful in the investigation of the localization of specific ribonucleic acid (RNA) targets or of the growth of tumor cells. One of the funny examples of using genetic

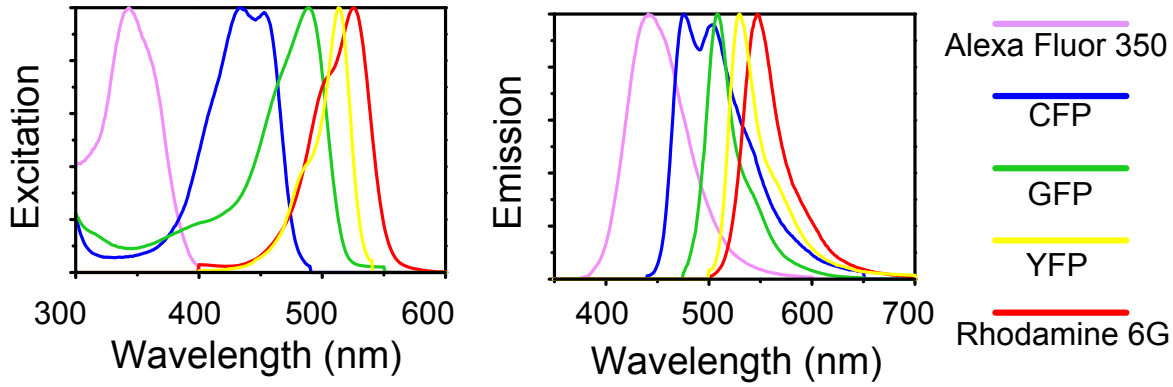

Figure 3.1.: Excitation and emission spectra of some organic fluorophores [117] (CFP - Cyan Fluorescent Protein, GFP - Green Fluorescent Protein, YFP - Yellow Fluorescent Protein).

modification with fluorescent proteins is the creation of Glofish (genetically modified fluorescent fish) [123].

It is also possible to use organic fluorescent molecules, for example, Rhodamine. However, they are toxic and can cause cancer [124], which is not preferable for living systems. Another negative point of using organic fluorophores, they have nonstable luminescence and can be fast and easily bleached [70].

3.1.2. Quantum dots

Quantum dots or semiconductor nanoparticles were discovered by the Russian scientist Alexey Ekimov in 1981 firstly in a glass matrix [125]. The energy levels in conduction and valence bands are quantized for nanosized semiconductor crystals [126]. The recombination of electrons from the levels in the conduction to the valance band levels give a few nearby sharp lines, this describes narrow luminescent spectra of quantum dots. Own to the same reason fluorescence of quantum dots strongly depends not only on the semiconductor material but also on the size of nanocrystals [127].

The possibility to choose a fluorescence wavelength is a big advantage for using quantum dots as optical markers, but they do not have high photostability. Quantum dots blink in time [128], and this makes the optical detection of quantum dots difficult. For biological application quantum dots can be functionalized with special proteins or molecules [129]. How-

ever, there is another problem to use them *in vivo*, since their components are toxic and are not preferred for living systems [130].

3.1.3. Metallic nanoparticles

Metallic nanoparticles, such as gold or silver [131], are good alternative to quantum dots or organic fluorophores in biological applications. First colloidal gold was obtained by J. Turkevich in 1951 , the size of the first gold nanoparticles was $2-3$ nm [132]. Fluorescent properties of metallic nanoparticles correspond to the surface plasmon resonance. The spectra of their fluorescence depend on the size of nanoparticles [133, 134]. The luminescence of gold nanoparticles is also very sensitive to the pH environment [135], and they can be used as pH sensors. But on the other hand the instability of their properties at different pH opens questions to use them in biological systems, where pH could change in a broad range in different cell parts. Gold and silver nanoparticles have big advantages related to the antibacterial effect and can be used as tumor targets for photothermal therapy [133, 136].

3.1.4. Nanodiamonds with color centers

Main problems of previously discussed optical markers in biological applications are related to their toxicity (especially for organic fluorophores and quantum dots) and photo-instability. Nanodiamonds with color centers can help to find the solution for such applications. Big advantage to use nanodiamonds as optical biomarkers is their nontoxicity. Nanodiamonds with the size more than 2 nm are nontoxic for cells [111] including human cells [137]. And as it was discussed in chapter 2.4 nanodiamonds with color centers have stable optical properties.

Nanodiamonds can be attached to proteins or molecules for their visualization [138]. Diamond nanocrystals can also be used for *in vivo* studies. They can penetrate into cells by two ways: small particles (with size up to 10 nm) by facilitated diffusion [139] and bigger nanocrystals by endocytosis [140, 141] (see appendix A.1). Nanodiamonds can easily penetrate into bacteria [142, 143] and living cells [144, 145].

They can find application not only at the level of single cells, but also inside big organisms, for example, worms [146] and mice [147]. Nanodiamonds' surface can adsorb different molecules from liquids. It might affect the charge state of NV center and can be detected optically. However, to have stable optical and hydrodynamical properties of color centers it

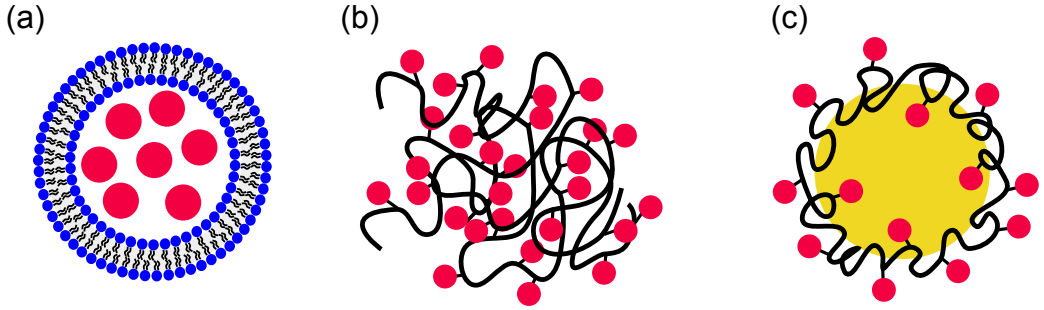

Figure 3.2.: Different systems for drug delivery (a) lipid nanoparticles, (b) polymer nanoparticles and (c) solid nanoparticles covered with polymer.

is necessary to protect nanodiamonds' surface with some chemical groups, molecules or proteins.

3.1.5. Drug delivery

One of the most important problems in medicine is an accurate drug delivery. For example, during usual chemotherapy, the drug would be absorbed by all tissues (tumor and healthy) and damage them. It means that medical treatment is a competition between healthy and cancer cells, which would died first and which would survive. Targeted drug delivery should help to exclude injuries of healthy organs. For drug delivery many different kinds of nanoparticles can be used [148–151]. For example, it can be nanoparticles formed of liposomes (fig. 3.2, (a)) [152], where the drug is protected by a lipid layer, which opens only in the right environment, or nanoparticles, which are created from polymer-drug conjugates (fig. 3.2, (b)) [153]. The drug can be attached to polymers by different pH sensitive chemical bound to provide its controlled release [154]. The reason for this is that tumor often has acidic pH level in comparison with healthy tissue [155]. It might be useful to utilize fluorescent nanoparticles (such as metallic nanoparticles [156] or quantum dots [157]) functionalized with polymer-drug system (fig. 3.2, (c)), which can be used not only for drug delivery but also for imaging of the drug trace. However, drug delivery system should be nontoxic itself, otherwise it is not very beneficial. For cancer therapy the preferable size of nanoparticles is $10 - 100$ nm [148]. Drug carriers should be easily functionalizable and be nontoxic by themselves. Nanodaimonds with color centers satisfy

to these criteria and can be considered as drug delivery system.

3.2. NV center as magnetic detector

Many different sensors for the detection of magnetic field can be found, such as Hall detectors, superconducting quantum interference devices (SQUID), inductive sensors, etc. Each of these detectors has a special area of applications in accordance to their size and sensitivity (fig. 3.3). For example, SQUID sensors are widely used in biomagnetometry [158]. However, for biological applications it would be nice to find a detector not only with high sensitivity, but also with nanoscale size for precise positioning. NV center in diamond has promising properties and can be utilized for such measurements. It can achieve very high sensitivity [159, 160] up to single spin. On the other hand optical manipulation and optical readout of the NV spin make possible to use this sensor *in vivo*. Such magnetic detector can be realized using shallow color centers in bulk diamond [19] or centers inside nanodiamonds [161], which are bound with biomolecules or put into the cells.

3.2.1. Detection of DC field by NV center

External constant magnetic field applied to NV center splits the spin levels at the ground state due to the Zeeman effect (fig. 3.4, (*a*) [17]) (for more details see chapters 2.2.2 and 2.2.3. The change of the splitting between states $|0\rangle$ and $|-1\rangle$ and states $|0\rangle$ and $|+1\rangle$ can be optically detected. The energy shift of the levels does not depend only on the strength of the applied magnetic field but also on the orientation of NV center in respect to this field and strains in the diamond crystal. The Hamiltonian of the system with the total electron spin equal to 1 and with the symmetry $C_{3\nu}$ is given by

$$\mathcal{H} = g\mu_B \mathbf{B} \cdot \mathbf{S} + D({S_z}^2 - S(S+1)/3) + E({S_x}^2 - {S_y}^2) \tag{3.1}$$

with g - the g-factor, μ_B - the Bohr magneton, $\mathbf{B}$ - external magnetic field, D and E are parameters of the zero-field splitting. From this the resonant frequencies of the transitions between $|0\rangle$ and $|\pm 1\rangle$ can be found by the formula [17]:

$$(g\mu_B B)^2 = \frac{1}{3}({\omega_1}^2 + {\omega_2}^2 - \omega_1\omega_2 - D^2) - E^2 \tag{3.2}$$

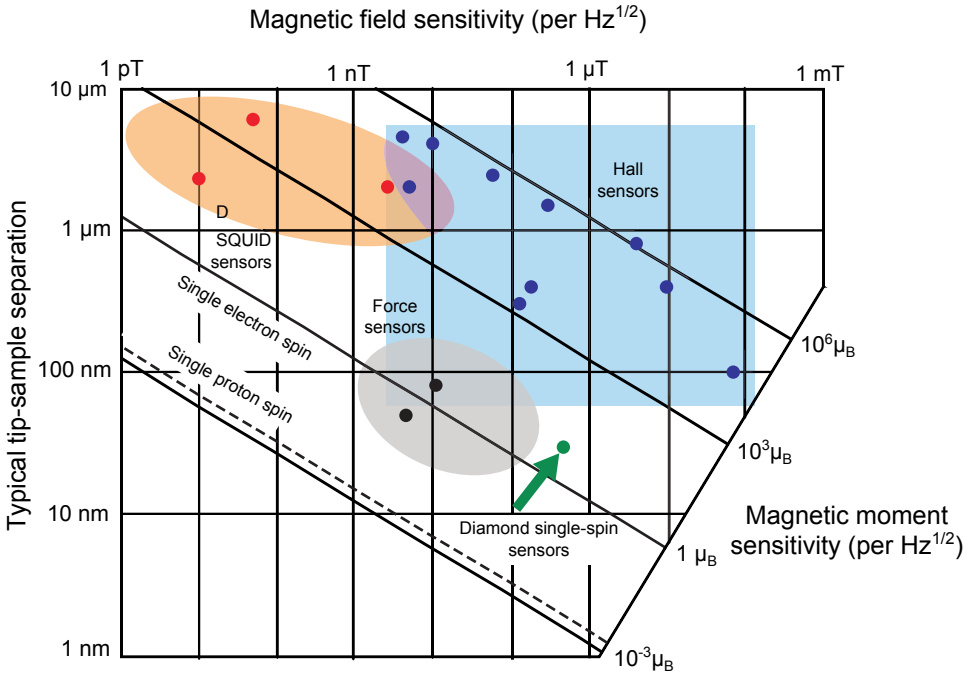

Figure 3.3.: Comparison of the sensitivity of different magnetic field detectors [162].

To determine the magnetic field measured by NV center it is necessary to know the crystal strain and applied electric filed, both are included in E (eqn. 3.2) and affect the splitting of the ODMR lines. However, the crystal strain also can be used as detector, not for magnetic filed but for pressure. Applied pressure to diamond crystal changes the internal strain and as a result the splitting between the resonant transition [163]. Thus NV center in diamond can be used as a pressure detector. This can open another areas of application of the color center.

The measurement of constant magnetic field enables the possibility to detect slow changes of the magnetic field in time or in space. The experimental demonstration of the magnetic field gradient detection was presented in the paper by G. Balasubramanian et al. in 2008 [17]. They scanned the magnetic tip of an atomic-force microscope (AFM) across the NV center in nanodiamond and simultaneously collected the fluorescence from the center, while continuous microwave field with constant frequency was applied (fig. 3.4, (b)). When the distance between NV center and the end of the magnetic tip was changed, the fluorescence level was influenced. This is due to the continuous tuning of the resonant transition frequency of NV spin by the varied magnetic field. At some point the resonant transition

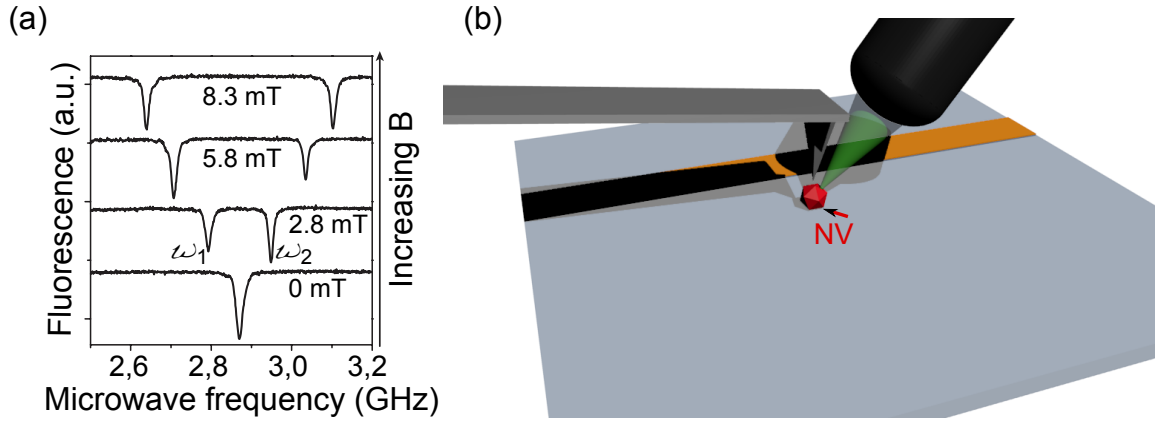

Figure 3.4.: (a) ODMR lines corresponding to different strengths of the applied magnetic field [17]. The figure shows the case when the principal axis of NV center coincides with the direction of the field. (b) Setup for scanning magnetic object around an NV center.

frequency crossed the applied microwave frequency, and the fluorescence decreased.

The sensitivity of the DC field can be improved by using Ramsey-type sequence [18]. In this case the spin prepared in either $|0\rangle$ or $|1\rangle$ state is fliped by $\pi/2$-pulse into coherent superposition $\frac{1}{\sqrt{2}}|0\rangle + \frac{1}{\sqrt{2}}|1\rangle$. Placed in an external magnetic field B the superposition state acquires a relative phase ϕ during the free evolution time τ. Second $\pi/2$-pulse converts coherence into population, which can be read out optically. The minimum detectable magnetic field (B_{min}) can be determined by formula

$$B_{min} = \frac{\hbar}{g\mu_B} \frac{1}{\sqrt{\tau T}} \tag{3.3}$$

with μ_B - the Bohr magneton, $g \approx 2$ for the NV center in diamod, T - total averaging time [164]. To decrease B_{min} field T and τ should be increased. The evolution time τ is limited by the T_2^*, and at maximum can reach this value. From this the sensitivity of a magnetometer based on a single electron spin can be estimated as it is shown in [165]

$$\eta_{DC} \approx \frac{\hbar}{g\mu_B C \sqrt{T_2^*}} \tag{3.4}$$

where

$$C \approx \frac{N_0 - N_1}{\sqrt{2(N_0 + N_1)}} \tag{3.5}$$

is a function of the N_0 and N_1, which are photon numbers collected from the state $m_s = 0$ and $m_s = 1$, correspondingly (fig. 3.5, (c), blue line). The sensitivity can be up to ~ 1 μT Hz$^{-1/2}$ [166]. Collection efficiency improvement leads to an increase of sensitivity, which was observed in Ref. [167], where they enhanced this value up to ~ 120 nT Hz$^{-1/2}$ by utilizing a plasmonic structure.

3.2.2. Detection of AC field by NV center

The detection of a periodic magnetic field can be done by Hahn's spin-echo method [64]. The π-pulse in Hahn-echo sequence refocuses the spin (fig. 3.5, (a)). It filters the effect from the periodically fluctuating magnetic field. But in case when the period of the magnetic field is equal to the free evolution time τ the Hahn-echo filter is blind to that field (fig. 3.5, (a)). This magnetic fluctuations affect the coherence time T_2 and decrease it. The observation of such changes in T_2 time gives the information about the external magnetic field. The sensitivity of the detection is limited now by the coherence time T_2 and can be expressed as

$$\eta_{AC} \approx \frac{\pi\hbar}{2g\mu_B C\sqrt{T_2}} \tag{3.6}$$

where parameter of the photon collection C can be count by formula 3.5 [165]. The optimal sensitivity is obtained for the field with frequency $\nu \sim 1/T_2$ (fig. 3.5, (c), orange line). Actually coherence time can be prolonged by adding more refocusing π-pulses, how it was proposed in 1954 by Carr and Purcell [168]. Such continuous refocusing effectively decouples the system from the environment and improves the sensitivity of the detection [168]. Meiboom and Gill in 1958 modified the sequence proposed by Call and Purcell. They demonstrated that the spin rotation around different axes x and y makes the sequence insensitive to inaccuracy of the π-pulse, so that T_2 coherence time is prolonged [169]. This new sequence was named CPMG and further used for the nuclear magnetic resonance measurements (fig. 3.5, (b)). As the result, this method gives better sensitivity (fig. 3.5, (c), green line).

3.2.3. Nuclear magnetic resonance by NV center

The presented method of the detection of AC field can be applied for the Nuclear Magnetic Resonance (NMR) spectroscopy. The NV center in di-

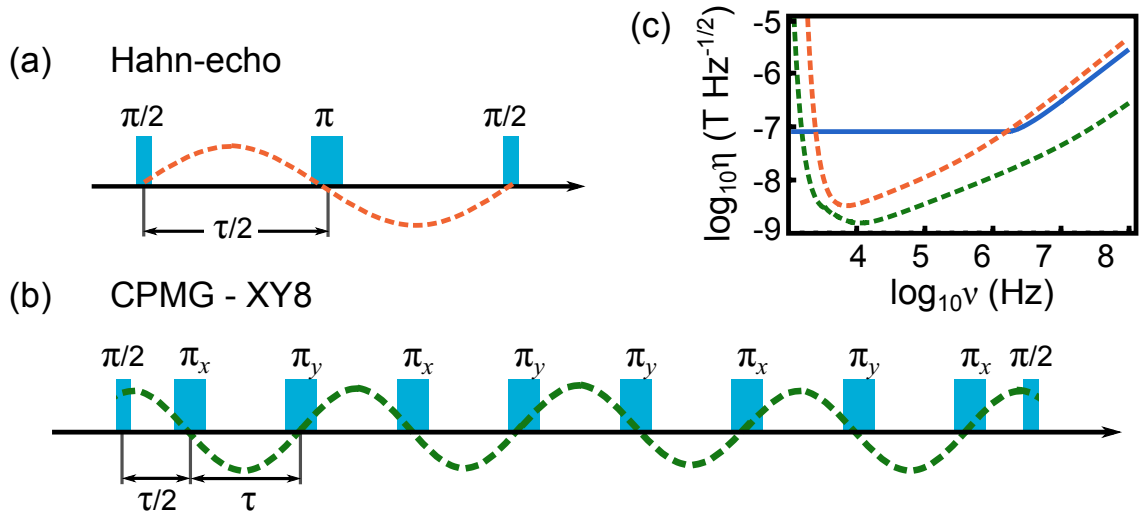

Figure 3.5.: (a) Hahn-echo sequence for the AC field measurements. (b) CPMG XY8 sequence for the AC field measurements. (c) The sensitivity to DC (solid line) AC (dot line) magnetic fields for a single NV center as function of signal frequency ν. Orange line - detection by Hahn-echo method. Green line - CPMG (XY8) sequence. [165]

amond interacts with atoms or molecules, which have non-zero nuclear spins and can be positioned close to the color center. This interaction can be determined by Hahn-echo or CPMG measurement, which were discussed before. The π-pulse in the T_2 time measurements refocuses the spin and reduces the dephasing, which comes from the fast oscillating external magnetic field. This elongates the T_2 time. But the period of the field fluctuation should be shorter than the waiting time $\tau/2$ between MW pulses (fig. 3.5). In case when fluctuations are slower, the dephasing produced by them would not be compensated. If the half of the period of the oscillating magnetic field is equal to the waiting time τ (fig. 3.5), the echo sequence is blind to it. In this case CPMG sequence can not decouple spin system from external field. Vice-versa, the phase is not canceled by refocusing pulses but accumulated, and it results in loss of coherence of the system. In the measurement we observe the drop down of T_2 time at the waiting time τ, which is equal to $1/2\nu$, where ν is frequency of magnetic field oscillations. In case of NMR measurements the Larmor frequency of spins is detected. Although, magnetic field produced by spin precession experiences random change of the amplitude and phase, the frequency by Larmor precession is preserved and can be detected by the described method. The increase of the number of π-pulses prolongs the coherence

time T_2 and decreases the waiting time τ [168, 169]. It makes the sensitivity higher and increase bandwidth of detectable frequencies. The sequence with additional π-pulses applied to NV center in diamond was suggested in Ref. [170, 171]. The detection of the hydrogen ^1H and carbon ^{13}C was demonstrated in Ref. [19, 20]. The sensitivity of NV center is limited by the radius of interaction between electron and nuclear spins. For example, a shallow implanted NV center, which is $\sim$ 5 nm under the surface, will interact with nuclear spins, which are localized on the diamond surface in the volume of $\sim$(5 nm)^3 [19].

4. Experimental setups

4.1. Optical measurements

4.1.1. Confocal microscopy

The basis of all optical measurements with NV centers in diamond is a confocal microscope. This technique was developed in 1955 [172] and patented in 1961 [3] by Marvin Minsky. The principal scheme of a confocal microscope is presented in figure 4.1. The pinhole installed before the detector cuts off all fluorescence, which is not originated from the focal point of the objective (fig. 4.1, red dashed line). The resolution of image in this case is defined by the excitation wavelength (λ) and the numerical aperture (NA) of the objective:

$$r_{lateral} = 0.61\frac{\lambda}{NA} \tag{4.1}$$

where $r_{lateral}$ is a radius of the focal spot in xy-dimension. In case of visualization of NV centers when wavelength of the excitation laser is equal to 532 nm and oil objective with high $NA = 1.35$ is used, the focus spot is $r_{lateral} = 240$ nm. In z-dimension the size of the spot (z_{axial}) is larger and effective detected area is defined by optical detection channel too, the approximate number can be estimated by formula

$$z_{axial} = 1.4\lambda\frac{n}{NA^2} \tag{4.2}$$

where n is the index of refraction of the material. In case of diamond and previous explanation of the setup, $z_{axial} = 980$ nm.

For the manipulation of the NV spin the pulses of the laser and the microwaves (MW) should be applied. To produce laser pulses an acousto-optical modulator is used (fig. 4.1, (2)). To apply MW pulses a wire is spanned close to the NV centers directly on the diamond surface. For better transmission of MW field a lithographic structure can be fabricated on top of diamond or on a glass substrate for nanodiamonds.

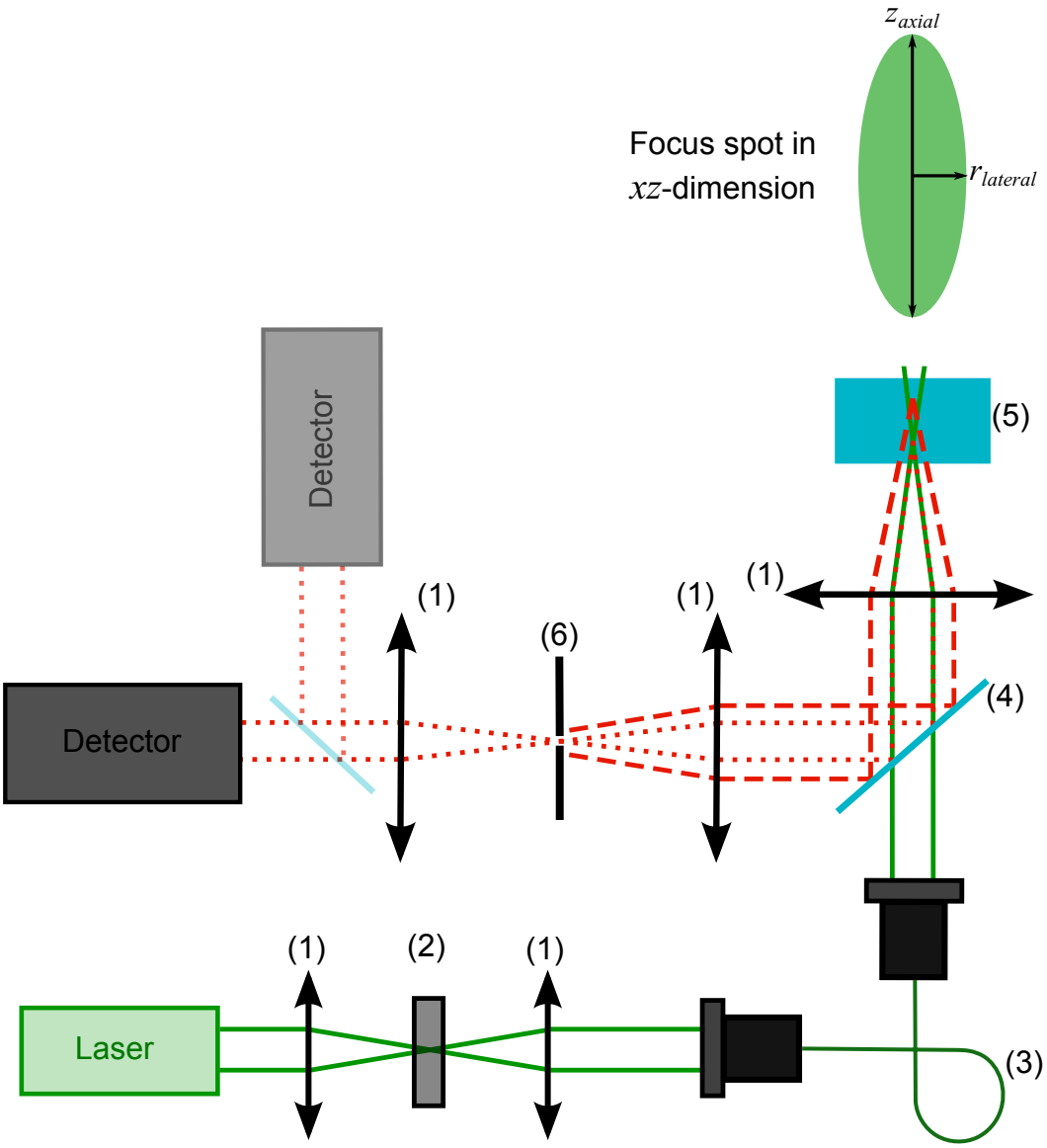

Figure 4.1.: Principle scheme of a confocal microscope, its (1) – focusing lenses, (2) – acousto-optical modulator (AOM), (3) – optical fiber, (4) – dichroic mirror, (5) – sample, (6) – pinhole.

4.1.2. Fluorescence correlation spectroscopy

Fluorescence correlation spectroscopy (FCS) [173–175] of a single emitter is a good method to analyze its dynamic parameters, as the excited state lifetime or the diffusion of fluorescent particles. A standard confocal microscope is the base of FCS measurements, only with modified detection channel (fig. 4.1).

The analysis of the stochastic events is realized in FCS measurements. If one event (for example, excitation) happens at the time $t = 0$, then what is the probability to find next event after time τ? To show this probability a correlation function should be constructed. For some period of time the data is collected and then the time between two events is analyzed. The photon correlation technique based on second-order correlation function was proposed in 1976 [176, 177]. The autocorrelation function of this data is given by

$$g^2(\tau) = \frac{\delta F(t) \cdot \delta F(t+\tau)}{\langle F(t) \rangle^2} \tag{4.3}$$

where $F(t)$ is a fluorescence signal and

$$\delta F(t) = F(t) - \langle F(t) \rangle, \tag{4.4}$$

$$\langle F(t) \rangle = \frac{1}{T} \int_0^T F(t) dt \tag{4.5}$$

FCS data can be used in different measurements, such as antibunching or detection of the diffusion of fluorescent particles in a solution. Each experiment requires some modification of the setup.

Antibunching measurements

The first application of the FCS technique found in antibunching measurements [178–182]. Avalanche photodiodes can not detect the difference between one, two or more simultaneous photons. It can give one electrical pulse, when the light is caught by the detector. Second photon can be detected only after some time (so called dead time), which is necessary for the detector to come into the initial state. The number of obtained pulses in time unit (per second) shows the intensity of the fluorescence. The maximum sensitivity is limited by the saturation of the detector. To distinguish the number of single photon emitters or the number of emitted photons from one light source a special technique can be used. For that

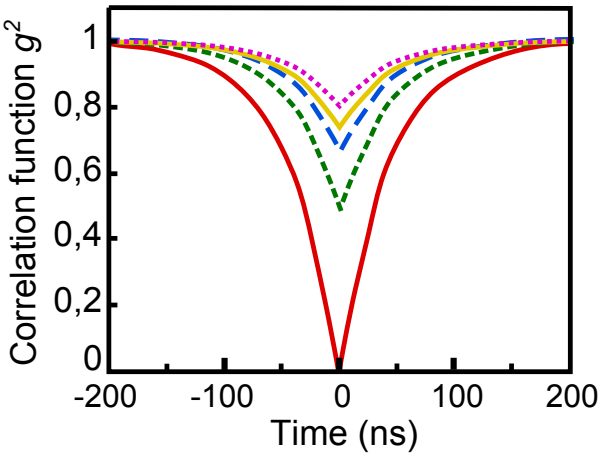

Figure 4.2.: The correlation functions for antibunching measurements for different numbers of emitters N. $N = 1$ - red, $N = 2$ - green, $N = 3$ - blue, $N = 4$ - yellow, $N = 5$ - pink.

the antibunching should be measured.

To measure the antibunching the fluorescence should be split into two channels by a beam splitter (fig. 4.1). It is also possible to increase the number of detected channels, if the potential number of simultaneous photons is more than two. However, if the question is whether the emitter gives one or more photons, the two channel setup is enough. The two photosignals give possibility to calculate the correlation function by formula 4.3. In this case we look at the time, when photons come at both detectors at the same time. For one single photon emitter only one detector can observe the light at the time moment $t = 0$. Second photon can reach any of the two detectors only after time, which is determined by the lifetime of the excited state of emitter. So at time $t = 0$, when one detector registers a photon, the second detector should show zero. For one single photon source the minimum $g^{(2)}(t = 0)$ is equal 0 (fig. 4.2, red line). In case of two simultaneous photons next situations can be realized. First, each photodiodes detect photons at the same time. Second, both photons come to the same detector. This means that at the time $t = 0$ second detector with equal probability can show "zero" or "non-zero" signal. The minimum $g^{(2)}(t = 0)$ for two possible simultaneous photons is equal 1/2 (fig. 4.2, green line).

The minimal value of the $g^{(2)}$-function dip at zero delay can be found by the formula:

$$g^2_{t=0} = \frac{N-1}{N}, \tag{4.6}$$

where N is the number of emitters. The maximum of $g^{(2)}(t = 0)$ is determined by the noise such as background fluorescence, dark counts of the photodiode. For high background level the number of the emitters can be hard to distinguish. This usually implies that single photon source can be confidently determined only if $g^{(2)}(t = 0)$ is in a range between 0 and 0.5.

Diffusion measurements

Such measurements requires one detector and constant periodic time pulses. In this case not the time between two emission processes is analyzed but the time how long a fluorescent particle stays in the focus and emits light. The decay of diffusion autocorrelation function is determined by the diffusion time

$$\tau_D = \frac{r^2_{lateral}}{4 \cdot D}, \tag{4.7}$$

where $r_{lateral}$ is the radius of the focal spot, which is coming from the Abbe limit (eq. 4.2), D is a diffusion coefficient, which can be found by

$$D = \frac{k \cdot T}{6\pi \cdot \eta_\nu \cdot R_h}, \tag{4.8}$$

where k is the Boltzmann constant, T is the temperature, η_ν is the viscosity of the solution, and R_h is the hydrodynamic radius of the diffusing particles. The hydrodynamic radius can be found from the equations 4.7 and 4.8 as

$$R_h = \frac{2\tau_D \cdot k \cdot T}{3\pi \cdot \eta_\nu \cdot r^2_{lateral}}. \tag{4.9}$$

The hydrodynamic radius is not the real size of fluorescent particle, it is includes the interaction between the particle and the solution. In case of particles with different sizes, the sum of several exponential function can be observed. Each function corresponds to each type of particles. Depending on the investigated system it is also possible to do two-, three- [183], or higher-order [184] photon correlations.

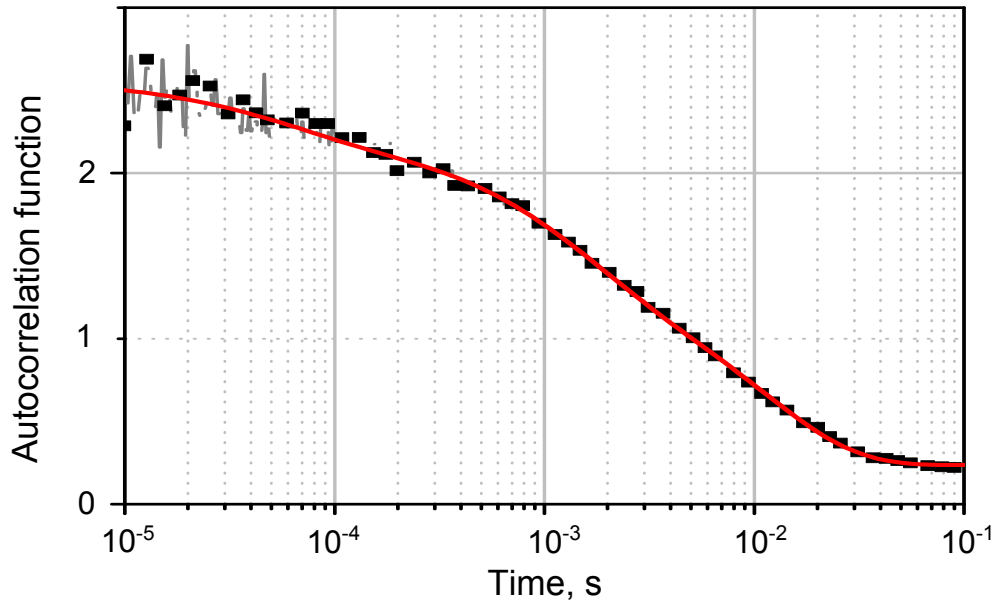

Figure 4.3.: The autocorrelation function in case of diffusion measurements.

4.2. Size and structure measurement

In 1986 the Nobel prize was shared between Ernst Ruska "for his fundamental work in electron optics, and for the design of the first electron microscope" and Gerd Binnig together with Heinrich Rohrer "for their design of the scanning tunneling microscope" [185, 186]. These two methods are an important way of structural investigation of objects until nowadays.

4.2.1. Atomic-force microscopy

The scanning tunneling microscope led to design of the atomic force microscope (AFM), which was presented in 1986 [187]. In this method to scan the sample surface a special AFM tip is used. It has a sharp needle at the end of a cantilever. An infrared laser is pointed at the AFM cantilever and goes to the detector after reflection from the cantilever. This detector consists of four parts and reacts on every movement of the AFM cantilever (fig. 4.4, (a)). The resolution of AFM depends on the tip sharpness and the stability of the setup and can reach $\mathring{A}$ level in the vertical direction [188].

The AFM can be operated in several modes: contact, tapping, non-contact, tuning fork and force [189]. All this modes are related to the

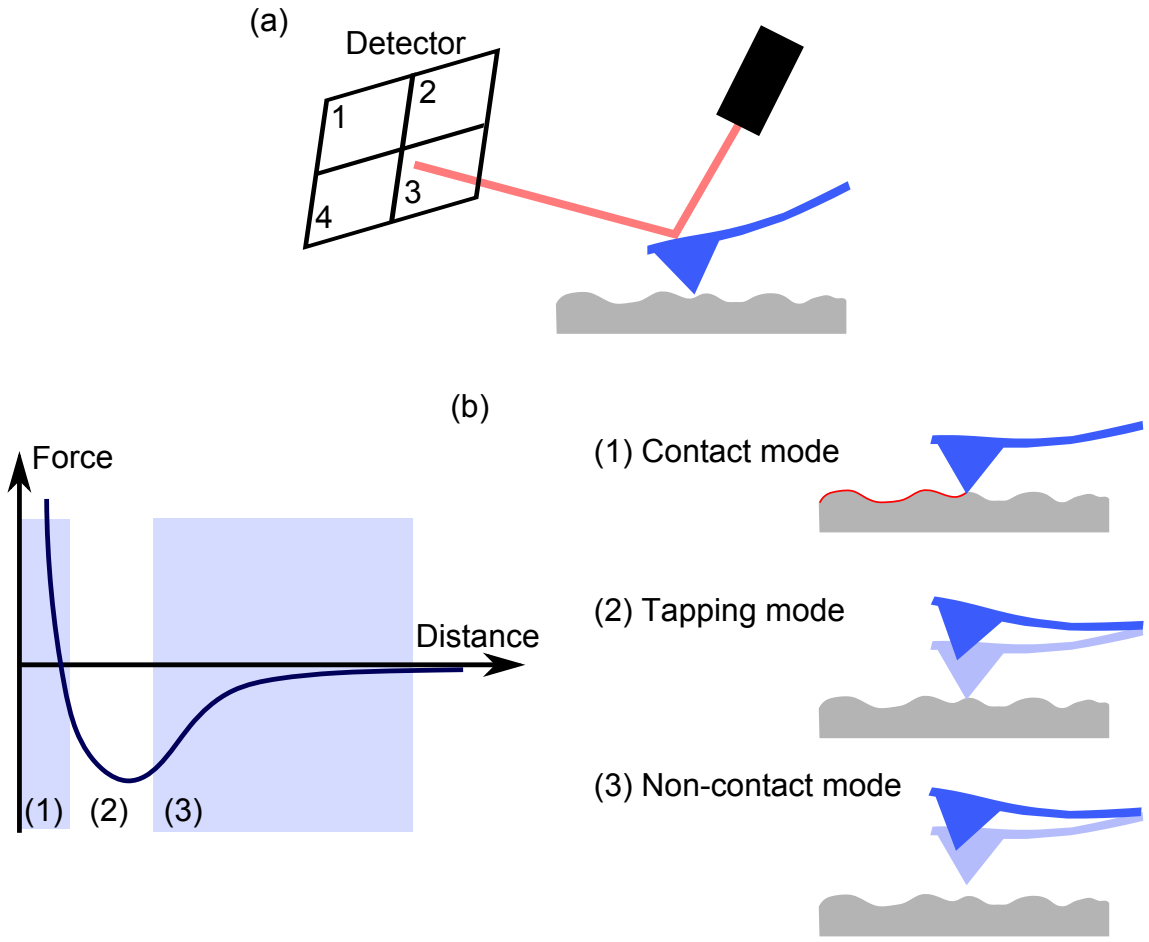

Figure 4.4.: (a) Principle scheme of the detection of the movement of the probe during the AFM scan. (b) Three modes of AFM scan and the interaction between the probe and the investigated sample for these modes.

interaction between AFM tip and sample surface (fig. 4.4, (b)). In a contact mode the AFM tip stays in a constant contact with the sample surface. In tapping and non-contact modes the tip is oscillating above the investigated surface. Depending on the amplitude of such oscillations the AFM tip will or will not touch the surface. The frequency and the amplitude of the AFM tip oscillation is related to the geometry and the material of the tip. It can be described as an usual mechanical oscillator, which has some length and mass. In a non-contact mode the typical work distance between the end of the tip and the sample surface is around $50 - 150$ $\mathring{A}$ [190].

AFM tip can be modified with different molecules. In this case the tip oscillations can be transfered to the interaction force between such molecules and surface, which also can be functionalized. Some nanoparticles also can be attached to the AFM tip. It makes possible to investigate how they interact with the sample.

4.2.2. Electron microscopy

In the beginning of 1930s Ernst Ruska and Max Knoll presented the prototype of an electron microscope [191, 192]. In this case the investigation of the sample is done by the scattering of the electron beam, from which the structure of the sample is reconstructed. There are two main types of electron microscopes. In both of them focused electron beam interacts with the investigated sample. Then transmitted (TEM) or scattered (SEM) electrons are detected [193, 194]. The resolution of the electron microscope depends on the electron energy and focusing system, which is not trivial for electron beam, and can achieve 0.5 $\mathring{A}$ [195]. Electron microscopy can give images with very high resolution up to single atoms for a crystal structure. However, it constrains strict rules onto the sample, which can be studied by this method. For example, for SEM the investigated object should be electrically connected to the holder. All measurements have to be implemented in the vacuum and at low temperatures. It is not applicable for living biological samples.

5. Optical markers based on nanodiamonds

5.1. Introduction

One of the possible application of nanodiamonds is to use them as optical markers, as it was discussed in chapter 3.1. Biomarkers should be biocompatible [196], non-toxic [111, 137] and also hydrophilic [196] to be placed inside the living systems without negative consequences. Also they should have stable properties in all environments. It is easy to show the significance of stable properties of nanoparticles for *in vivo* applications in case of a pill, which we take. In the beginning a tablet goes to the stomach, where pH level can go down to about 1 [197]. But after absorption the drug goes into the blood, which has pH level around 7.5 [197]. It means that at least in this pH range, the biomarkers should have the same hydrodynamic properties. The nanodiamonds penetrate into cells by endocytosis (see appendix A.1). If they aggregate inside cells, it might impede to push big clusters of nanoparticles out [196]. The aggregation of nanoparticals should be prevented for *in vivo* applications. For optical markers the fluorescent stability is extremely important. The stability of NV center inside nanodiamond is strongly related to its charge and the surface functionalization (see chapters 2.2.6, 2.4.3). Thus nanodiamonds for biological applications should be hydrophilic, have stable hydrodynamic and optical properties in different buffers, and do not form clusters.

Oxidized by acid treatment nanodiamonds are negatively charged and hydrophilic, but they have different hydrodynamical properties in different pH buffers [198]. The reason of this might be based on the fact that the nanodiamonds' surface can adsorb different charged molecules from the solvent. It can change the interaction between diamond nanocrystals and liquid. Also it would change the charge of the nanodiamonds' surface, and as result it might affect the charge of NV centers. The protection of the nanodiamonds' surface from the adsorption from the environment is necessary for the stabilization of their properties.

The stabilization of nanodiamonds in different solvents is an important

problem, that should be solved to use nanodiamonds inside living systems. One of the possible ways is to use polymer coating of nanocrystals, as it was demonstrated for quantum dots [199] or gold nanoparticles [200]. Here we present the stabilization of nanodiamonds by the protein coating. This system can be potentially used for drug delivery to tumor tissues. All presented chemical experiments were done in the collaboration with the group of Prof. Tanja Weil (Institute of Organic Chemistry III, University of Ulm).

The fluorescence of nanodiamonds depends on the color center. For *in vivo* applications it is more appropriate to use particles with more red shifted fluorescence where transparency of living tissues is higher. In case of diamond nanocrystals it might be SiV center. However, NV center has good magnetic properties and can be used as magnetic field detector. Thus it would be useful to combine both of this centers in one nanocrystal. The fabrication of such nanodiamonds is presented in the section 5.5.

5.2. Functionalization of nanodiamonds

In our experiments we decided to use Human serum albumin (HSA) protein for coating of nanodiamonds. This is a good protein for *in vivo* experiments, since it is monomeric and soluble in water. It is produced by the liver. The human blood plasma on 50 % consists of HSA protein [201]. The total surface of HSA is very large, and therefore it can be used for transport of non water-soluble particles in blood [202, 203]. The proteins' attachment to the nanodiamonds' surface was done by electrostatic interaction. For that the proteins were modified to become positively charged (fig. 5.1). Nanodiamonds were treated in the three acid mixture 2.4.3, which results in negatively charged surface of the crystals..

5.2.1. Protein modification

In the beginning HSA proteins were marked by Rhodamine molecules to visualized them (fig. 5.1, step 1). During that reaction each protein had only one dye molecule. After that 1-Ethyl-3-(3-dimethylaminopropyl)carbodiimide (EDC) coupling and denaturalization by urea (fig. 5.1, step 2 and 3) were used to unfold the proteins and stabilize them for the attachment of polyethylene glycol (PEG) chains [204]. It is possible to control the length of PEG chains and as a result the number of functional groups at the chosen places [205]. In the end of such modification HSA proteins became positively charged biopolymers, which

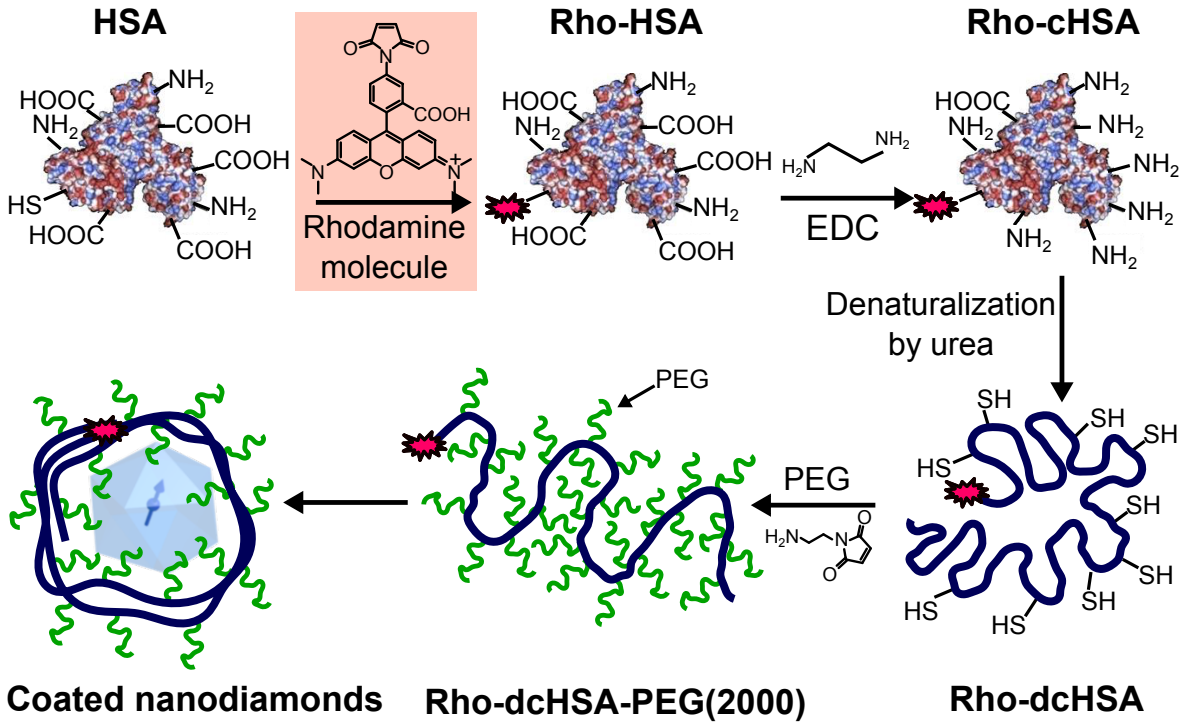

Figure 5.1.: The schema of the modification of HSA protein for further coating of nanodiamonds. First step is attaching of Rhodamine molecule to the protein. After that the latter is modified as it is depicted to have positively charged linear protein. At the last step proteins are electrostatically attached to acid treated nanodiamonds.

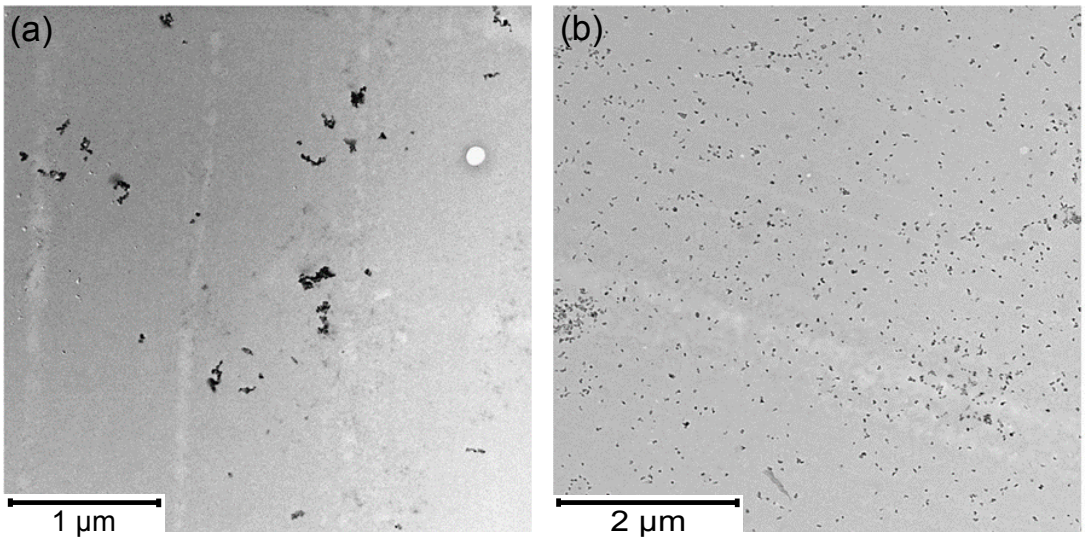

Figure 5.2.: The images of uncoated (a) and coated (b) nanodiamonds obtained by transmission electron microscope.

we called dcHSA-PEG.

Nanodiamonds with average size 50 nm were cleaned in the three acid mixture and had negatively charged surface 2.4.3. Thus the produced biopolymer can be attached to diamonds' surface by electrostatic interaction. Depends on the nanocrystals' size one particle can be coated in few proteins. The nanodiamonds' surface was completely protected by HSA proteins. Coated nanocrystals also have the PEG chains at the outer sheath. This makes new complex particles positively charged, and this might prevent the aggregation of nanodiamonds.

Before and after coating nanodiamonds were measured at the transmission electron microscope (TEM) (fig. 5.2). This data shows that after coating nanocrystals are more isolated one from another than before. However, to have more certain information about the properties of HSA coated nanodiamonds it is better to use independent verification method such as FCS measurements (chapter 4.1.2). It makes possible to study the hydrodynamic properties and aggregation inside the solution of coated nanocrystals.

5.3. Colocalization of nanodiamonds and protein

5.3.1. pH stability

Nonfluorescent nanodiamonds were chosen for the first experiments to test stability of the protein coating at different pH levels in range from 2 to 8. Proteins were marked with Rhodamine molecules (HSA-Rho, fig. 5.1) for visualization. It was done to show the attachment of proteins to nanodiamonds by the diffusion properties of small and big particles. For small particles such as free proteins the diffusion time should be shorter. If proteins are attached to the nanodiamonds, the fluctuating particles become bigger and corresponding diffusion time should be longer. To determine the diffusion times the autocorrelation function of fluctuated particles were measured by fluorescence correlation spectroscopy (FCS). The FCS method was explained in the chapter 4.1.2.

In the beginning we measured the diffusion time of free proteins marked with Rhodamine in the buffer with pH level 5. The autocorrelation data was fitted by single exponential function (fig. 5.3, grey line). The diffusion time of free protein (τ_{Rho}) is equal to $(4.0 \pm 0.2) \times 10^{-4}$ s.

Coated nanodiamonds were prepared in four different buffers: pH 2, pH 4, pH 6, and pH 8. The autocorrelation functions of coated diamond nanocrystals are presented in the fig. 5.3. Obtained data can be well fitted by the sum of two exponential functions (solid lines, fig. 5.3). One component is related to the diffusion time of free protein with Rhodamine (τ_{Rho}) and the second exponent corresponds to the movement of coated nanodiamonds (τ_{ND}). Nanodiamonds inside the solutions have distribution in their sizes, meaning that they would have different diffusion times. It is also possible to fit data with a sum of multiple exponential functions, where slightly better fitting can be found. However, the diffusion times, which are not related to free Rhodamine, are very close to each other. Thus we can fit all nanodiamonds with one average diffusion time. The diffusion times obtained from the fitting can be found in the table 5.1.

The diffusion times related to free protein with attached Rhodamine molecules are in good agreement with control measurement (fig. 5.3, grey data). Diffusion times corresponding to coated nanodaimons diffusion times are very close to each other and values are in the order of few milliseconds (tab. 5.1).

The obtained diffusion times might be used for the calculation of the diffusion coefficients and the hydrodynamic radii. For this the formula 4.8

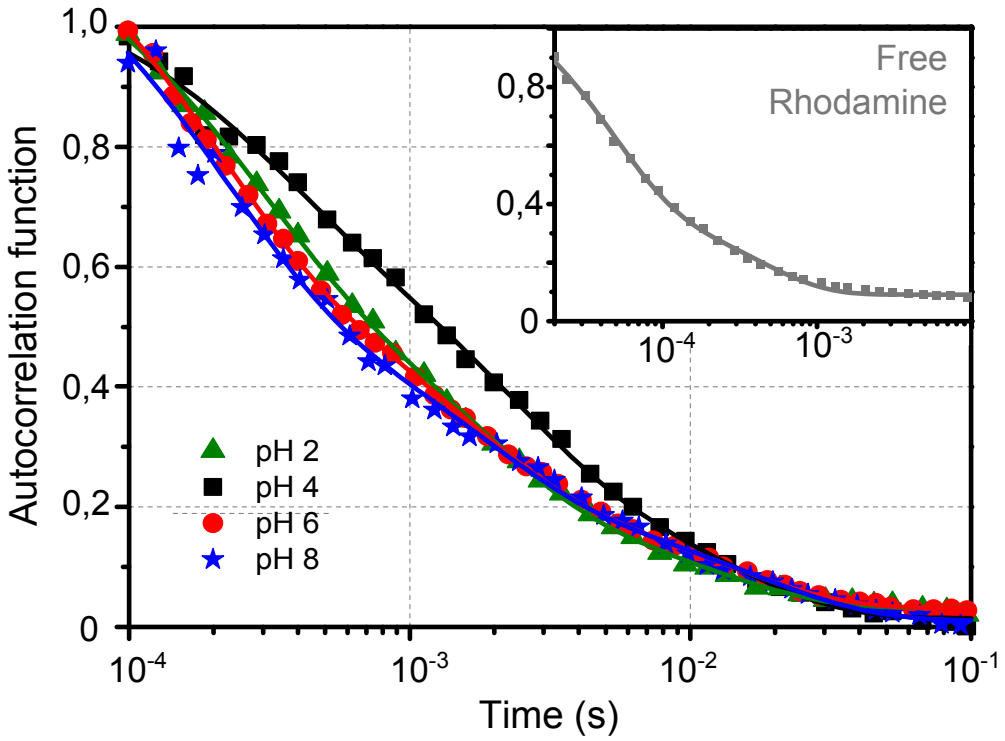

Figure 5.3.: The autocorrelation functions of fluorescent particles. The inset - grey data - the diffusion of free HSA proteins marked with Rhodamine molecules. Solid grey line - the fit to the data by single exponential function. The colorful data - the autocorrelation functions of coated non-fluorescent nanodiamonds in the buffers with different pH levels. The solid curves are the sum of two exponential functions, one of which is related to free proteins, and another presents coated nanodiamonds.

Table 5.1.: Diffusion times of free proteins marked with Rhodamine molecules and coated nanodiamonds in buffers with pH levels 2, 4, 6, and 8.

	τ_{Rho}, s	$\Delta\tau_{Rho}$	τ_{ND}, s	$\Delta\tau_{ND}$
pH 2	$3.9 \cdot 10^{-4}$	$0.1 \cdot 10^{-4}$	$4.5 \cdot 10^{-3}$	$0.1 \cdot 10^{-3}$
pH 4	$6.0 \cdot 10^{-4}$	$0.2 \cdot 10^{-4}$	$6.5 \cdot 10^{-3}$	$0.2 \cdot 10^{-3}$
pH 6	$3.2 \cdot 10^{-4}$	$0.1 \cdot 10^{-4}$	$5.2 \cdot 10^{-3}$	$0.1 \cdot 10^{-3}$
pH 8	$3.3 \cdot 10^{-4}$	$0.1 \cdot 10^{-4}$	$6.6 \cdot 10^{-3}$	$0.3 \cdot 10^{-3}$

Table 5.2.: Hydrodynamic properties of coated nanodiamonds in the buffers with pH levels 2, 4, 6, and 8.

	τ_{ND}, s	D_{ND}, m^2/s	R^h_{ND}, m
pH 2	$4.5 \cdot 10^{-3}$	$1.06 \cdot 10^{-12}$	$56.7 \cdot 10^{-9}$
pH 4	$6.5 \cdot 10^{-3}$	$1.52 \cdot 10^{-12}$	$81.3 \cdot 10^{-9}$
pH 6	$5.2 \cdot 10^{-3}$	$1.21 \cdot 10^{-12}$	$64.7 \cdot 10^{-9}$
pH 8	$6.6 \cdot 10^{-3}$	$1.54 \cdot 10^{-12}$	$82.1 \cdot 10^{-9}$

and 4.9 can be used, respectively. The calculations were done for the viscosity of water at room temperature. The diffusion coefficients and the hydrodynamic radii of coated nanodiamonds are presented in the table 5.2.

The hydrodynamic radii of coated nanodiamonds in all buffers are very similar. It means that coated nanodiamonds do not adsorb any molecules from the environment. In case of nanodiamonds' aggregation the autocorrelation curves have to give diffusion times, which are multiple by a factor of two or more greater compared to single nanoparticle. It would be visible as some "steps" at the autocorrelation functions. In presented data such "steps" are missing. The fit shows that observed size of nanoparticles are similar for all tested solutions. It proves that coated nanodiamonds do not suffer of aggregation inside the measured buffers.

5.3.2. Cell stability

In case of biological applications nanodiamonds' coating should be stable in real living system. The colocalization of nanodiamonds with HSA proteins was tested in two systems. First test *in vitro* was performed on a glass substrate. Second *in vivo* was realized in living HeLa cells. To verify

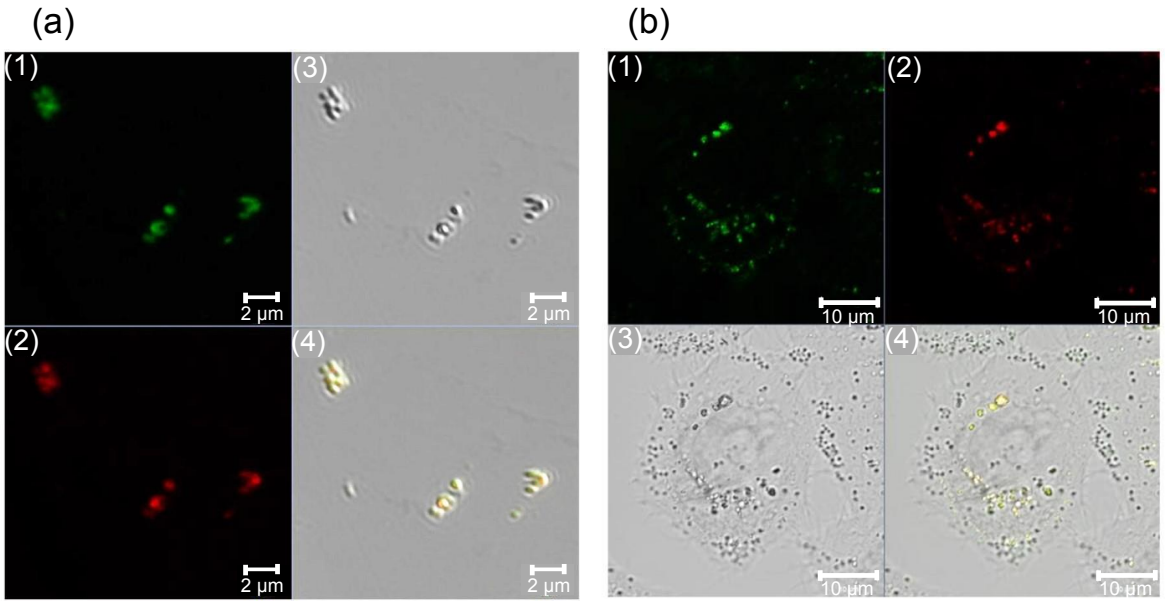

Figure 5.4.: The colocalization of fluorescent nanodiamonds and marked proteins at the glass substrate (a) and inside the HeLa cells (b). Channels: (1) - Rhodamine fluorescence, (2) - NV center fluorescence, (3) - differential interference contrast microscopy, (4) - sum of channels from 1 to 3.

the colocalization fluorescent nanodimonds with NV centers were coated with HSA protein. Proteins were marked with Rhodamine molecules as it was shown in figure 5.1. In this case it is possible to collect the fluorescence from nanodiamonds and from proteins separately. The colocalization measurements were carried out on a commercial confocal microscope (Zeiss LSM 710). Rhodamine molecules were excited by laser light with wavelength 514 nm, and the excitation of NV center was done by laser at 561 nm. To collect the emissions from fluorescent particles bandpass filters were used: $525 - 550$ nm for Rhodamine and $685 - 720$ nm for NV centers accordingly.

Firstly the colocalization of nanodiamonds and proteins was examined on glass slide on which crystals covered by biopolymer were spin-cast (fig. 5.4, (a)). Data shows that fluorescence in both detection channels corresponding to the NV and Rhodamine originates from the same points (fig. 5.4, (a) (1, 2, 4)) which proves the protein is attached to nanodiamonds.

The second step was the colocalization measurements inside the living HeLa cells [206]. HeLa cells were incubated with coated fluorescent nanodi-

amonds in physiological buffer for 12 *hours*. Coated diamond nanocrystals were uptaken by cells (appendix A.1) and transported to the cytoplasm region (fig. 5.4, (b)). The emission from NV centers is presented in figure 5.4, (b), (2). For each nanodiamond we can compare the fluorescence from Rhodamine molecules, which are shown at figure 5.4, (b), (1). Even after 24 hours of incubation, fluorescence collected from each point of the sample by both detection channels confirmed that proteins remain bound to nanodimonds inside the cells. This result implies that the non-covalent electrostatic interaction between modified HSA proteins and acid treated nanodiamonds is very strong so that the complex does not dissociate during the time it is inside the cell.

5.4. Drug delivery by nanodiamonds

Drug delivery is one of the important problems in medicine. It might be necessary to bring the drug to some specific organs and not to all other parts of organism. It is specially important for chemotherapy, as the toxic medicines attack all tissues. To minimized the negative effect from cancer drug to healthy tissues it is necessary to deliver medicaments only to tumors. There are many protein systems, which can be used for drug delivery [148–151].The release of drug is triggered by pH level or temperature, for example [154, 155]. For visualization of the process of drug delivery absorption the optical markers can be useful. Nanodiamonds due to their properties are promising for this purpose.

5.4.1. Doxorubicin

Doxorubicin (DOX) (fig. 5.5) is a drug used for cancer chemotherapy [207, 208], and as all drugs for such application, it has negative side effects. Especially Doxorubicin affects strongly the heart and blood systems [209]. One of the important questions, which needs to be solved, the drug is delivered only to the tumor tissue and does not influence healthy tissues.

Doxorubicin itself has a fluorescence [210]. This is very convenient for the preliminary experiments on drug delivery, because it is possible to trace nanodiamonds and drug molecules together.

5.4.2. Nanodiamonds with Doxorubicin

HSA proteins were modified by the same way as it is shown in figure 5.1 (steps 2 - 4). Doxorubicin molecules were conjugated onto biopoly-

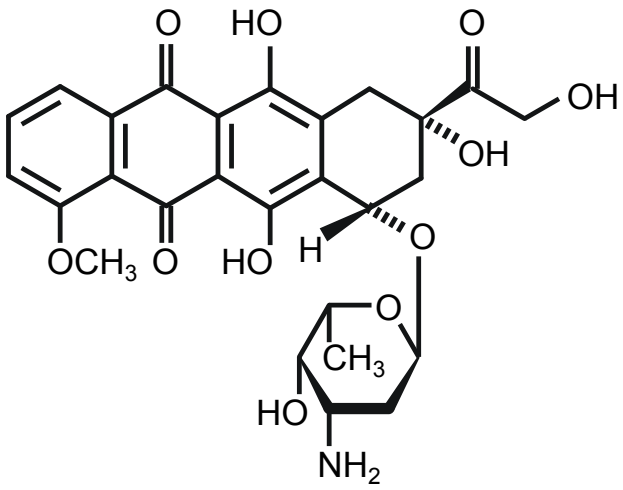

Figure 5.5.: The Doxorubicin molecule [207].

mer dcHSA-PEG [9, 211]. It was done by using the Doxorubucin prodrug N-ε-maleimidocaproic acid hydrazide-DOX. The drug is attached to the protein by pH sensitive bond, which is shown at figure 5.6. The Doxorubicin molecules release at pH level 5.5 or lower. Then HSA proteins with attached Doxorubicin molecules were coated to nanodiamonds by electrostatic interaction.

The measurements of Doxorubicin release were carried out in two systems. First test had to prove that release occurs at specific level of pH and was performed in buffers with different acidity level. Second test was done inside HeLa cells, to observe pharmaceutical effect.

5.4.3. Buffer measurements

The release of Doxorubicin molecules was firstly measured in different buffers with pH level 5 and 7. The release in buffer was analyzed by FCS method explained in the chapter 4.1.2. For measurements in buffer we took non-fluorescent nanodiamonds. This choice was dictated by the fact, that fluorescence of the drug is much weaker compared to NV center. Moreover, their fluorescence lies in the same spectral region and cannot be separated by optical filters. Absorption band of the Doxorubicin is reminiscent to NV center, therefore drug is excited by the same green laser used for NV centers.

The autocorrelation function of free drug in the buffer with pH level 5 is depicted in figure 5.7 (green line). Fit to the data reveals the diffusion time of free drug to be $\tau_{DOX} = 1.58 \cdot 10^{-3}$ s. It shows the diffusion

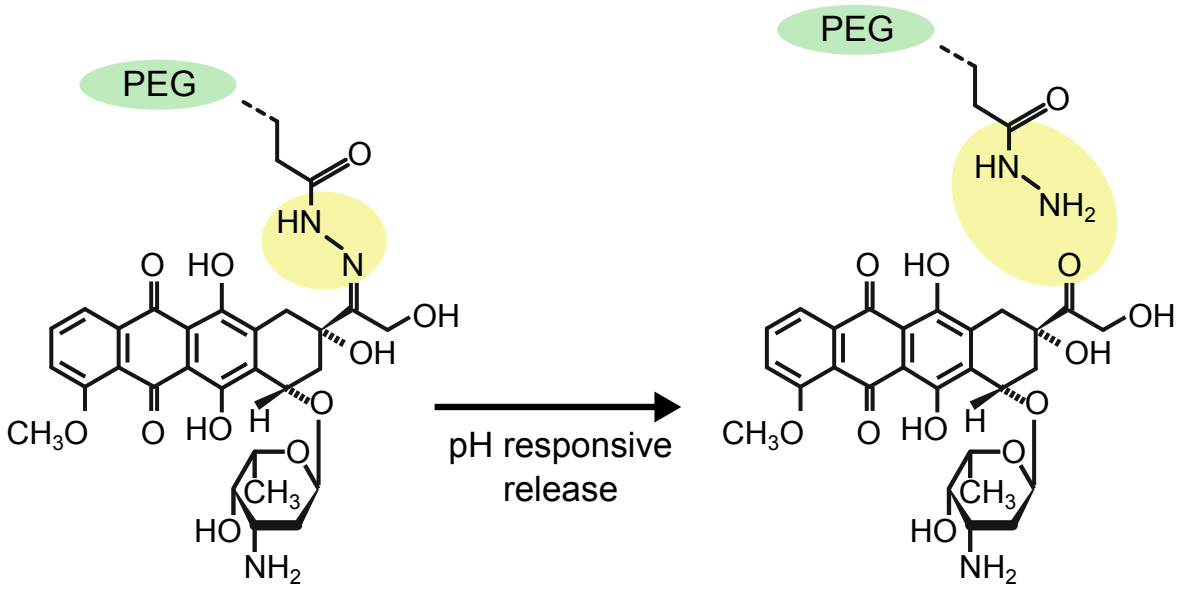

Figure 5.6.: The pH sensitive bond used to attach Doxorubicin molecule to the HSA protein. The release of the drug should be at pH level low than 5.5.

Table 5.3.: Diffusion times and hydrodynamic properties of free Doxorubicin molecules at pH level 5 and drug attached to nanodiamonds at pH level 7.

sample	τ, s	$\Delta\tau$	D, m^2/s	R^h, m
DOX pH5	$1.58 \cdot 10^{-3}$	$0.5 \cdot 10^{-4}$	$9.5 \cdot 10^{-12}$	$22.6 \cdot 10^{-9}$
NDs-DOX pH 7	$12.9 \cdot 10^{-3}$	$3.4 \cdot 10^{-3}$	$1.2 \cdot 10^{-12}$	$178 \cdot 10^{-9}$

properties of free drug, which should be expected when drug is released from nanodiamonds. Then non-fluorescent nanodiamonds in HSA protein shell with attached Doxorubicin molecules (ND-DOX) were measured at the pH level 7 (fig. 5.7, blue line). In this case the diffusion time extracted from the fit is $\tau_{ND-DOX} = 12.9 \cdot 10^{-3}$ s. Diffusion time for free drug is 10 times shorter than the time for drug attached to nanodiamonds. Diffusion parameters of free Doxorubicin molecules at pH 5 and of nanodiamonds with attached drug at pH 7 are listed in the table 5.3.

Strongly diluted hydrochloric acid (HCl) was added to the solution of nanodiamonds with Doxorubicin at the pH level of 7, thus reducing it to the pH of 5. Immediately repeated FCS measurements gave the same

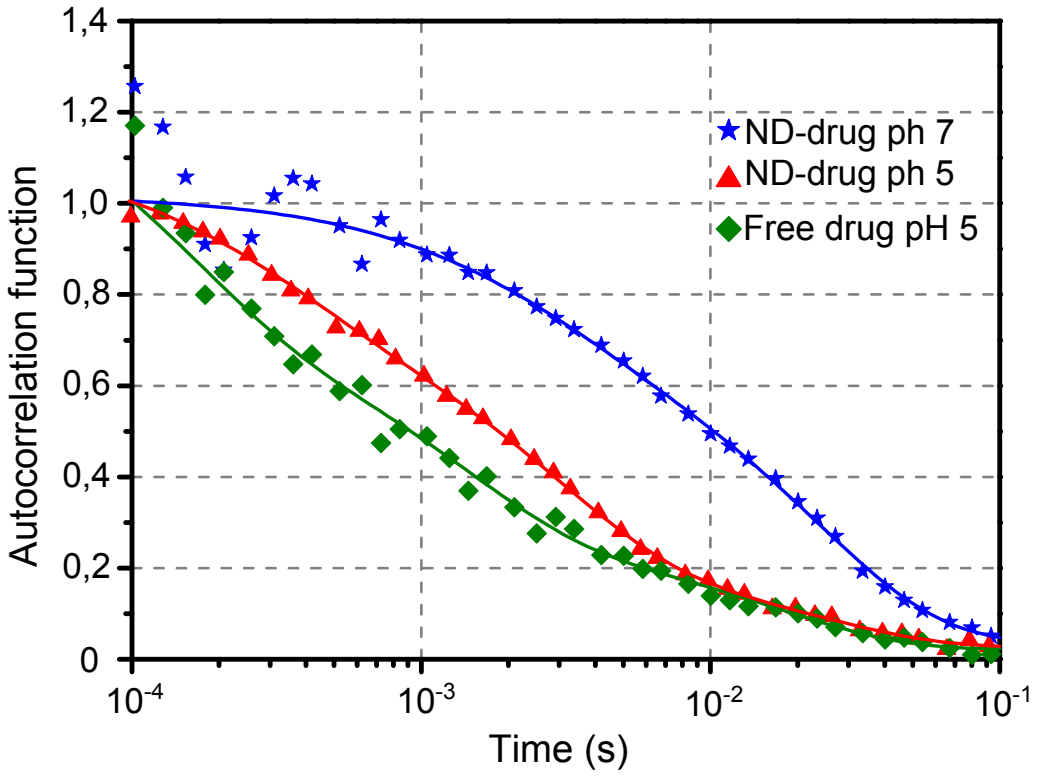

Figure 5.7.: The autocorrelation functions of free Doxorubicin molecules in the buffer with pH level 5 (green data), of Doxorubicin attached to HSA coated nanodiamonds at pH level 7 (blue data), and of Doxorubicin at nanodiamonds after 24 h at pH level 5 (red data). The changes between curves for nanodiamonds with attached drug at pH level 7 and 5 show the release of Doxorubicin molecules from nanodiamonds.

Table 5.4.: Concentration of released Doxorubicin molecules and of attached drug molecules to the nanodiamonds at the pH level 5 after 24 h.

Sample	τ, s	Coefficient	Error Coefficient	Concentration, %
NDs-DOX	$12.9 \cdot 10^{-3}$	0.29	0.01	30
free DOX	$1.58 \cdot 10^{-3}$	0.66	0.02	70

autocorrelation function, as for pH 7. However, 24 hours later the autocorrelation function changed to the curve, which is presented by red line in figure 5.7. This reduction of the diffusion time indicates the release of Doxorubicin molecules from the nanodiamonds.

It is reasonable to fit the autocorrelation function of released Doxorubicin molecules from nanodiamonds at pH level 5 (fig. 5.7, red data) by the sum of two exponential functions:

$$g^2(t) = C_{DOX} \cdot e^{-\frac{t}{\tau_{DOX}}} + C_{ND-DOX} \cdot e^{-\frac{t}{\tau_{ND-DOX}}}. \tag{5.1}$$

One term is related to the released drug molecules, and the other one corresponds to diffusion of Doxorubicin attached to nanodiamonds. In formula 5.1 the coefficients C_{DOX} and C_{ND-DOX} define the ratio between concentrations of small and big fluctuating particles [174, 175]. To find more precisely the coefficients C_{DOX} and C_{ND-DOX} diffusion times τ_{DOX} and τ_{ND-DOX} should be known. For this fit we can take diffusion times from the table 5.3. Obtained from the fit coefficients are listed in the table 5.4.

From the numbers presented in the table 5.4, it is possible to conclude that after 24 hours in buffer with pH level 5 approximately 70 % of Doxorubicin molecules are released from nanodiamonds coated with HSA proteins.

5.4.4. Cell measurements

The next part of drug delivery measurements was aimed at release of Doxorubicin molecules from the coated nanodiamonds inside HeLa cells [206]. This time we took fluorescent nanodiamonds, to be able to track drug molecules and nanodiamonds simultaneously. Monitoring of the movement of fluorescent particles inside the cells were done on home built confocal microscope. Three different samples were prepared. HeLa cells were incubated for 24 hours: i) with free Doxorubicin molecules (fig. 5.8, (a-b)),

ii) with coated fluorescent nanodiamonds but without drug (fig. 5.8, (c-d)), and iii) with Doxorubicin molecules attached to coated nanodiamonds (fig. 5.8, (e-f)). The particles penetrate into the cells by endocytosis (explained in appendix A.1).

Confocal images of HeLa cells incubated with free Doxorubicin molecules are presented in figure 5.8, (a, b). Cells were scanned in two dimensions: XY-plane (fig. 5.8, (a)) and XZ-plane (fig. 5.8, (b)). The cell's cytoplasm and nucleus show strong homogeneous fluorescence. This luminescence can be caused only by Doxorubicin molecules, which easily penetrate into cell nucleus [208].

The fluorescence of nanodiamonds without drug is visible inside the cell (figure 5.8, (c)). The fluorescence is not homogeneous as for DOX molecules and is concentrated in several spots. However, these spots visualize shape of the cell very obscurely and it is not possible to understand in which parts of the cell the nanodiamonds are localized. To visualized cells and nucleus a membrane dye was added to HeLa cells (fig. 5.8, (d)). Combining these two pictures (c) and (d), we find that nanodiamonds stay only inside the cytoplasm and don't penetrate into the nucleus of HeLa cells.

In the third sample we added coated nanodiamonds with attached Doxorubicin molecules to HeLa cells. Confocal pictures (fig. 5.8, (e, f) were obtained after 24 hours of incubation incubation time. In the cytoplasm of the HeLa cell we detected many bright spots, as it was in the case of free nanodiamonds (fig. 5.8, (c)). The cytoplasm also shows the dim homogeneous luminescence. The nucleus of the cells exhibits brighter fluorescence compared to the cytoplasm (fig. 5.8, (f)). Because only Doxorubicin molecules can penetrate into the nucleus, it reasonably suggests that detected light originates from the drug.

To understand unambiguously the nature of the obtained fluorescence, spectra were measured. The typical spectrum of one of the bright spot is presented in figure 5.9, (a) - black line (1). After 5 minutes of strong laser illumination the obtained spectrum had changed (fig. 5.9, (a) – red line (2)). It might be related to the bleaching of Doxorubicin. After bleaching, spectrum becomes quite reminiscent to NV's one with typical characteristic peaks. To prove that changes between black and red lines in figure 5.9, (a) corresponds to the bleaching of drug molecules, we can compare the difference between this spectrum and spectrum of Doxorubicin from cell nucleus. The spectrum of the free drug obtained from cell nucleus is presented in figure 5.9, (b) – black line (3). The calculated difference between spectra before and after laser bleaching is shown in figure 5.9, (b) - red line (4). The two spectra are in good agreement.

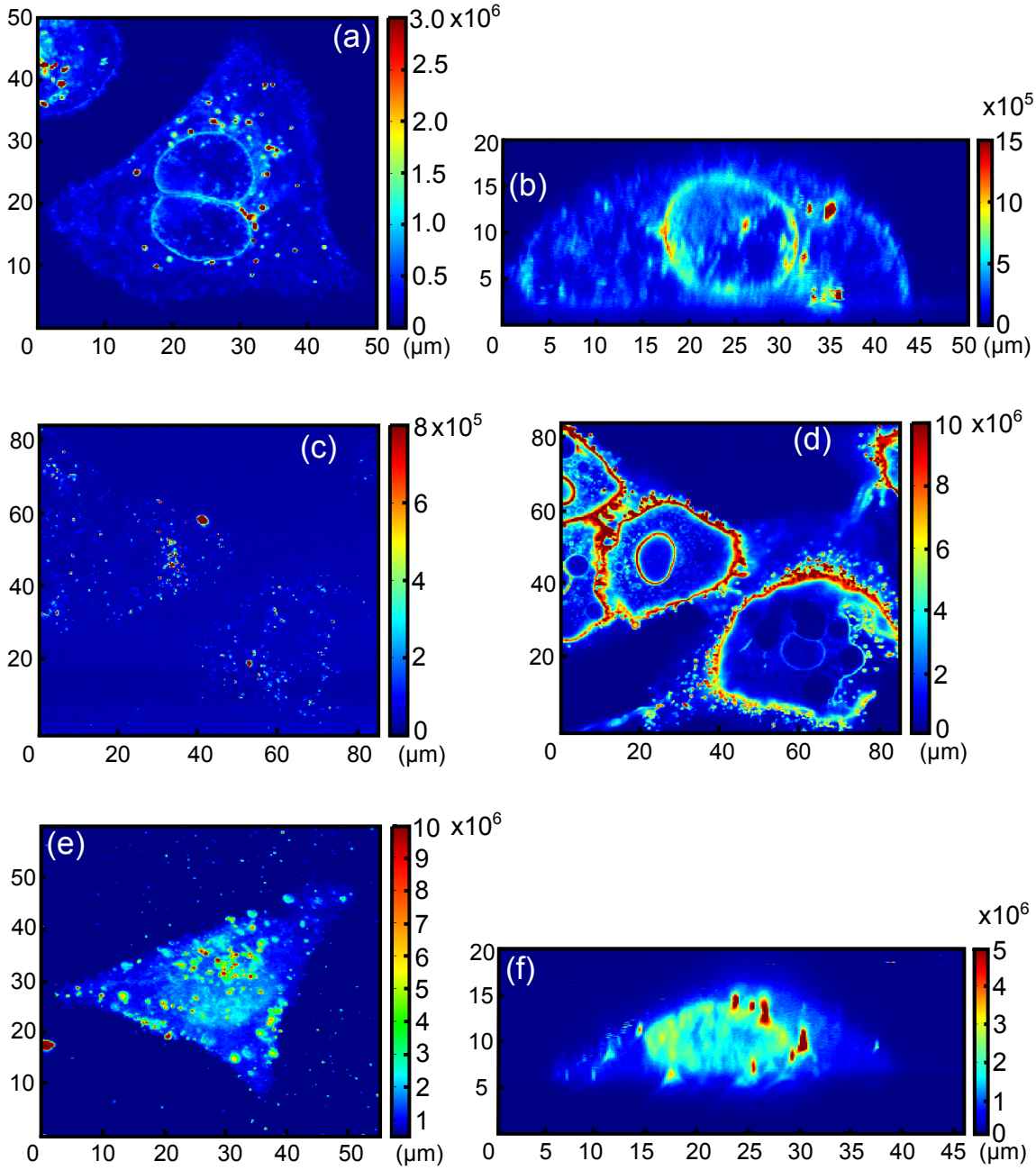

Figure 5.8.: Confocal images of HeLa cells after 24 hours of incubation time. The color-coded scale bar is in photocounts per seconds. Free Doxorubicin molecules inside the cells: (a) - XY-plane, (b) - XZ-plane. Free coated nanodiamonds without drug inside the cells: (c) - XY-plane, (d) - XY-plane with added membrane dye to visualize cells. Coated nanodiamonds with attached Doxorubicin molecules inside the cells: (e) - XY-plane, (f) - XZ-plane.

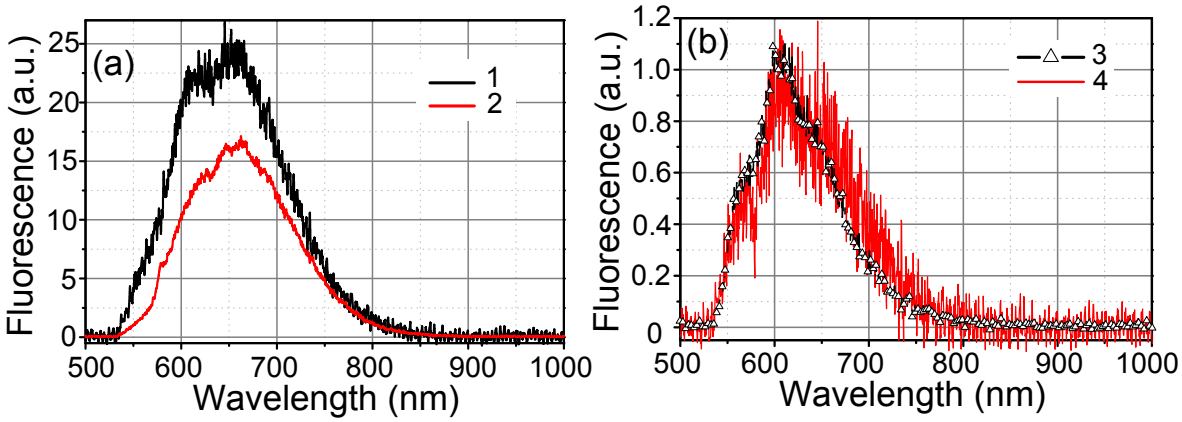

Figure 5.9.: (a) - spectra of NV center and Doxorubicin (1) and only NV center after the Doxorubicin bleaching (2). (b) - spectra of Doxorubicin (3) measured in the nucleus of HeLa cell, (4) obtained from the difference between (1) and (2) from fig. (a).

Obtained data proves that there are nanodiamonds with attached Doxorubicin molecules inside the cell cytoplasm, but only the drug penetrates into the cell nucleus. Also no NV center spectra were detected from the cell nucleus. It means that diamond nanocrystals stay only in cell cytoplasm.

5.4.5. Pre-clinical test

The clinical pre-test research was done in the collaboration with the Institute of Pharmacology of Natural Products and Clinical Pharmacology (University of Ulm) and the Institute of Pharmacology and Toxicology (University of Ulm, Medical Center). All measurements were done using clinical equipment in order to prove that the data which we obtained can be measured by standard medical tests.

Firstly the drug release from the system of nanodiamonds and HSA proteins (ND-HSA) was tested in different buffers (fig. 5.10, (a)). Those two buffers were the same as in our laboratory experiments – pH levels 5 and 7. Here, lysosomal mimicking environment was used, which better reflects the real cell environment. The release process was measured at ambient conditions. Nanodiamonds with attached Doxorubicin molecules were placed in different buffers for different time (up to 48 hours). After this time the nanodiamonds were separated from the free drug by centrifugation of the solution. Thus all unattached molecules were washed out. The fluores-

cence of solutions before and after centrifugation shows the concentration of released Doxorubicin molecules. The tests show that after 24 hours 75 % of the DOX molecules were released from ND-HSA system in the buffer with pH 5 and 60 % in lysosomal mimicking condition (fig. 5.10, (a)).

To study the antitumor effect of Doxorubicin molecules attached to nanodiamonds the chick chorioallantoic membrane model (CAM) was used. For that the human breast cancer cells were xenotransplanted into the chrioallantoic membrane of fertilized chicken eggs. Samples were incubated with two different concentration of drug (0.1 and 0.3 μmol/kg) free and attached to nanodiamonds (fig. 5.10, (b, c)). The tumor tissue was marked with red fluorescent proteins, where the integrated luminescence of tissue represents its size. The tumor luminescence normalized to initial fluorescence was obtained after different incubation times (1, 2 and 3 days). For free drug with a concentration of 0.1 μmol/kg the antitumor effect became visible only after 3 days of incubation with drug. For higher concentration 0.3 μmol/kg of free drug the size of tumor tissue has already decreased after one day of incubation. However, the efficiency of the drug is not high enough (fig. 5.10, (b)). The drug attached to the nanodiamonds shows higher efficiency than free drug (fig. 5.10, (c)). The antitumor effect is visible even for a small drug concentration (0.1 μmol/kg). It means that for the same medical effect can be achieved with much less amount of drug if ii is attached to nanodiamonds. Thus it reduces the negative effect to the healthy tissue.

The absorption of Doxorubicin molecules in different organs for free drug and drug attached to nanodiamonds was checked during the experiments on a mice model (fig. 5.10, (d)). Firstly the background fluorescence at the wavelength corresponding to the drug luminescence was obtained from different organs in phosphate-buffered saline (fig. 5.10, (d) - PBS). Two other mice were treated with free Doxorubicin molecules (DOX) and molecules attached to HSA proteins (HSA-DOX). The drug concentration in tumor tissue in both cases is almost the same. However, the drug is absorbed much less in healthy organs, if molecules are attached to the HSA proteins. For example, in heart no presence of Doxorubicin was observed. It proves that drug attached to protein-nanodiamond system has higher efficiency even for smaller concentration than free drug. The less absorption in healthy tissue decreases their damages during chemotherapy and increases the chance of surviving.

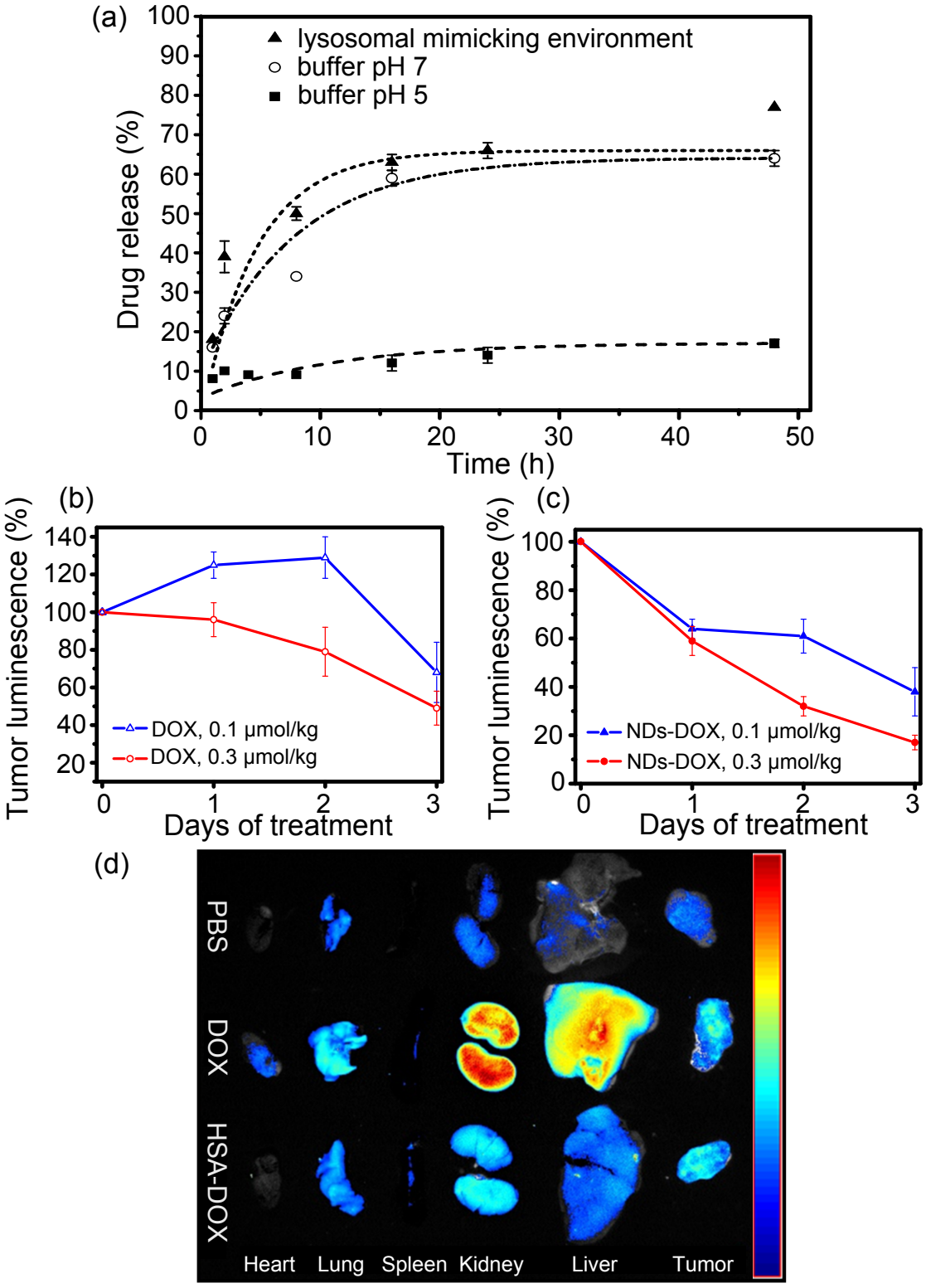

Figure 5.10.: (a) - Drug release from ND-HSA systems in buffers with pH 5 and pH 7 and in lysosomal mimicking environment. The efficiency of Doxorubicin in tumor tissue for CAM model in case of (b) free drug and (c) drug attached to proteins and nanodiamonds. Absorption of drug in different tissues in a mice model (d) - normalized fluorescence collected for: PBS - back ground of tissue in phosphate-buffered saline, DOX - free drug, HAS-DOX - drug released from HSA protein.

5.5. Nanodiamonds with two color centers

As it was already shown, nanodiamonds can be good biomarkers since they are not toxic and highly biocompatible. The emission wavelength wavelength of nanodiamonds with color centers is independent on the size of the particles as it occurs for quantum dots, for example. Nanodiamonds spectra are only related to the crystal defect. Different color centers embedded in nanodiamonds can broaden their applications. In case of biological markers it is better to have more red shifted fluorescence, because the absorption in living tissue is less in that spectral region [11]. From this point of view a SiV center inside nanodiamonds has more suitable properties as biomarker. Another interesting system might be diamond nanocrystals with both color centers: NV and SiV. They include red shifted fluorescence of SiV defect and magnetic property of NV center. These color centers can be excited and detected separately. In our work we tried to create nanodiamonds with two simultaneously occurring defects: NV and SiV. For that milled diamond nanocrystals with NV centers where grown in CVD chamber with silicon doping. This work was done in a collaboration with Prof. Irog I. Vlasov (General Physics Institute, Russian Academy of Sciences).

5.5.1. Sample preparation

Nanodiamonds were produced by mechanical milling of HPHT diamond with high concentration of nitrogen impurities. The particles' size was around 20 nm. Nanodiamonds' powder was firstly diluted in water and then stabilized with bovine albumin [10]. Nanodiamonds' solution was spin-coated on a silicon substrate. There HPHT nanocrystals were used as a seed for the further CVD growth. The time of the diamond growth was 15, 30, 60, 90, 120, and 180 s. During that time different diamond layers were grown around the initial nanodiamonds. New layers were doped with Si atoms, which were etched from the substrate. After CVD diamond growth nanocrystals were annealed for 1 hour in air at the temperature 550 ^{o}C. During the annealing the surfaces of the nanodiamonds were changed from being hydrogen to oxygen terminated. The oxygen at the diamond surface stabilizes negative charge of NV and SiV centers [75, 77].

5.5.2. Size measurements

The size of the nanodiamonds after different growth times was measured on electron microscope (fig. 5.11, (b)) and on atomic-force micro-

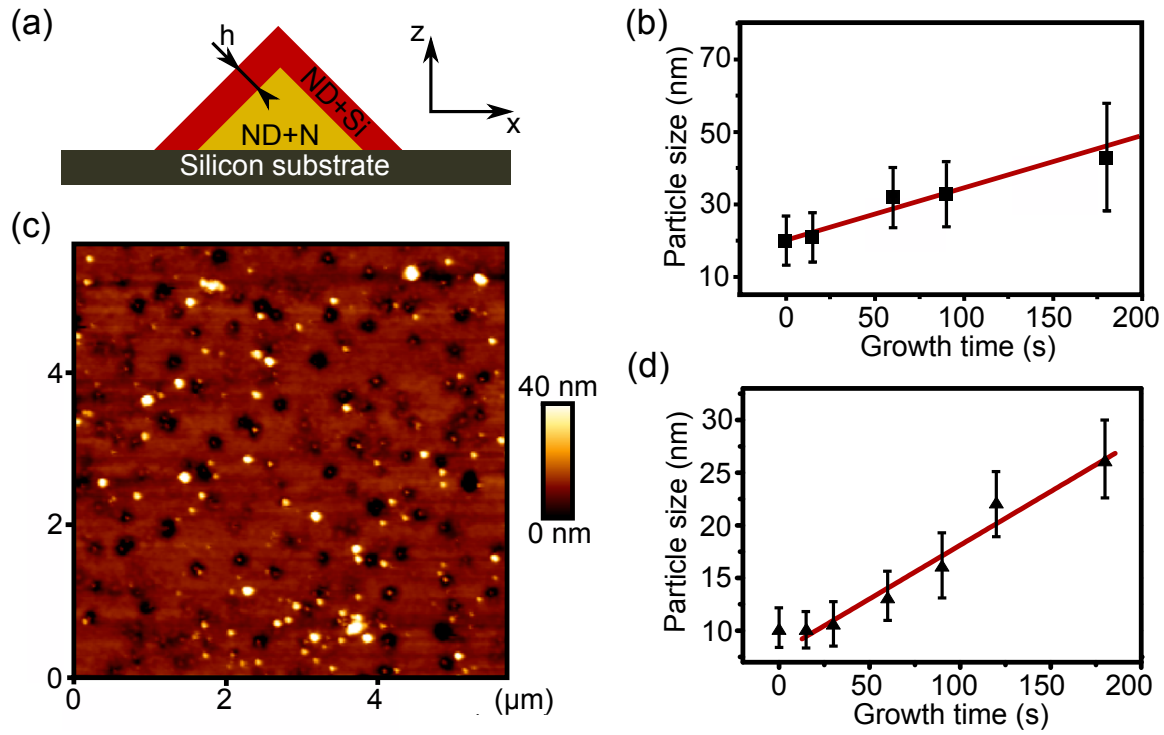

Figure 5.11.: (a) - The model of the growth of the nanodiamonds in X- and Z-axes, where yellow area - the seed is a HPHT diamond with high concentration of nitgoren atoms, red layer - the grown CVD diamond layer with the silicon impurities. (b) - Size of the diamond nanocrystals measured by electron microscopy. (c) - AFM data of the sample grown 180 s. (d) - Size of the diamond nanocrystals measured by AFM setup.

scope (fig. 5.11, (d)). During the growth for 15 and 30 s the size of the nanodiamonds was not noticeably changed. The grown diamond layers became visible after 60 s inside the CVD chamber (fig. 5.11, (b, d)). The observed size increase was different in case of electron microscopy and AFM measurements. It can be explained from the growth process, which is presented in figure 5.11, (a). Milled nanodiamonds often have the form of an elongated regular octahedron or the elongated truncated octahedron. It is related to the crystal structure of diamond. For spin-coated nanodiamonds the preferable position in space is when each nanocrystal has the maximum surface for contact with the substrate. It means that in the horizontal direction the size of the nanocrystals might be bigger than in vertical. This is the reason why AFM measurements show the smaller size of nanodiamonds than electron microscopy data. They look at the sample in different dimensions. AFM measures the hight of nanocrystals (fig. 5.11, (a)), whereas electron microscope characterizes nanodiamonds in lateral directions – XY plain (fig. 5.11, (a)). During the growth process new layers on the nanodiamonds appear at the surfaces, which have no contact with the substrate. The new diamond layers make a contribution in the increase of the vertical size of the nanocrystals only one time, but in horizontal direction two times, as shown in figure 5.11, (a). After 180 s of the growth the new diamond layer is around 12 nm.

During the CVD process not only nanodiamonds grow but also silicon substrate is etched. The AFM pictures of the nanodiamonds at the silicon wafer after 180 s inside the CVD chamber is presented in figure 5.11, (c). At all silicon surfaces arose dimples with the depth around $3 - 4\ nm$. Evaporated silicon atoms can integrate into the new diamond layer. It can induce the formation of the Si defects in diamond including SiV centers.

5.5.3. Fluorescence measurements

Nanodiamonds' fluorescence was measured before and after the CVD growth on the confocal microscope described in chapter 4.1.1. The original nanodiamonds, which were used as diamond seeds, show in the spectra only presence of NV centers (fig. 5.12, (d)), but their fluorescence is unstable in time, as depicted in figure 5.12, (a). It can be caused by the short distance between the color centers and nanodiamonds' surface. Nanocrystals' surfaces may contain a lot of molecules, which play role of acceptors and can capture electrons from NV centers and quench them. During the CVD growth we can expect the stabilization of NV luminescence, because the new diamond layer increases the distance between color centers and

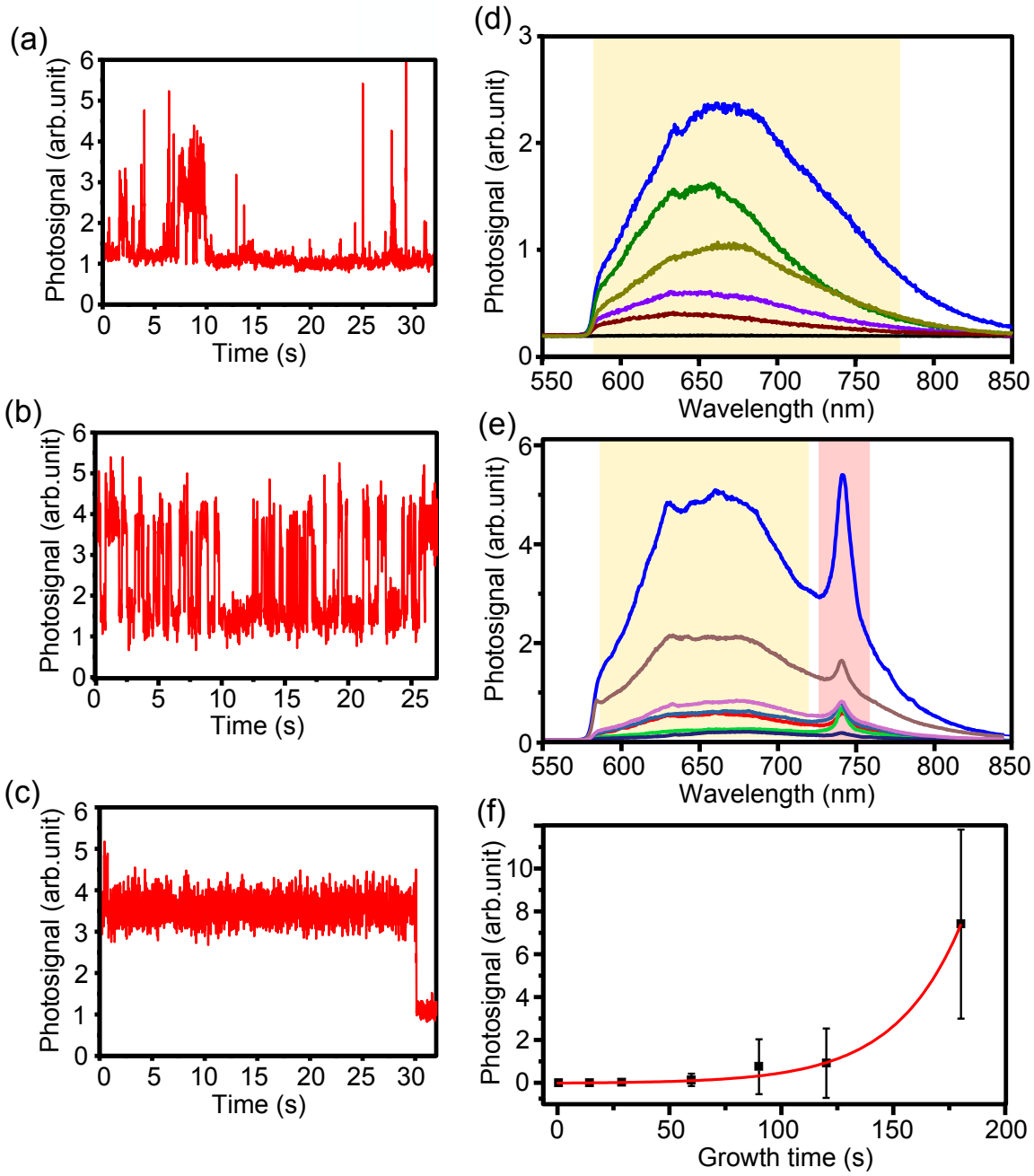

Figure 5.12.: Stability of the fluorescence of NV centers in nanodiamonds before CVD growth (a), after 30 s (b) and after 180 s (c) in CVD reactor. Spectrum of nanodiamonds' fluorescence before CVD growth (d) and after 180 s (e). The yellow shaded areas are related to the NV defects in nanodiamonds. The red area shows, the spectral region for SiV centers. Dependence of the fluorescent intensity of SiV centers on the growth time (f).

the surface. After 30 s inside the CVD reactor, nanodiamonds do not increase in size much, as it was shown by AFM measurements (fig. 5.11, (d)). However, after 30 s of CVD growth the time, which NV centers spend in a fluorescent state, becomes longer (fig. 5.12, (b)). Though nanodiamonds still blink after such short growing time. After 180 s in CVD chamber nanodiamonds increase thickness of the of the new layer by 12 nm, and NV centers turn to their constantly stable fluorescent state (fig. 5.12, (c)). By the way the intensity of the NV fluorescence does not increase much with the used growing time (fig. 5.12, (d,e), yellow areas). It can be explained from the point that during the growth new nitrogen impurities are not added, but some NV centers, which are located close to the nanodiamonds' surfaces, are converted to the stable fluorescent state due to increasing the distance between color centers and the surfaces.

As it was already mentioned, during the CVD growth silicon atoms can be evaporated from the substrate and can be incorporated into nanodiamond crystal lattice. They can create SiV centers in the nanocrystals. All samples were checked for the presents of SiV defects before and after annealing (550 ^{o}C in air for 1 hour). Samples without annealing do not exhibit a presence of SiV luminescence in the fluorescence spectra. But SiV centers are observed in the spectra of nanodiamonds after the annealing (fig 5.12, (e), red area). The number of the SiV defects is increasing with the time of the growth (fig. 5.12, (f)). The increase occurs with nonlinear behaviour, as opposed to the width increasing of the new diamond layers (fig. 5.12, (f)). Nonlinearity can be related to the point that number of the SiV centers grow proportionally to the volume of the new nanodiamonds. The model of the half sphere can be used to simulate the change of the volume of the nanodiamonds. In case of regular octahedron or truncated octahedron the volume is still proportional to the sphere radius to the power of three. For half sphere the new volume can be calculated as:

$$\Delta V = \frac{2}{3}\pi(h^3 + 3h^2R + 3hR^2), \tag{5.2}$$

where h is a height of the new CVD diamond layer and is a function of time, R - the radius of the sphere, which represents the nanodiamonds. For the short growing time nanodiamonds do not increase in size much (fig. 5.11, (b, d)). The presence of SiV centers is detected only after 90 s of the growing time (fig. 5.12, (f)). The new layer of nanodiamonds is comparable with the size of initial seed after 120 s inside the CVD chamber. For longer times we can expect that the number of SiV centers inside nanodiamonds increase nonlinearly in the beginning a function of time to

the power of two and later as the power of three (eq. 5.2). This is what we see in the data presented in figure 5.12, (f).

5.6. Conclusion

In modern biology and medicine there are many problems, which can be solved by using optical markers. They have to fulfill some requirements such as biocompatibility, non-toxicity and possess stable emission. Nanodiamonds with color centers have high potential to be used for these purposes.

In this chapter it was demonstrated that nanodiamonds with NV centers can be used as optical markers in living systems and for drug delivery for chemotherapy. We show that nanodiamonds coated with modified HSA proteins have stable diffusion properties in the buffers with pH level in the range from 2 to 8. Coated diamond nanocrystals do not aggregate in all tested solutions. The protein coating is stable in buffers with pH levels $2-8$ and in living systems (HeLa cells). HSA proteins can be modified to attach drug molecules by pH sensitive bonds. Drug molecules are released from the coated nanodiamonds at the pH level less than 5.5. Coated nanodiamonds with attached drug molecules were tested inside HeLa cells, where modified particles penetrate into the cells as one system. Drug molecules are released from nanodiamonds inside the cells and penetrate into the cell nucleus. Clinical tests demonstrate that in 24 h 75% of the drug molecules are released from coated nanodiamonds in the buffer with pH level 5 and 60 % in lysosomal mimicking condition. The presented results for the stabilization of nanodiamonds and their use as drug delivery system were published in [9].

SiV centers have red shifted fluorescence compared to NV defects. It might broaden the *in vivo* applications of diamond nanocrystals with such color centers. However, nanodiamonds with NV centers can also be used to detect magnetic field, which is not possible with SiV defects. In that case diamond nanocrystals with two different color centers can find even wider application than particles with one type of defect. CVD growth of nanodiamonds on silicon substrate can be a good strategy to create diamond nanocrystals with two color centers: nitrogen-vacancy and silicon-vacancy. For the initial seed we used milled diamond nanocrystals with high concentration of NV centers. Nanodiamonds were spin coated on the silicon substrate and grown in a CVD chamber for different times between 15 and 180 s. The SiV centers became visible in optical spectra after 90 s of

growth time. After that time the new diamond layer at the nanodiamonds is 5 nm thick. The number of color centers increased nonlinearly with the growth time. Obtained results were published in [10].

6. Magnetic sensors based on NV center

6.1. Introduction

There are many problems in biology and medicine, which are related to nanoscale magnetic detection. It is important for understanding of magnetic proteins, for example, biocompasses [212] or measuring magnetic field of proteins. NV centers in diamond can be used for detection of constant and oscillating magnetic fields (see chapter 3.2). NMR measurements based on NV center can help with the investigation of protein or molecule structure (see chapter 3.2.3). For that color centers should be placed close to the investigated system. It ca be realized on bulk diamond with shallow implanted NV centers [19, 20] or on nanodiamonds containing NV centers. Diamond nanocrystals have big advantages compared to a bulk diamond. This is related to the size of nanodiamonds. They might be attached to the interesting molecules or proteins or placed *in vivo* close enough to the investigated objects.

In this work we are interested in the detection of metallo-protein, which is called ferritin. This is a protein, which contains iron atoms in a non-toxic state inside different living organisms. It is found not only inside higher organism [213], but also inside plants and microorganisms [214]. In human body problems with ferritin can lead to many diseases. For example the low number of iron atoms per one protein causes anemia [215, 216]. Contamination of the ferritin core with another metal atoms can provoke Alzheimer's disease in case of aluminum [217, 218] or Parkinson's disease for zinc [219, 220]. It will be useful to know not only the number of the ferritin molecules in the blood, but also know what the single protein contains. Firstly we would like to detect the presence of ferritin molecules by NV centers inside nanodiamonds. Later this technique can be improved for a single molecule detection.

6.2. Ferritin

For the first time ferritin was obtained in 1942 by S. Granick from horse spleen [213]. That molecule consists of a protein shell "apoferritin" and an iron core [221, 222]. The total size of the ferritin is equal to 12 nm, the core size is around 6 nm (fig. 6.1) [222, 223]. Ferritin is the main iron store in human organisms, which is used for the production of globins such as hemoglobin and myoglobin.

Apoferritin consists of 24 subunits, which self-assemble. Its subunits can be of two types L (light) and H (heavy) [224–226]. They have different molecular masses, antigenic and isoelectric properties. The production of L- and H-subunits depends on the genes, and the ratio between them are different for ferritin molecules produced in different organs. For example, the concentration of L-subunits is higher for proteins from liver and spleen, but the concentration of H-subunits is higher for molecules produced in heart and tumor tissues [224, 227].

Ferritin's core is colloidal iron hydroxide. Iron saturated ferritin molecules contains metal atoms up to 27 % of they molecular weight. It is equivalent to approximately 4500 Fe^{3+} atoms per one ferritin molecule. To capture iron in state 3^+ it is necessary to have oxidizing agent. In this case oxidized iron Fe^{3+} can be formed by electron transfer from Fe^{2+} atom to oxygen. The chemical formula of the ferritin core is $[FeO(OH)_8][FeO(H_2PO_4)]$, which is called ferrihydride [228, 229]. The concentration of ferritin molecules in blood serum correlates with the stored iron in an organism. The low number of ferritin molecules in the blood or of the iron atoms per one molecule results in anemia. The determination of the ferritin concentration is a well-tested medical investigation. However, the detection of iron number per one molecule is more complicated method. The ferritin core might also contain atoms of another metal, for example, aluminum [217, 218] or zinc [219, 220]. This lead to problems with brain and all organism totally.

The mineral ferritin core has low symmetrical crystal structure with antiferromagnetic oriented spins of Fe^{3+} atoms [229]. Small fluctuations of the uncompensated Fe^{3+} spins create a total magnetic moment around 300 μ_B [230]. The strong magnetisation of ferritin core is observed at low temperature [231, 232].

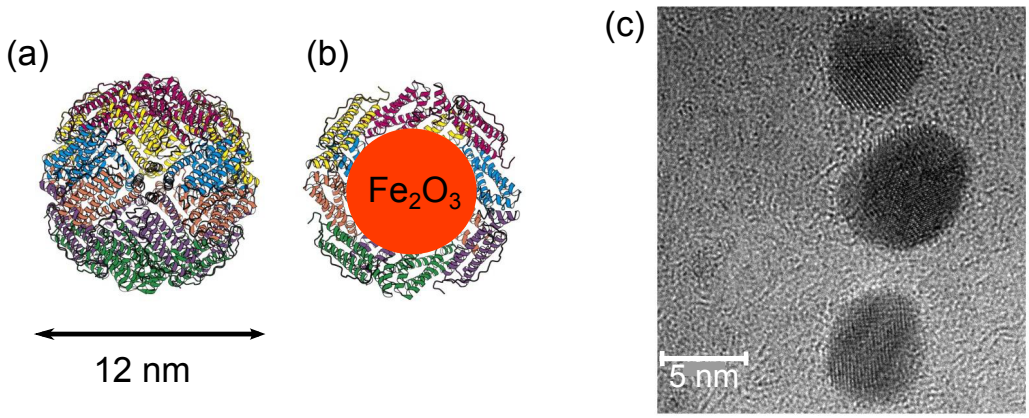

Figure 6.1.: The structure of ferritin molecules: (a) - apoferritin - protein shell consists of 24 subunits, (b) - apoferritin with iron core inside. (c) - electron microscopy picture of ferritin molecules, where only iron cores are visible.

6.3. Sample preparation

For this experiment we used fluorescent nanodiamonds from Prof. Dr. H. C. Chang's group (Institute of Atomic and Molecular Sciences, Academia Sinica, Taiwan) [233]. The average size of the diamond nanocrystals was 30 nm. The diamond powder was produced from the synthetic type *Ib* crystals, which had high level of nitrogen impurities. Nanodiamonds were irradiated by He^+ ions with energy 40 keV and dose of 1×10^{13} ions/cm^2. The irradiation produces vacancies inside nanocrystals, which are used for the formation of NV centers. Almost every nanodiamond had one or more color centers.

Firstly nanodiamonds were treated with three acid mixture (see chapter 2.4.3). This results in carboxyl groups at the diamond surface (fig. 6.2). These groups can be used for futher attachment of the ferritin moleculs by EDC (1-Ethyl-3-(3-dimethylaminopropyl)carbodiimide) coupling (fig. 6.2) [234]. The typical pH level for EDC reaction is in the range of $4.0 - 6.0$ [234, 235]. However, it is not acceptable for ferritin molecules, which are stable at pH level higher than 7 [227]. With low pH apoferritin is disintegrated to 24 subunits. This means that during this chemical reaction pH level plays an important role and should be strictly controlled.

The ferritin attachment was checked by electron microscopy. The images of nanodiamonds with attached ferritin molecules before and after

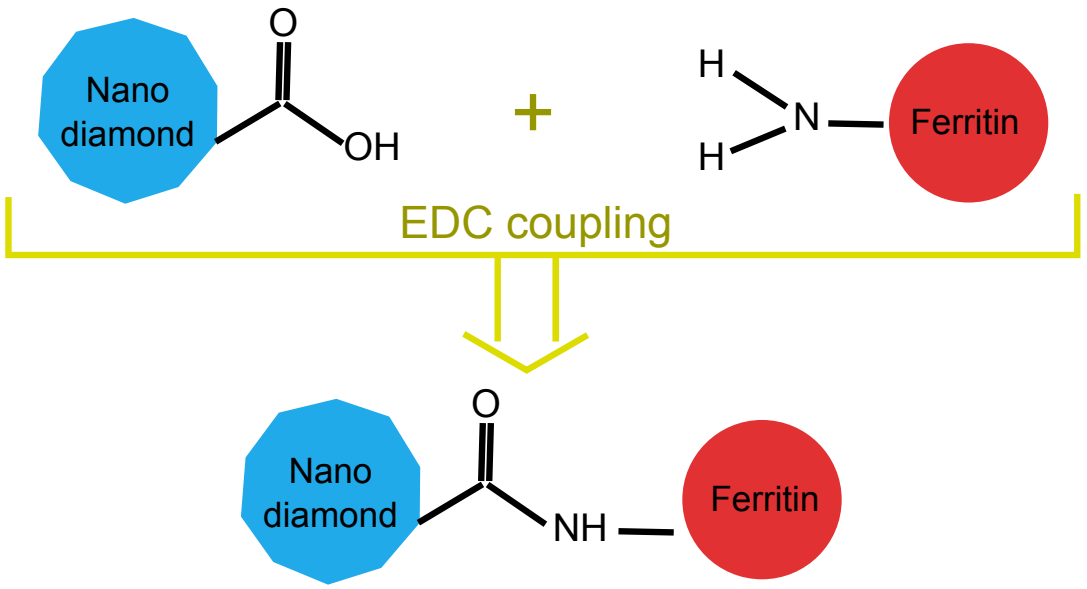

Figure 6.2.: Schematic picture of EDC coupling of the attached ferritin to the nanodiamond.

the purification from free proteins are presented in figure 6.3. The electron microscope with high resolution allows to resolve the single atoms and to identify the crystal structure of diamond and ferritin core. These measurements were done in a collaboration with Prof. Dr. Ute Kaiser's group (Electron Microscopy Group of Materials Science, University of Ulm). The obtained data shows that one nanodiamond is connected to 10 ± 2 molecules (fig. 6.3).

6.4. Coherence time measurements

Nanodiamonds with and without ferritin molecules were spin-coated on glass substrates with lithographic microwave structure. All measurements were done on a home built confocal microscope, which is presented in chapter 4.1.1. We chose nanodiamonds only with single NV center inside. This was proven by antibunching measurements (see chapter 4.1.2). To speed up selection of nanodiamonds with single NV center inside, detected photocount level was correlated with number of centers. For our experiment we chose 32 nanodiamonds with single NV centers from both samples with and without metallo-proteins.

The measurements were done in a low external magnetic field of about

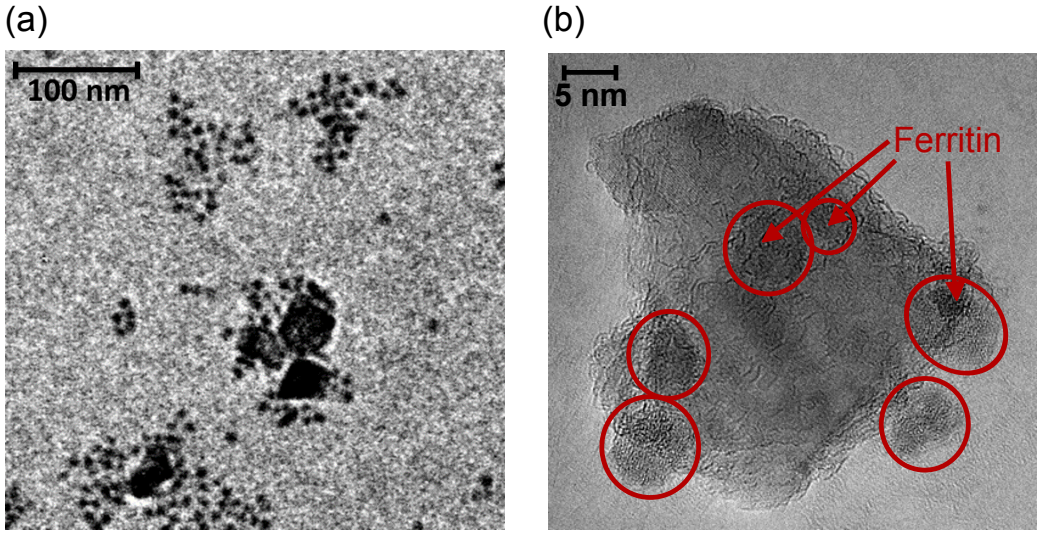

Figure 6.3.: Electron microscopy images of nanodiamonds with attached ferritin molecules before (a) and after (b) purification.

20 G. This field splits the ODMR lines of NV centers but should not polarize the core of the ferritin molecules. The splitting of $m_S = -1$ and $m_S = +1$ states depends not only on the magnitude and orientation of external magnetic field, but also on the crystal strains (see formula 3.2). All diamond nanocrystals lie in random orientations. It means that the applied magnetic field has different effective component in the direction of the axis of NV center. All NV centers should exhibit splitting of ODMR lines. Firstly the Rabi frequency was found for all chosen NV center according to the technique presented in chapter 2.2.5. After the determination of the π- and $\frac{\pi}{2}-$pulse the coherence times T_1 and T_2 have been measured, as explained in chapter 2.2.5.

The relaxation times of NV centers are strongly dependent on the environment (ref. 6.4.3). In bulk diamond the main role for the decreasing of coherence times plays lattice defects and impurities, which have magnetic moments. For nanocrystals the decreasing of coherence times of color centers is rather associated with the chemical groups and molecules attached to the surface or situated close to it. There are many of these groups. It is possible to make pure bulk diamond with extremely low concentration of impurities. However, it is not possible to protect completely the diamond surface from all molecules. This means that NV centers, which are close to the surface, have shorter coherence time. In nanodiamonds all color centers are close to the surface. This allows to use diamond nanocrystals

with NV centers as magnetic sensors *in vivo* and *in vitro*.

The distance between color centers and magnetic molecules at the diamond surface is very important for relaxation times and for sensitivity. To estimate the distance between NV center and molecules at the surface we have to know the location of the color center inside the nanodiamond and the location of molecules at the surface. First important criterion for that is the size of the nanocrystal. It defines the minimum and maximum possible distance. In a solution nanodiamonds have a broad size distribution. Selection of crystals by size with a resolution of 1 nm is hardly possible. Normally we can expect at least some deviation from average size by ± 5 nm. It means that it is necessary to characterize the real size of each nanodiamond before measurements, but usually it is not possible. There is another important question, which is related to the position of color center inside the nanodiamond itself. The probability to find a color center in certain volume inside nanocrystal depends on the radial position of NV defect (R_{NV}, fig. 6.4). For a spherical model of nanodiamonds the probability to find the color center depends on the radius of the particle R. For example, the probability is equal to 0.1, when the color center is in a central part of nanodiamond with radius $0.47 \times R$. It means that the probability is much higher, when the distance of NV center from the center of the nanodiamond is growing. The relative position of magnetic molecules around NV center is also important. However, the number of ferritin molecules varies from nanocrystal to nanocrystal. In that case we have two unknown parameters: the distance from color center to nanodiamond surface (ΔR, fig. 6.4) and the number and position of ferritin molecules.

Another important issue while working with nanodiamond is that it is not possible to make measurements on clean sample and then repeat it on the chemically modified sample. All measurements can only be carried out on different groups of nanodiamonds. It means that measurements should be statistically averaged, because the coherence time of NV centers in nanocrystals varies within one sample.

6.4.1. T_1 time measurements

The measurements of the longitudinal relaxation time T_1 were done by the method discussed in chapter 2.2.5. Obtained values of the T_1 time for nanodiamonds without ferritin molecules are mostly in a range from 30 μs to 90 μs (fig. 6.5, (c), red distribution). The average T_1 time of color centers in free diamond nanocrystals is 46 μs. A typical curve is presented in figure 6.5, (a).

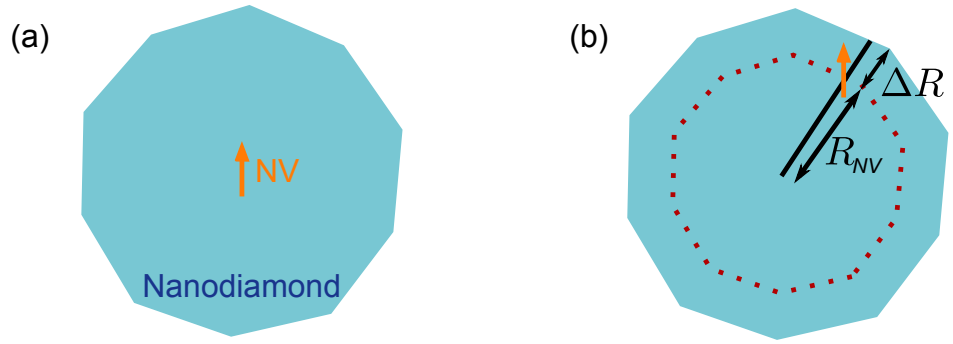

Figure 6.4.: The different positions of NV center inside a nanodiamond. (a) NV center in a center of nanocrystal – rare situation. (b) NV center is close to nanodiamond's surface. The probability to find NV center is higher for bigger radial position R_{NV}.

The attachment of ferritin molecules decreases the relaxation time T_1 of NV center (fig. 6.5 (b)). The range of measured T_1 times is between 2 μs and 17 μs (fig. 6.5, (c), blue distribution). The mean value of T_1 time for NV centers inside nanodiamonds with ferritin molecules drops to 6.6 μs. This is 7 times shorter than T_1 for nanocrystals without metallo-proteins.

Both distributions of the spin-lattice relaxation time T_1 for NV centers inside nanodiamonds with (blue data) and without (red data) ferritin molecules are presented in figure 6.5, (c). The measured times for two groups are not overlapping. This allows to distinguish the presence of the ferritin molecules by the T_1 time measurements.

6.4.2. T_2 time measurements

Coherence time T_2 was measured using the sequence discussed in chapter 2.2.5. The typical curve for nanodiamonds without ferritin molecules is depicted in figure 6.6, (a). All observed T_2 times for that group of diamond nanocrystals are in a range from 2.4 μs to 10.4 μs (fig. 6.6, (c), red distribution). The average T_2 time without metallo-proteins is equal to 6.7 μs.

Nanodiamonds conjugated with ferritin molecules show shorter T_2 time. The total range of observed coherence times is between 0.3 μs and 1.4 μs (fig. 6.6, (c), blue distribution). The typical curve of NV centers inside nanodiamonds with attached ferritin molecules is presented in figure 6.6, (b). Their mean value is 0.7 μs. It is approximately 9 times shorter than for clean diamond nanocrystals.

Well separated numbers of T_2 coherence times (fig. 6.6, (c)) give possibil-

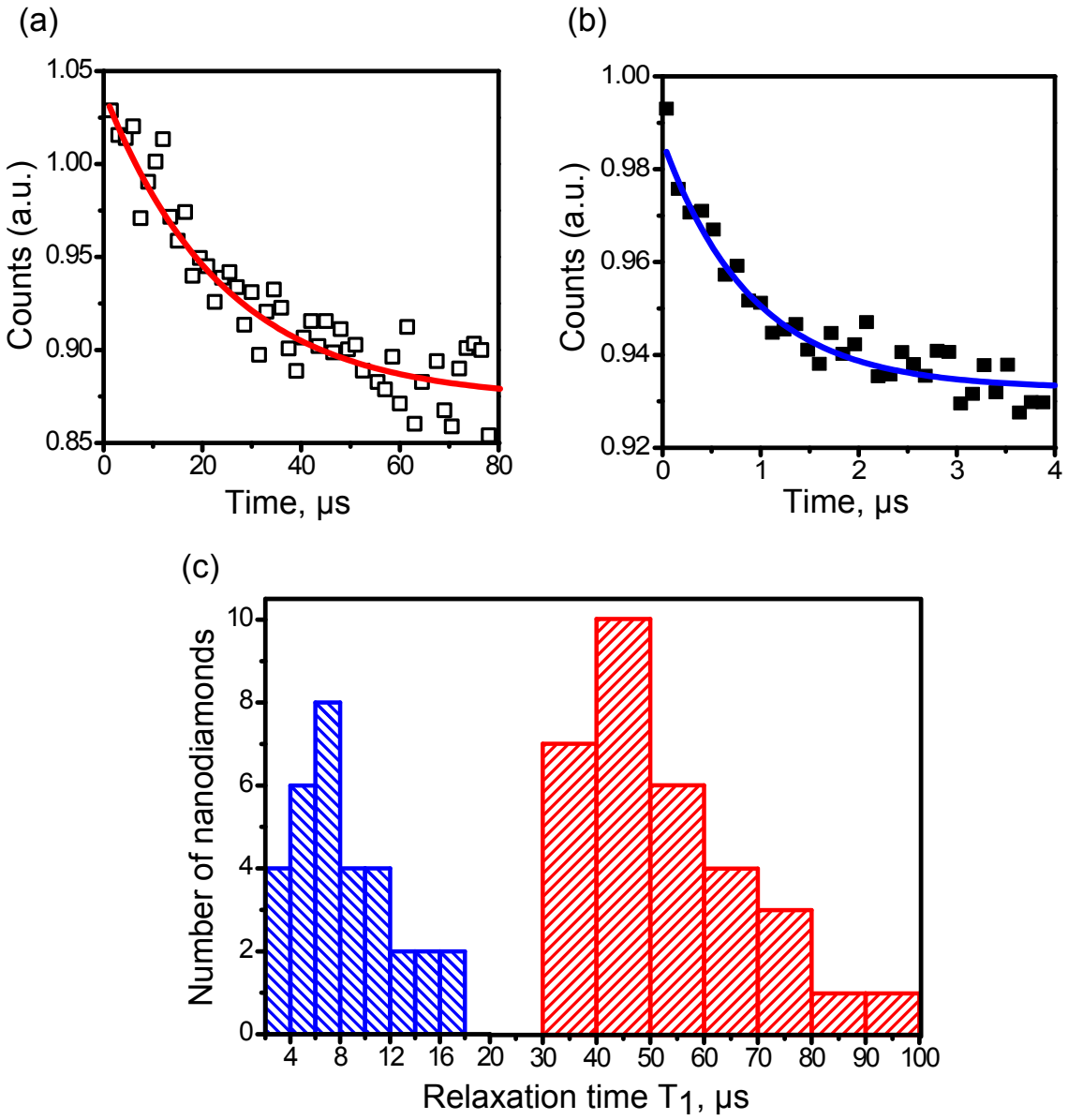

Figure 6.5.: Typical relaxation time T_1 of free nanodiamonds (a) and of nanodiamonds with attached ferritin molecules (b). The distribution of the relaxation time T_1 for free nanodiamonds (red) and of nanodiamonds with attached ferritin molecules (blue) (c).

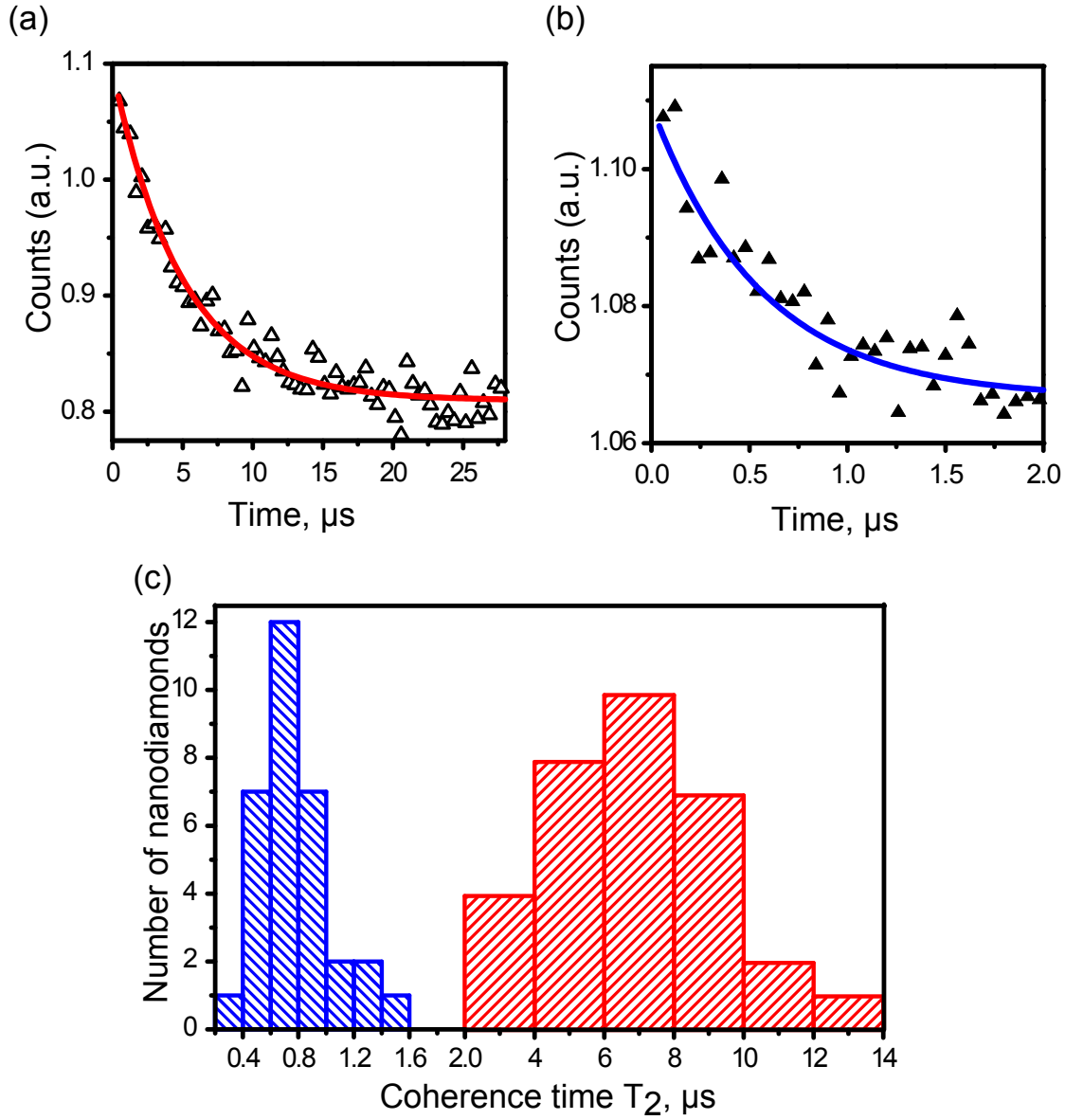

Figure 6.6.: Typical coherence time T_2 of free nanodiamonds (a) and of nanodiamonds with attached ferritin molecules (b). The distribution of the coherence time T_2 for free nanodiamonds (red) and of nanodiamonds with attached ferritin molecules (blue) (c).

ity for further experiments to determine the presence of metallo-proteins at the nanodiamonds' surface.

6.4.3. Theoretical model

It would be good to see not only the presence of ferritin molecules itself, but also to determine the number of metallo-proteins. For this we, in the collaboration with the group of Prof. Dr. Martin B. Plenio (Institute for theoretical physics, University of Ulm), developed a theoretical model of the observed system.

The hyperfine coupling between nitrogen nuclear spin and electron spin of NV center is neglected. It means that the properties of the NV's ground state can be described by the Hamiltonian:

$$\mathcal{H} = SDS + g\mu_B B_0 S_z, \tag{6.1}$$

where $S = (S_x, S_y, S_z)$ is the operator of the electron spin of NV center with spin number $S = 1$, $D = 2.87\ GHz$ is the splitting of states $m_S = |\pm 1\rangle$ and $m_S = |0\rangle$ at zero field, g is g-factor, μ_B is the Bohr magneton, and B_0 is the applied constant magnetic field, which in our case was approximately 20 G.

The ferritin core holds Fe^{3+} ions, which have an electron spin equal to 5/2. The flip-flops of these spins produce a fluctuating magnetic field, which affect the spin of the color center inside nanodiamonds. We can present this process at room temperature classically as a random exchange of polarization between iron spins at a rate of 2.1 GHz. This is taken from the line width of the electron spin resonance spectrum of ferritin molecule [236].

The transversal component $S^{\perp}$ (see chapter 2.2.5), which is perpendicular to the NV's symmetry axis, of the fluctuating magnetic field of metallo-protein induces flips of the electron spin of the color center. That component leads to faster relaxation and shorter value of T_1 relaxation time. In set terms the noise spectrum $S^{\perp}(\omega)$ at the frequency, which corresponds to the resonance spin transition of the ground state of NV center at zero-field (i.e., $\omega_0 \approx 2.87\ GHz$), permits to make accurate estimation of T_1 time as $1/S^{\perp}(\omega = \omega_0)$.

The changes in T_2 coherence time are related to the longitudinal component $S^{\parallel}$ of the fluctuating magnetic field (see chapter 2.2.5). The T_2 time can be calculated by the decay of the spin echo signal SE, which is dependent on the noise spectrum $S^{\parallel}(\omega)$ of ferritin core [237]:

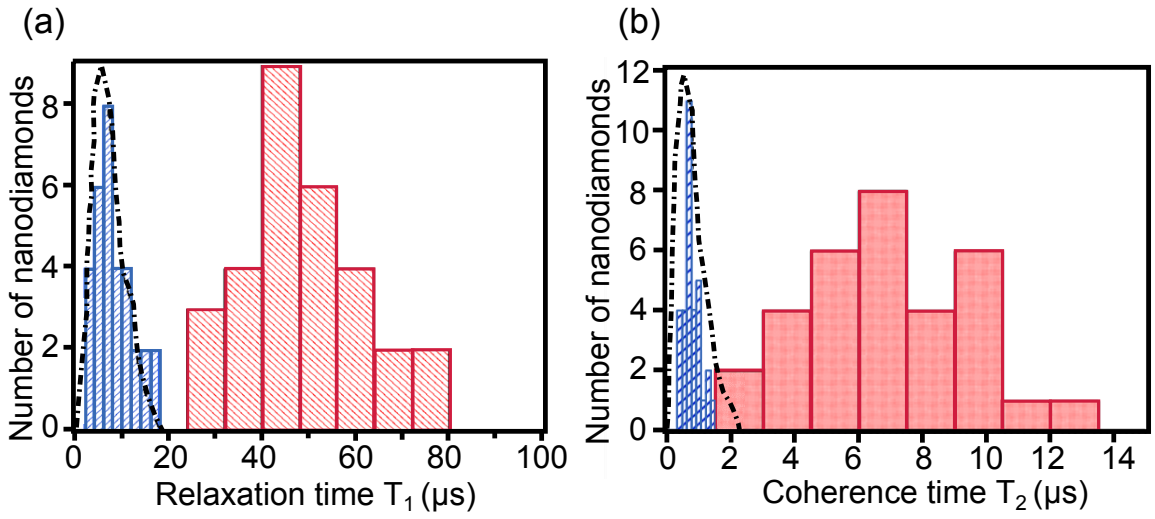

Figure 6.7.: The distribution of the relaxation time T_1 (a) and T_2 (b) for free nanodiamonds (red) and of nanodiamonds with attached ferritin molecules (blue). The black dashed lines are result of numerical simulations.

$$SE = 8 \int_0^\infty \frac{1}{\pi} S^{\parallel}(\omega) \cdot \sin^4(\frac{\omega t}{4}) \frac{1}{\omega^2} \, d\omega. \tag{6.2}$$

It should be also noticed that all nanodiamonds have size distribution and the positions of the color centers inside them are not defined. On the other hand we do not know the exact positions of ferritin molecules at the nanocrystals' surface. It means that the distance between NV center and ferritin molecules are variable. The number of metallo-proteins is different from nanodiamond to nanodiamond and is in the range of $8-15$ molecules per one nanoctystal. Thus the effective magnitude of the fluctuating magnetic field cannot be precisely found. The numerical simulation was done with the variation of these two parameters (distance between NV and ferritin molecules and number of proteins per one nanodiamond). The results for T_1 and T_2 relaxation times are shown as dashed lines in figure 6.7. The total number of simulated nanodiamonds is 1000 for each group. The theoretical prediction is in a good agreement with the obtained experimental results.

This model has one fixed parameter – number of iron atoms inside ferritin core – and two variables – distance between color center and molecules

and number of metallo-proteins. Such model can be used to distinguish the number of iron atoms in one ferritin molecule.

6.5. Further experiments

The main interest in studies of ferritin molecules is the identification of the number of iron atoms in the ferritin core and the presence of the other atoms inside it. In presented experiments a few metallo-proteins with given iron number were attached to the nanodiamond. However, in modern medicine there is another problem – to distinguish the unknown iron number per single protein. If we find the number of attached molecules and their relative position, we can calculate the iron number with our theoretical method (chapter 6.4.3). The one of possible solutions is to use a single metallo-protein and to detect it's interaction with NV center at different known distances. It can be done using a combination of confocal and atomic-force microscopes [17]. The combination of this technique and NMR measurement at the NV center in diamond [19, 20] can allow to discover the chemical composition of the ferritin core. Single protein sensing can be done with small amount of the specimen. It can be applied to the proteins, which are isolated from different organs, not only from the serum. It can improve the medical diagnostic of different diseases.

6.5.1. Single protein sensing

Single protein sensing can be realized using a combination of confocal and atomic-force microscopes. These measurements can be performed in two ways. First, the AFM tip with attached NV center is scanned around the metallo-protein. That type of AFM tip can be produced by gluing the nanodiamond with NV center to the end of an AFM needle [17]. Other possible way is the fabrication of the AFM tip directly of the diamond with the shallow implanted color centers [238]. Second possible experimental realization is in opposite configuration. The investigated protein is attached to the AFM cantilever. It can be either a needle or a spherical tip. This tip can be scanned around the shallow NV center inside a flat bulk diamond [239, 240] or inside a nanodiamond. Color center should be shallow implanted to have a smallest possible distance to the protein or molecule. The bulk diamond is more preferable than small nanocrystals. The coherence time of an NV center in a bulk diamond is usually longer than in nanodiamond. It is important parameter for high sensitivity of

magnetic field using NV centers. The position of color center in nanocrystal is indeterminate. This makes the estimation of distance between NV center and investigated object hardly possible.

The production of the sharp diamond tips with NV center with long relaxation times is currently under extensive work. According to the discussed above we proposed the configuration when proteins are attached to the AFM tip and that tip is scanned around shallow NV center in a bulk diamond. For this we used thin bulk diamond (square-shaped 4×4 mm, thickness 80 μm). The implantation of ^{14}N was done with energy 2.5 keV which corresponds to a depth of approximately 5 nm below the diamond surface.

First test experiments were done with an AFM tip, to which ferritin was attached by adsorption. The AFM cantilever with the SiO_2 spherical particle (diameter 3.5 μm, fig. 6.8 (a,b)) was placed into the ferritin solution. After drying in air some molecules were stuck by Van der Waals forces at the silica particle (fig. 6.8 (c)). In this case the concentration of the proteins at the tip is high and they are distributed inhomogeneously. However the high concentration of the ferritin molecules should result in strong and easily detectable changes of the T_1 and T_2 times.

The localization of ferritin molecules at the AFM tip is unknown. Tip with attached ferritin molecules was scanned around selected NV center. At the same time for each position of the tip the change of spin relaxation time of the NV center was measured. Obtained map of the relaxation time change shows influence of ferritin molecules onto NV's spin. For such experiment it is hard to collect for each point entire curves of either T_1 or T_2 times. However, the times can be estimated by the photon count rate (fig. 6.9), which are coming from the color center when special sequence is applied. For example, for T_2 time measurement the sequence is as in chapter 2.2.5 $\frac{\pi}{2} - \frac{\tau}{2} - \pi - \frac{\tau}{2} - \frac{\pi}{2}$, where τ is a fixed delay time. The photosignal would be stronger for longer T_2 time (fig. 6.9). The constant time τ is chosen as a mean value among two extreme values of coherence time, namely: undisturbed one – the longest, and in presence of ferritin in close proximity – the shortest one. For the T_1 time the measurements are similar, except the MW sequence (chapter 2.2.5). To obtain better statistic the measurements should be repeated as many time as possible. The chosen time τ defines the time of one run of the measurement. The T_2 time is shorter than T_1, and it means that necessary constant waiting time is shorter for T_2 scanning measurement. Therefore, for the same measurement time per point statistical averaging is higher for T_2 sequence than for T_1. It gives high contrast and less noise. So that for scanning measure-

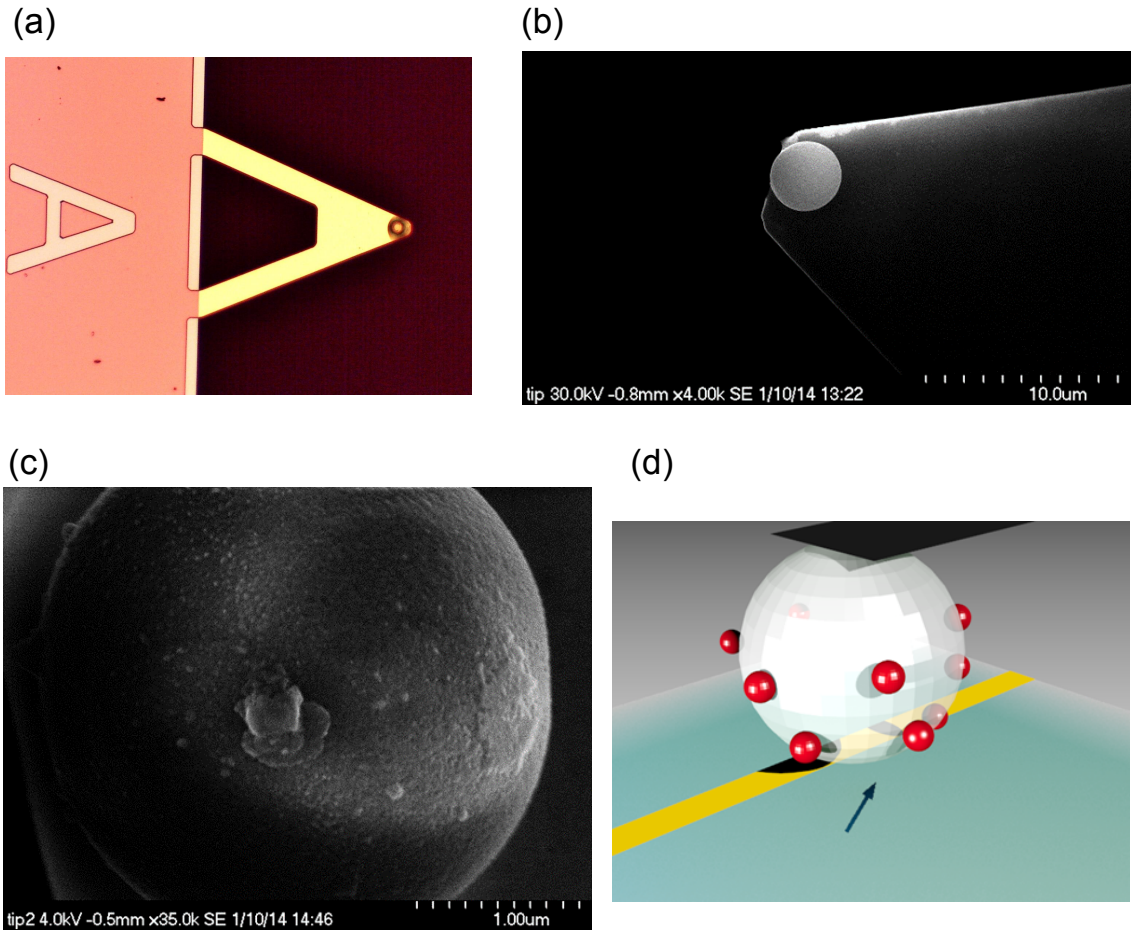

Figure 6.8.: The image of the AFM tip with silica spherical particle (3.5 μm in diameter) in optical (a) and electron (b) microscopes. SEM picture of silica AFM tip with attached ferritin molecules (c). The schematic picture of the setup configuration, where the AFM tip with ferritin molecules (red beads) is scanned around shallow NV center (denoted by arrow) in bulk diamond (d).

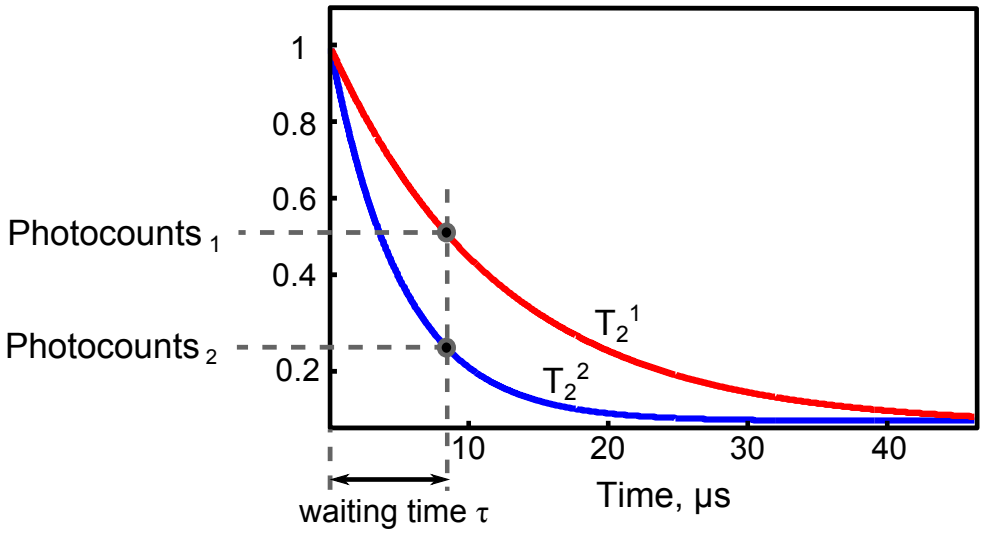

Figure 6.9.: Typical plot of coherence time T_2 of free shallow NV center (red line) and of color center with close ferritin molecules around it (blue line). Constant waiting time τ can be chosen at the middle of the relaxation curve to distinguish T_2 times by the photon count rate level.

ments the detection of T_2 time is more efficient than T_1.

A few NV centers in the shallow implanted diamond were tested by measurements of coherence. We detected T_2 time of the color centers, when the AFM tip with ferritin molecules was far away from the diamond surface (T_2^{free}) and when AFM tip was in a contact with the diamond surface around NV center ($T_2^{ferritin}$). The best obtained data was $T_2^{free} = 12$ μs and $T_2^{ferritin} = 5$ μs. The detected $T_2^{ferritin}$ time might not be the shortest possible coherence time. The points of the measurements were chosen randomly, and the coherence times strongly depend on the position of the ferritin at the AFM tip in respect to the position of the NV center in diamond.

Our experiments revealed that scanning measurements of the T_2 time by the described above method is not optimal and has some problems. Firstly, the AFM tip can quench the NV fluorescence and because of this the change of the photosignal can be independent of the coherence time change. Another undesirable influence might be caused by some small changes of the magnetic field during scan, which in our case lasted more than 3 hours. It can lead to the mechanical instability and also to the shift of ODMR lines. The MW frequency is not changed during the scan, and

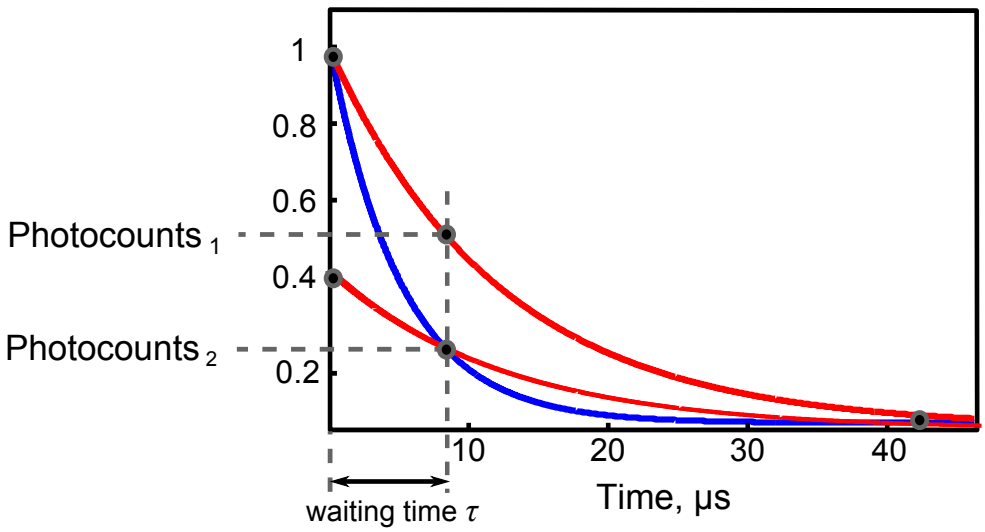

Figure 6.10.: Typical coherence time T_2 curve of NV center with close ferritin molecules (blue line) and of free color center with different optical contrast (two red lines). The photosignal at constant waiting time τ is indistinguishable or real change of relaxation time from just reduction of contrast for any other reason. Two additional points on the curve help to overcome this problem.

it affects the contrast of the coherence time curve (fig. 6.10). It might be that for the same value of coherence time with different contrast or total numbers of photons we see different photosignals and interpret them as different coherence times, which would not be correct.

The solution of such problems can be in the counting not just one point of the coherence time curve, but thee or more points (fig. 6.10). Such points can serve as references and aid to differentiate change of coherence time from all other undesirable effects. It increases the measurement time for each point and imposes new conditions for stability on the setup and the environment. In parallel to this problem we also work on the fabrication of AFM tip with single attached ferritin molecule. One of the promising way to do it is the attachment of magnetic protein by a part of DNA, how it was shown in Ref. [241].

6.6. Conclusion

The new step in medical diagnostic of different diseases can be done by the investigation of single molecules or proteins produced in organism. One of the such interesting objects is ferritin, which structural change might be an evidence of anemia, Alzheimer's or Parkinson's diseases. To look inside such a small protein we have to have high sensitive nanoscale magnetic detector. An NV center in diamond is a good candidate for it.

As demonstrated here, NV center in nanodiamonds can be used as a sensor to detect the presence of ferritin molecules. The fluctuating magnetic field affects the coherence times of the color center. For 10 ± 2 metalloproteins per one nanocrystal the detected decrease of relaxation times was by factor of 7 for T_1 time and 9 for T_2 time (fig. 6.5 and 6.6). Observed data helps to develop a theoretical model of the interaction between ferritin molecules and NV center in nanodiamond. All results on the detection of ferritin molecules by NV center in nanodiamonds were published in [21]. In our experiments we used molecules with known number of iron atoms in the core (4500 atoms per molecule). Presented numerical simulation can be used for the determination of iron atoms number if given that exact distance between single molecule and color center is known. The single protein detection can be done by the combination of confocal and atomic-force microscopes.

A. Appendix

A.1. Membrane transport

A.1.1. Cell membrane

Cell membrane plays an extremely important role in its physiology. In the first place it protects cell from the external objects, which can be injurious for it. On the other hand cell receives through the membrane all elements, which are necessary for cell's life.

The basic structure of cell membrane is a lipid bilayer that includes many different kind of protein molecules and protein channels, which are responsible for transport of special molecules through the membrane (fig. A.1). This lipid-globular protein mosaic model of membrane structure was presented in 1972 by Singer and Nicolson [242]. Cell membrane has channels to transport different molecules. They can identify right objects by chemical groups. The transport through the lipid bilayer can be defined as passive and active.

A.1.2. Passive membrane transport

Passive transport through the cell membrane is conditional to the concentration gradient inside the cell and in extracellular fluid. The work process of this transport is direct diffusion through the lipid bilayer (fig. A.2(a)) or facilitated diffusion (fig. A.2(b)), which is realized through the protein channels, and osmosis. The diffusion way is available for small objects such as non-polar molecules (for example, oxygen and carbon dioxide). Polar molecules or ions such as bigger compounds – glucose or retinol, can go through cell membrane by means of facilitated diffusion. For example, nanodiamonds with the size up to 10 nm also can penetrate into cells by the facilitated diffusion [139].

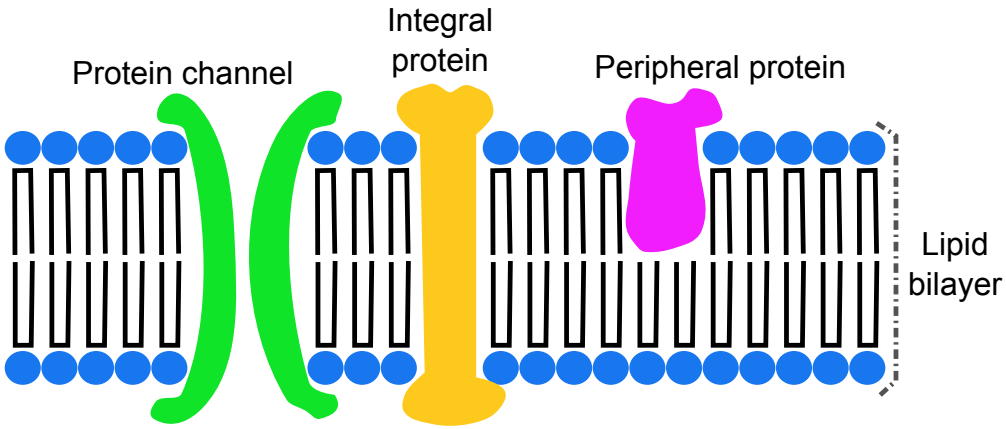

Figure A.1.: Mosaic structure of cell membrane, which includes lipid bilayer, protein channels, integral and peripheral proteins.

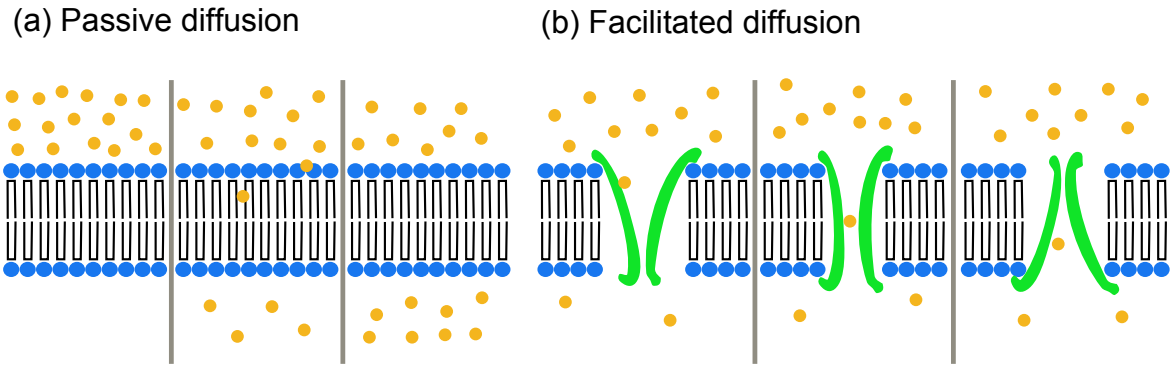

Figure A.2.: The mechanism of passive transport through cell membrane.

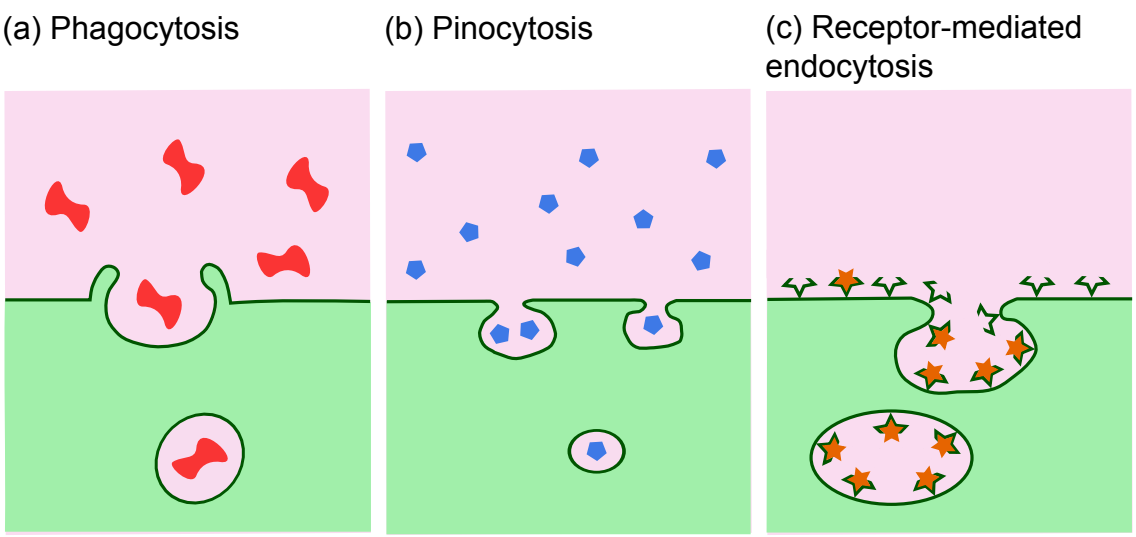

Figure A.3.: The mechanism of active transport through cell membrane - endocytosis.

A.1.3. Active membrane transport

Active transport happens in despite of the concentration gradient and is realized by different kind of channels in the cell membrane. This process occurs by using energy from adenosine triphosphate (ATP). This mechanism is responsible for transport of especially important elements to achieve high concentration of them inside the cells. The active transport can be realized by endocytosis (fig. A.3) or exocytosis. For nanoparticles endocytosis plays more important role, because of exocytosis particles should be initially coated into the lipid bilayer.

Endocytosis is a type of active cell absorption of particles. There are two main mechanisms of endocytosis: phagocytosis and pinocytosis, which also consists of clathrin-dependent endocytosis, caveolae-dependent endocytosis, cacropinocytosis and clathrin- and caveolae-independent endocytosis. The typical size of particles for endocytosis is between 10 and 500 nm [140]. Nanodiamonds are normally penetrate into the cells by endocytosis.

B. Bibliography

[1] W. Shockley. Circuit element utilizing semiconductive materials, June 22 1954. URL http://www.google.ch/patents/US2681993. US Patent 2,681,993. 1

[2] Karl Pearson. *The Grammar of Science*. Adam & Charles Black, second edition, 1900. 1

[3] M. Minsky. Microscopy apparatus, December 19 1961. URL http://www.google.com/patents/US3013467. US Patent 3,013,467. 1, 43

[4] M. J. Rust, M. Bates, and X. Zhuang. Sub-diffraction-limit imaging by stochastic optical reconstruction microscopy (STORM). *Nature Methods*, 3:793–796, 2006. 2

[5] E. Betzig, G. H. Patterson, R. Sougrat, O. W. Lindwasser, S. Olenych, J. S. Bonifacino, M. D. Davidson, J. Lippincott-Schwartz, and H. F. Hess. Imaging intracellular fluorescent proteins at nanometer resolution. *Science*, 313(5793):1642–1645, 2006. doi: 10.1126/science.1127344. 2

[6] S. W. Hell and J. Wichmann. Breaking the diffraction resolution limit by stimulated emission: stimulated-emission-depletion fluorescence microscopy. *Opt. Lett.*, 19(11):780–782, 1994. doi: 10.1364/OL.19.000780. URL http://ol.osa.org/abstract.cfm?URI=ol-19-11-780. 2

[7] B. R. Smith, D. W. Inglis, B. Sandnes, J. R. Rabeau, A. V. Zvyagin, D. Gruber, C. J. Noble, R. Vogel, E. Ōsawa, and T. Plakhotnik. Five-nanometer diamond with luminescent nitrogen-vacancy defect centers. *Small*, 5(14):1649–1653, 2009. ISSN 1613-6829. doi: 10.1002/smll.200801802. URL http://dx.doi.org/10.1002/smll.200801802. 2, 30

[8] I. I. Vlasov, A. A. Shiryaev, T. Rendler, S. Steinert, S.-Y. Lee, D. Antonov, M. Vörös, F. Jelezko, A. V. Fisenko, L. F. Semjonova,

J. Biskupek, U. Kaiser, O.I. Lebedev, I. Sildos, P.R. Hemmer, V. I. Konov, A. Gali, and J. Wrachtrup. Molecular-sized fluorescent nanodiamonds. *Nature Nanotechnology*, 9:54–58, 2014. doi: 10.1038/nnano.2013.255. 2, 30

[9] Y. Wu, A. Ermakova, W. Liu, G. Pramanik, T.M. Vu, A. Kurz, L. McGuinness, B. Naydenov, S. Hafner, R. Reuter, J. Wrachtrup, J. Isoya, C. Frtsch, H. Barth, T. Simmet, F. Jelezko, and T. Weil. Programmable biopolymers for advancing biomedical applications of fluorescent nanodiamonds. *Advanced Functional Materials*, 25(42): 65766585, 2015. doi: 10.1002/adfm.201502704. 2, 60, 74

[10] V. A. Shershulin, V. S. Sedov, A. Ermakova, U. Jantzen, L. Rogers, A. A. Huhlina, E. G. Teverovskaya, V. G. Ralchenko, F. Jelezko, and I. I. Vlasov. Size-dependent luminescence of color centers in composite nanodiamonds. *physica status solidi (a)*, pages n/a–n/a, 2015. ISSN 1862-6319. doi: 10.1002/pssa.201532204. URL http://dx.doi.org/10.1002/pssa.201532204. 2, 29, 69, 75

[11] S. L Jacques. Optical properties of biological tissues: a review. *Physics in Medicine and Biology*, 58(11):R37, 2013. URL http://stacks.iop.org/0031-9155/58/i=11/a=R37. 2, 69

[12] D. B. Tretyakov, I. I. Beterov, V. M. Entin, and I. I. Ryabtsev. Cold atoms in optical lattices as qubits for a quantum computer. *Russian Microelectronics*, 35(2):74–77, 2006. ISSN 1608-3415. doi: 10.1134/S1063739706020028. URL http://dx.doi.org/10.1134/S1063739706020028. 2

[13] J. Clarke and F. K. Wilhelm. Superconducting quantum bits. *Nature*, 453:1031–1042, 2008. doi: 10.1038/nature07128. 2

[14] J. Gorman, D. G. Hasko, and D. A. Williams. Charge-qubit operation of an isolated double quantum dot. *Phys. Rev. Lett.*, 95:090502, 2005. doi: 10.1103/PhysRevLett.95.090502. URL http://link.aps.org/doi/10.1103/PhysRevLett.95.090502. 2

[15] A. Gruber, A. Drbenstedt, C. Tietz, L. Fleury, J. Wrachtrup, and C. von Borczyskowski. Scanning confocal optical microscopy and magnetic resonance on single defect centers. *Science*, 276(5321): 2012–2014, 1997. doi: 10.1126/science.276.5321.2012. URL http://www.sciencemag.org/content/276/5321/2012.abstract. 2, 8, 14, 17

[16] L. J. Rogers, K. D. Jahnke, M. H. Metsch, A. Sipahigil, J. M. Binder, T. Teraji, H. Sumiya, J. Isoya, M. D. Lukin, P. Hemmer, and F. Jelezko. All-optical initialization, readout, and coherent preparation of single silicon-vacancy spins in diamond. *Phys. Rev. Lett.*, 113:263602, 2014. doi: 10.1103/PhysRevLett.113.263602. URL http://link.aps.org/doi/10.1103/PhysRevLett.113.263602. 2, 28

[17] G. Balasubramanian, I. Y. Chan, R. Kolesov, M. Al-Hmoud, J. Tisler, C. Shin, C. Kim, A. Wojcik, P. R. Hemmer, A. Krueger, T. Hanke, A. Leitenstorfer, R. Bratschitsch, F. Jelezko, and J. Wrachtrup. Nanoscale imaging magnetometry with diamond spins under ambient conditions. *Nature*, 455:648–651, 2008. doi: 10.1038/nature07278. 2, 37, 38, 39, 88

[18] G. Balasubramanian, P. Neumann, D. Twitchen, M. Markham, R. Kolesov, N. Mizuochi, J. Isoya, J. Achard, J. Beck, Tissler. J., V Jacques, P. R. Hemmer, F. Jelezko, and J. Wrachtrup. Ultralong spin coherence time in isotopically engineered diamond. *Nature Materials*, 8:383–387, 2009. doi: 10.1038/nmat2420. 2, 39

[19] T. Staudacher, F. Shi, S. Pezzagna, J. Meijer, J. Du, C. A. Meriles, F. Reinhard, and J. Wrachtrup. Nuclear magnetic resonance spectroscopy on a $(5 - Nanometer)^3$ sample volume. *Science*, 339(6119): 561–563, 2013. doi: 10.1126/science.1231675. 2, 9, 37, 42, 77, 88

[20] H. J. Mamin, M. Kim, M. H. Sherwood, C. T. Rettner, K. Ohno, D. D. Awschalom, and D. Rugar. Nanoscale nuclear magnetic resonance with a nitrogen-vacancy spin sensor. *Science*, (6119):557–560, 2013. doi: 10.1126/science.1231540. 2, 9, 42, 77, 88

[21] A. Ermakova, G. Pramanik, J.-M. Cai, G. Algara-Siller, U. Kaiser, T. Weil, Y.-K. Tzeng, H. C. Chang, L. P. McGuinness, M. B. Plenio, B. Naydenov, and F. Jelezko. Detection of a few metallo-protein molecules using color centers in nanodiamonds. *Nano Letters*, 13(7): 3305–3309, 2013. doi: 10.1021/nl4015233. URL http://dx.doi.org/10.1021/nl4015233. PMID: 23738579. 3, 93

[22] M. C. Tappert R. Tappert. *Diamonds in Nature A Guide to Rough Diamonds*. Springer, 2011. 5

[23] Anke Krueger. *Carbon Materials and Nanotechnology*. Wiley, 2010. 5

[24] R. Robertson, Fox J. J., and Martin A. E. Two type of diamond. *Proc. R. Soc. A*, 232:463–535, 1934. 5, 9

[25] R. Robertson, Fox J. J., and Martin A. E. Further work on two types of diamond. *Proc. R. Soc. A*, 157(892):579–593, 1936. 5

[26] W. Kaiser and W. L. Bond. Nitrogen, a major impurity in common type i diamond. *Phys. Rev.*, 115(4):857–863, 1959. 5, 9

[27] C. M. Breeding and J. E. Shigley. The "type" classification system of diamonds and its imporrtance in gemology. *Gems & Gemology*, pages 96–111, 2009. 6

[28] F. P. Bundy, H. T. Hall, H. M. Strong, and R. H. Wentorf. Man-made diamonds. *Nature*, 176:5155, 1955. 6

[29] R. C. Burns, J. O. Hansen, R. A. Spits, M. Sibanda, C. M. Welbourn, and D. L. Welch. Growth of high purity large synthetic diamond crystals. *Diamond and Related Materials*, 8(89): 1433 – 1437, 1999. ISSN 0925-9635. doi: http://dx.doi.org/10.1016/S0925-9635(99)00042-4. URL http://www.sciencedirect.com/science/article/pii/S0925963599000424. 7

[30] C. Venkateswaran, K. Anbukumaran, . Victor Jaya, N, and S. Natarajan. Design and performance of a belt-type high pressure, high temperature apparatus. *Review of Scientific Instruments*, 68(1):189–192, 1997. doi: http://dx.doi.org/10.1063/1.1147807. URL http://scitation.aip.org/content/aip/journal/rsi/68/1/10.1063/1.1147807. 7

[31] Yu. N. Pal'yanov, A. G. Sokol, Yu. M. Borzdov, A. F. Khokhryakov, and N. V. Sobolev. Diamond formation from mantle carbonate fluids. *Nature*, 400:417–418, 1999. 7

[32] R. S. Balmer, J. R. Brandon, S. L. Clewes, H. K. Dhillon, J. M. Dodson, I. Friel, P. N. Inglis, T. D. Madgwick, M. L. Markham, T. P. Mollart, N. Perkins, G. A. Scarsbrook, D. J. Twitchen, A. J. Whitehead, J. J. Wilman, and S. M. Woollard. Chemical vapour deposition synthetic diamond: materials, technology and applications. *Journal of Physics: Condensed Matter*, 21(36):364221, 2009. URL http://stacks.iop.org/0953-8984/21/i=36/a=364221. 7

[33] Z.P. Belich L.A. Vasiliev. *Diamonds. Its properties and applications.* Moscow, Nedra, 1983. 7, 8

[34] W. C. Walker and J. Osantowski. Ultraviolet optical properties of diamond. *Phys. Rev.*, 134:A153–A157, 1964. doi: 10.1103/PhysRev.134.A153. URL http://link.aps.org/doi/10.1103/PhysRev.134.A153. 8

[35] W. Saslow, T. K. Bergstresser, and Marvin L. Cohen. Band structure and optical properties of diamond. *Phys. Rev. Lett.*, 16:354–356, 1966. doi: 10.1103/PhysRevLett.16.354. URL http://link.aps.org/doi/10.1103/PhysRevLett.16.354. 8

[36] A. T. Collins. The characterisation of point defects in diamond by luminescence spectroscopy. *Diamond and Related Materials*, 1 (56):457 – 469, 1992. ISSN 0925-9635. doi: http://dx.doi.org/10.1016/0925-9635(92)90146-F. URL http://www.sciencedirect.com/science/article/pii/092596359290146F. Proceedings of the Second European Conference on Diamond, Diamond-like and Related Coatings. 8

[37] A. M. Zaitsev. *Optical Properties of Diamond*. Springer-Verlag, 2001. 8, 9

[38] J. H. N. Loubser and J. A. van Wyk. Electron spin resonance in the study of diamond. *Reports on Progress in Physics*, 41(8):1201, 1978. URL http://stacks.iop.org/0034-4885/41/i=8/a=002. 8, 14

[39] D. A. Redman, S. Brown, R. H. Sands, and S. C. Rand. Spin dynamics and electronic states of N- V centers in diamond by epr and four-wave-mixing spectroscopy. *Phys. Rev. Lett.*, 67:3420–3423, 1991. doi: 10.1103/PhysRevLett.67.3420. URL http://link.aps.org/doi/10.1103/PhysRevLett.67.3420. 8, 14

[40] G. Davies and M. F. Hamer. Optical studies of the 1.945 ev vibronic band in diamond. *Proc. R. Soc. A*, 348:285–298, 1976. 8

[41] M. Orrit, J. Bernard, and R. I. Personov. High-resolution spectroscopy of organic molecules in solids: from fluorescence line narrowing and hole burning to single molecule spectroscopy. *The Journal of Physical Chemistry*, 97(40):10256–10268, 1993. doi: 10.1021/j100142a003. URL http://dx.doi.org/10.1021/j100142a003. 8

[42] F. Dolde, I. Jakobi, B. Naydenov, N. Zhao, S. Pezzagna, C. Trautmann, J. Meijer, P. Neumann, F Jelezko, and J Wrachtrup. Room-

temperature entanglement between single defect spins in diamond. *Nature Physics*, 9:139–143, 2013. doi: 10.1038/nphys2545. 9, 10

[43] L. T. Hall, G. C. G. Beart, E. A. Thomas, D. A. Simpson, L. P. McGuinness, L.H. Cole, J. H. Manton, R. E. Scholten, F Jelezko, Jrg Wrachtrup, S. Petrou, and Hollenberg L. C. L. High spatial and temporal resolution wide-field imaging of neuron activity using quantum nv-diamond. *Scientific Reports*, 2(401), 2012. doi: 10.1038/srep00401. 9

[44] J. Meijer, B. Burchard, M. Domhan, C. Wittmann, T. Gaebel, I. Popa, F. Jelezko, and J. Wrachtrup. Generation of single color centers by focused nitrogen implantation. *Applied Physics Letters*, 87(26):261909, 2005. doi: http://dx.doi.org/10.1063/1.2103389. URL http://scitation.aip.org/content/aip/journal/apl/87/26/10.1063/1.2103389. 9

[45] B. Naydenov, V. Richter, J. Beck, M. Steiner, P. Neumann, G. Balasubramanian, J. Achard, F. Jelezko, J. Wrachtrup, and R. Kalish. Enhanced generation of single optically active spins in diamond by ion implantation. *Applied Physics Letters*, 96 (16):163108, 2010. doi: http://dx.doi.org/10.1063/1.3409221. URL http://scitation.aip.org/content/aip/journal/apl/96/16/10.1063/1.3409221. 10

[46] T. Yamamoto, C. Müller, L. P. McGuinness, T. Teraji, B. Naydenov, Sh. Onoda, T. Ohshima, J. Wrachtrup, r Jelezko, F., and J Isoya. Strongly coupled diamond spin qubits by molecular nitrogen implantation. *Phys. Rev. B*, 88:201201, 2013. doi: 10.1103/PhysRevB.88.201201. URL http://link.aps.org/doi/10.1103/PhysRevB.88.201201. 10

[47] Susumu Namba, editor. *Ion Implantation in Semiconductors*. Springer, 1975. 10

[48] J. F. Prins. Vacancy diffusion and trapping in electron-irradiated type IaA diamonds. *Diamond and Related Materials*, 10(1):87 – 93, 2001. ISSN 0925-9635. doi: http://dx.doi.org/10.1016/S0925-9635(00)00425-8. URL http://www.sciencedirect.com/science/article/pii/S0925963500004258. 10

[49] I. Kiflawi, A. T. Collins, K. Iakoubovskii, and D. Fisher. Electron irradiation and the formation of vacancyinterstitial pairs in diamond.

Journal of Physics: Condensed Matter, 19(4):046216, 2007. URL http://stacks.iop.org/0953-8984/19/i=4/a=046216. 10

[50] A. Gali, M. Fyta, and E. Kaxiras. *Ab initio* supercell calculations on nitrogen-vacancy center in diamond: Electronic structure and hyperfine tensors. *Phys. Rev. B*, 77:155206, 2008. doi: 10.1103/PhysRevB.77.155206. URL http://link.aps.org/doi/10.1103/PhysRevB.77.155206. 11

[51] M. W. Doherty, N. B. Manson, P. Delaney, F. Jelezko, J. Wrachtrup, and L. C.L. Hollenberg. The nitrogen-vacancy colour centre in diamond. *Physics Reports*, 528(1):1 – 45, 2013. ISSN 0370-1573. doi: http://dx.doi.org/10.1016/j.physrep.2013.02.001. URL http://www.sciencedirect.com/science/article/pii/S0370157313000562. The nitrogen-vacancy colour centre in diamond. 11

[52] M. W. Doherty, J. Michl, F. Dolde, I. Jakobi, P. Neumann, N. B. Manson, and J. Wrachtrup. Measuring the defect structure orientation of a single nv^- centre in diamond. *New Journal of Physics*, 16 (6):063067, 2014. URL http://stacks.iop.org/1367-2630/16/i=6/a=063067. 11

[53] A. Batalov, V. Jacques, F. Kaiser, P. Siyushev, P. Neumann, L. J. Rogers, R. L. McMurtrie, N. B. Manson, F. Jelezko, and J. Wrachtrup. Low temperature studies of the excited-state structure of negatively charged nitrogen-vacancy color centers in diamond. *Phys. Rev. Lett.*, 102:195506, 2009. doi: 10.1103/PhysRevLett.102.195506. URL http://link.aps.org/doi/10.1103/PhysRevLett.102.195506. 11

[54] P. Neumann, R. Kolesov, V. Jacques, J. Beck, J. Tisler, A. Batalov, L. Rogers, N. B. Manson, G. Balasubramanian, F. Jelezko, and J. Wrachtrup. Excited-state spectroscopy of single NV defects in diamond using optically detected magnetic resonance. *New Journal of Physics*, 11(1):013017, 2009. URL http://stacks.iop.org/1367-2630/11/i=1/a=013017. 13, 15

[55] G. D. Fuchs, V. V. Dobrovitski, R. Hanson, A. Batra, C. D. Weis, T. Schenkel, and D. D. Awschalom. Excited-state spectroscopy using single spin manipulation in diamond. *Phys. Rev. Lett.*, 101:117601,

2008. doi: 10.1103/PhysRevLett.101.117601. URL http://link.aps.org/doi/10.1103/PhysRevLett.101.117601. 13

[56] L. J. Rogers, R. L. McMurtrie, M. J. Sellars, and N. B. Manson. Time-averaging within the excited state of the nitrogen-vacancy centre in diamond. *New Journal of Physics*, 11(6):063007, 2009. URL http://stacks.iop.org/1367-2630/11/i=6/a=063007. 13

[57] A. Batalov, C. Zierl, T. Gaebel, P. Neumann, I.-Y. Chan, G. Balasubramanian, P. R. Hemmer, F. Jelezko, and J. Wrachtrup. Temporal coherence of photons emitted by single nitrogen-vacancy defect centers in diamond using optical rabi-oscillations. *Phys. Rev. Lett.*, 100: 077401, 2008. doi: 10.1103/PhysRevLett.100.077401. URL http://link.aps.org/doi/10.1103/PhysRevLett.100.077401. 15

[58] J. R. Maze, A. Gali, E. Togan, Y. Chu, A. Trifonov, E. Kaxiras, and M. D. Lukin. Properties of nitrogen-vacancy centers in diamond: the group theoretic approach. *New Journal of Physics*, 13(2): 025025, 2011. URL http://stacks.iop.org/1367-2630/13/i=2/a=025025. 15

[59] J. Harrison, M. J. Sellars, and N. B. Manson. Optical spin polarisation of the N-V centre in diamond. *Journal of Luminescence*, 107 (14):245 – 248, 2004. ISSN 0022-2313. doi: http://dx.doi.org/10.1016/j.jlumin.2003.12.020. URL http://www.sciencedirect.com/science/article/pii/S0022231303001972. Proceedings of the 8th International Meeting on Hole Burning, Single Molecule, and Related Spectroscopies: Science and Applications. 16

[60] M. Steiner, P. Neumann, J. Beck, F. Jelezko, and J. Wrachtrup. Universal enhancement of the optical readout fidelity of single electron spins at nitrogen-vacancy centers in diamond. *Phys. Rev. B*, 81:035205, 2010. doi: 10.1103/PhysRevB.81.035205. URL http://link.aps.org/doi/10.1103/PhysRevB.81.035205. 16

[61] I. I. Rabi. Space quantization in a gyrating magnetic field. *Phys. Rev.*, 51:652–654, 1937. doi: 10.1103/PhysRev.51.652. URL http://link.aps.org/doi/10.1103/PhysRev.51.652. 20

[62] A. Jarmola, V. M. Acosta, K. Jensen, S. Chemerisov, and D. Budker. Temperature- and magnetic-field-dependent longitudinal spin relaxation in nitrogen-vacancy ensembles in diamond.

Phys. Rev. Lett., 108:197601, 2012. doi: 10.1103/PhysRevLett.108.197601. URL http://link.aps.org/doi/10.1103/PhysRevLett.108.197601. 22

[63] E. L. Hahn. Nuclear induction due to free larmor precession. *Phys. Rev.*, 77:297–298, 1950. doi: 10.1103/PhysRev.77.297.2. URL http://link.aps.org/doi/10.1103/PhysRev.77.297.2. 23

[64] E. L. Hahn. Spin echoes. *Phys. Rev.*, 80:580–594, 1950. doi: 10.1103/PhysRev.80.580. URL http://link.aps.org/doi/10.1103/PhysRev.80.580. 23, 40

[65] N. Bar-Gill, L. M. Pham, A. Jarmola, D. Budker, and R. L. Walsworth. Solid-state electronic spin coherence time approaching one second. *Nature Communications*, 4, 2013. 25

[66] H. S. Knowles, D. M. Kara, and M. Atatüre. Observing bulk diamond spin coherence in high-purity nanodiamonds. *Nature Materials*, 13 (21-25), 2014. doi: 10.1038/nmat3805. 25

[67] F. Jelezko and J. Wrachtrup. Single defect centres in diamond: A review. *physica status solidi (a)*, 203(13):3207–3225, 2006. ISSN 1862-6319. doi: 10.1002/pssa.200671403. URL http://dx.doi.org/10.1002/pssa.200671403. 25

[68] N. Mizuochi, T. Makino, H. Kato, D. Takeuchi, M. Ogura, H. Okushi, M. Nothaft, P. Neumann, A. Gali, F. Jelezko, J. Wrachtrup, and S. Yamasaki. Electrically driven single-photon source at room temperature in diamond. *Nature Photonics*, 6:299–303, 2012. doi: 10.1038/nphoton.2012.75. 25

[69] B. Grotz, M. V. Hauf, M. Dankerl, B. Naydenov, S. Pezzagna, J. Meijer, F. Jelezko, J Wrachtrup, M. Stutzmann, F. Reinhard, and J. A. Garrido. Charge state manipulation of qubits in diamond. *Nature Communications*, 3:729, 2012. doi: 10.1038/ncomms1729. 25

[70] N. C. Shaner, P. A Steinbach, and R. Y. Tsien. A guide to choosing fluorescent proteins. *Nature Methods*, 2:905–909, 2005. doi: 10.1038/nmeth819. 25, 33, 34

[71] J. Tang and R. A. Marcus. Mechanisms of fluorescence blinking in semiconductor nanocrystal quantum dots. *The Journal of Chemical Physics*, 123(5):054704, 2005. doi: http://dx.doi.org/10.

1063/1.1993567. URL http://scitation.aip.org/content/aip/journal/jcp/123/5/10.1063/1.1993567. 25

[72] P. Siyushev, H. Pinto, M. Vörös, A. Gali, F. Jelezko, and J. Wrachtrup. Optically controlled switching of the charge state of a single nitrogen-vacancy center in diamond at cryogenic temperatures. *Phys. Rev. Lett.*, 110:167402, 2013. doi: 10.1103/PhysRevLett.110.167402. URL http://link.aps.org/doi/10.1103/PhysRevLett.110.167402. 25

[73] G. Waldherr, J. Beck, M. Steiner, P. Neumann, A. Gali, Th. Frauenheim, F. Jelezko, and J. Wrachtrup. Dark states of single nitrogen-vacancy centers in diamond unraveled by single shot nmr. *Phys. Rev. Lett.*, 106:157601, 2011. doi: 10.1103/PhysRevLett.106.157601. URL http://link.aps.org/doi/10.1103/PhysRevLett.106.157601. 25

[74] J. Tisler, T. Oeckinghaus, R. J. Stöhr, R. Kolesov, R. Reuter, F. Reinhard, and J. Wrachtrup. Single defect center scanning near-field optical microscopy on graphene. *Nano Lett.*, 13(7):3152–3156, 2013. doi: 10.1021/nl401129m. URL http://dx.doi.org/10.1021/nl401129m. PMID: 23795752. 25

[75] M. V. Hauf, B. Grotz, B. Naydenov, M. Dankerl, S. Pezzagna, J. Meijer, F. Jelezko, J. Wrachtrup, M. Stutzmann, F. Reinhard, and J. A. Garrido. Chemical control of the charge state of nitrogen-vacancy centers in diamond. *Phys. Rev. B*, 83:081304, 2011. doi: 10.1103/PhysRevB.83.081304. URL http://link.aps.org/doi/10.1103/PhysRevB.83.081304. 25, 69

[76] V. Petrakova, A. Taylor, I. Kratochvilova, F. Fendrych, J. Vacik, J. Kucka, J. Stursa, P. Cigler, M. Ledvina, A. Fiserova, P. Kneppo, and M. Nesladek. Luminescence of nanodiamond driven by atomic functionalization: Towards novel detection principles. *Adv. Funct. Mater.*, 22(4):812–819, 2012. ISSN 1616-3028. doi: 10.1002/adfm.201101936. URL http://dx.doi.org/10.1002/adfm.201101936. 25, 26, 30

[77] C. Osterkamp, J. Lang, J. Scharpf, C. Mller, L. P. McGuinness, T. Diemant, R. J. Behm, B. Naydenov, and F. Jelezko. Stabilizing shallow color centers in diamond created by nitrogen delta-doping using sf6 plasma treatment. *Appl. Phys.*

Lett., 106(11):113109, 2015. doi: http://dx.doi.org/10.1063/1.4915305. URL http://scitation.aip.org/content/aip/journal/apl/106/11/10.1063/1.4915305. 25, 69

[78] J. P. Goss, R. Jones, S. J. Breuer, P. R. Briddon, and S. Öberg. The twelve-line 1.682 ev luminescence center in diamond and the vacancy-silicon complex. *Phys. Rev. Lett.*, 77:3041–3044, 1996. doi: 10.1103/PhysRevLett.77.3041. URL http://link.aps.org/doi/10.1103/PhysRevLett.77.3041. 26

[79] S. S. Moliver. Electronic structure of neutral siliconvacancy complex in diamond. *Zhurnal Tekhnicheskoí Fiziki*, 73(11):9094, 2003. in Russian. 26

[80] M. Stammler, H. Eisenbei, J. Ristein, J. Neubauer, M. Gbbels, and L. Ley. Growth of high-quality homoepitaxial diamond films by HF-CVD. *Diamond and Related Materials*, 11(36):504 – 508, 2002. ISSN 0925-9635. doi: http://dx.doi.org/10.1016/S0925-9635(01)00627-6. URL http://www.sciencedirect.com/science/article/pii/S0925963501006276. 12th European Conference on Diamond, Diamond- Like Materials, Carbon Nanotubes, Nitrides & Silicon Carbide. 26

[81] S. Tamura, G. Koike, A. Komatsubara, T. Teraji, S. Onoda, L. P. McGuinness, L. Rogers, B. Naydenov, E. Wu, L. Yan, F. Jelezko, T. Ohshima, J. Isoya, T. Shinada, and T. Tanii. Array of bright silicon-vacancy centers in diamond fabricated by low-energy focused ion beam implantation. *Applied Physics Express*, 7(11):115201, 2014. URL http://stacks.iop.org/1882-0786/7/i=11/a=115201. 26

[82] C. Hepp, T. Müller, V. Waselowski, J. N. Becker, B. Pingault, H. Sternschulte, D. Steinmüller-Nethl, A. Gali, J. R. Maze, M. Atatüre, and C. Becher. Electronic structure of the silicon vacancy color center in diamond. *Phys. Rev. Lett.*, 112:036405, 2014. doi: 10.1103/PhysRevLett.112.036405. URL http://link.aps.org/doi/10.1103/PhysRevLett.112.036405. 26, 27

[83] V. S. Vavilov, A. A. Gippius, A. M. Zaitsev, B. V. Deryagin, B. V. Spitsyn, and A. E. Aleksenko. Investigation of the cathodoluminescence of epitaxial diamond films. *Soviet Physics: Semiconductors*, 14:1078–1079, 1980. ISSN 1063-7826. 26

[84] U. F. S. D'Haenens-Johansson, A. M. Edmonds, B. L. Green, M. E. Newton, G. Davies, P. M. Martineau, R. U. A. Khan, and D. J. Twitchen. Optical properties of the neutral silicon split-vacancy center in diamond. *Phys. Rev. B*, 84:245208, 2011. doi: 10.1103/PhysRevB.84.245208. URL http://link.aps.org/doi/10.1103/PhysRevB.84.245208. 26

[85] C. D. Clark, H. Kanda, I. Kiflawi, and G. Sittas. Silicon defects in diamond. *Phys. Rev. B*, 51:16681–16688, 1995. doi: 10.1103/PhysRevB.51.16681. URL http://link.aps.org/doi/10.1103/PhysRevB.51.16681. 26

[86] L. J. Rogers, K. D. Jahnke, M. W. Doherty, A. Dietrich, L. P. McGuinness, C. Müller, T. Teraji, H. Sumiya, J. Isoya, N. B. Manson, and F. Jelezko. Electronic structure of the negatively charged silicon-vacancy center in diamond. *Phys. Rev. B*, 89:235101, 2014. doi: 10.1103/PhysRevB.89.235101. URL http://link.aps.org/doi/10.1103/PhysRevB.89.235101. 26

[87] B. Pingault, J. N. Becker, C. H. H. Schulte, C. Arend, C. Hepp, T. Godde, A. I. Tartakovskii, M. Markham, C. Becher, and M. Atatüre. All-optical formation of coherent dark states of silicon-vacancy spins in diamond. *Phys. Rev. Lett.*, 113:263601, 2014. doi: 10.1103/PhysRevLett.113.263601. URL http://link.aps.org/doi/10.1103/PhysRevLett.113.263601. 28

[88] S. Wan, R. R. Anderson, and J. A. Parrish. Analytical modeling for the optical properties of the skin with in vitro and in vivo applications. *Photochemistry and Photobiology*, 34(4):493–499, 1981. ISSN 1751-1097. doi: 10.1111/j.1751-1097.1981.tb09030.x. URL http://dx.doi.org/10.1111/j.1751-1097.1981.tb09030.x. 28

[89] R. S. Lewis, T. Ming, J. F. Wacker, E. Anders, and E. Steel. Interstellar diamonds in meteorites. *Nature*, 326:160–162, 1987. doi: 10.1038/326160a0. 28

[90] M. Jerofejeff and P. Latschinoff. Der meteorit von Nowo-Ure. *Zapiski Rossijskogo Mineralogicheskogo obshchestva*, 24(1):263–294, 1888. 28

[91] R. Berman and J. Thewlis. The graphitediamond equilibrium. *Nature*, 176:834–836, 1955. doi: 10.1038/176834b0. 28

[92] J.-P. Boudou, P. A. Curmi, F. Jelezko, J. Wrachtrup, P. Aubert, M. Sennour, G. Balasubramanian, R. Reuter, A. Thorel, and E. Gaffet. High yield fabrication of fluorescent nanodiamonds. *Nanotechnology*, 20(23):235602, 2009. URL http://stacks.iop.org/0957-4484/20/i=23/a=235602. 28, 30

[93] P. S. De Carli and J. C. Jamieson. Formation of diamond by explosive shock. *Science*, 133(3467):1821–1822, 1961. doi: 10.1126/science.133.3467.1821. 28

[94] V.V. Danilenko. Thermodynamics of graphite to diamond transformation. *Fizika Goreniya i Vzryva*, 5:137–142, 1988. 28

[95] V. F. Anisichkin and I. Ju. Malkov. Thermodynamical stability of superdispersed diamond form. *Fizika Goreniya i Vzryva*, 5:135–137, 1988.

[96] N. R. Greiner, D. S. Phillips, J. D. Johnson, and F. Volk. Diamonds in detonation soot. *Nature*, 333:440–442, 1988. doi: 10.1038/333440a0. 28

[97] K. V. Volkov, V. V. Danilenko, and V. I. Elin. Diamond synthesis from the carbon of detonation products. *Fizika Goreniya i Vzryva*, 26:123–125, 1990. 28, 29

[98] V. N. Mochalin, O. Shenderova, D. Ho, and Yu. Gogotsi. The properties and applications of nanodiamonds. *Nat. Nanotechnol.*, 7:11–23, 2012. doi: 10.1038/nnano.2011.209. 28

[99] J. E. Butler and A.V. Sumant. The CVD of nanodiamond materials. *Chemical Vapor Deposition*, 14(7-8):145–160, 2008. doi: 10.1002/cvde.200700037. 29

[100] HOSOKAWA ALPINE Aktiengesellschaft. URL https://www.hosokawa-alpine.com. (Accessed 08.12.2016). 30

[101] FRITSCH GmbH. URL http://www.fritsch-milling.com. (Accessed 08.12.2016). 30

[102] Microdiamant AG. URL http://www.microdiamant.com/. (Accessed 08.12.2016). 30

[103] G. Dantelle, A. Slablab, L. Rondin, F. Lain, F. Carrel, Ph. Bergonzo, S. Perruchas, T. Gacoin, F. Treussart, and J.-F. Roch. Efficient

production of NV colour centres in nanodiamonds using high-energy electron irradiation. *Journal of Luminescence*, 130(9):1655 – 1658, 2010. ISSN 0022-2313. doi: http://dx.doi.org/10.1016/j.jlumin.2009.12.003. URL http://www.sciencedirect.com/science/article/pii/S0022231309005985. Special Issue based on the Proceedings of the Tenth International Meeting on Hole Burning, Single Molecule, and Related Spectroscopies: Science and Applications (HBSM 2009) - Issue dedicated to Ivan Lorgere and Oliver Guillot-Noel. 30

[104] J.-P. Boudou, J. Tisler, R. Reuter, A. Thorel, P. A. Curmi, F. Jelezko, and J. Wrachtrup. Fluorescent nanodiamonds derived from HPHT with a size of less than 10 nm. *Diamond and Related Materials*, 37:80 – 86, 2013. ISSN 0925-9635. doi: http://dx.doi.org/10.1016/j.diamond.2013.05.006. URL http://www.sciencedirect.com/science/article/pii/S0925963513001064. 30

[105] T. Gaebel, C. Bradac, J. Chen, J. M. Say, L. Brown, P. Hemmer, and J. R. Rabeau. Size-reduction of nanodiamonds via air oxidation. *Diamond and Related Materials*, 21:28 – 32, 2012. ISSN 0925-9635. doi: http://dx.doi.org/10.1016/j.diamond.2011.09.002. URL http://www.sciencedirect.com/science/article/pii/S0925963511003116. 30

[106] C. Bradac, T. Gaebel, C. I. Pakes, J. M. Say, A. V. Zvyagin, and J. R. Rabeau. Effect of the nanodiamond host on a nitrogen-vacancy color-centre emission state. *Small*, 9(1):132–139, 2013. ISSN 1613-6829. doi: 10.1002/smll.201200574. URL http://dx.doi.org/10.1002/smll.201200574. 30

[107] A. Kruger, Y. Liang, G. Jarre, and J. Stegk. Surface functionalisation of detonation diamond suitable for biological applications. *J. Mater. Chem.*, 16:2322–2328, 2006. doi: 10.1039/B601325B. URL http://dx.doi.org/10.1039/B601325B. 31

[108] V. R. Dhanak, Yu. V. Butenko, A. C. Brieva, P. R. Coxon, L. Alves, and L. Siller. Chemical functionalization of nanodiamond by amino groups: An X-ray photoelectron spectroscopy study. *J. Nanosci. Nanotechnol.*, 12(4):3084–3090, 2012. doi: http://dx.doi.org/10.1166/jnn.2012.4547. 31

[109] A. S. Karakoti, R. Shukla, R. Shanker, and S. Singh. Surface functionalization of quantum dots for biological applica-

tions. *Advances in Colloid and Interface Science*, 215:28 – 45, 2015. ISSN 0001-8686. doi: http://dx.doi.org/10.1016/j.cis.2014.11.004. URL http://www.sciencedirect.com/science/article/pii/S0001868614002887. 31

[110] J. Zhou, J. Ralston, R. Sedev, and D. A. Beattie. Functionalized gold nanoparticles: Synthesis, structure and colloid stability. *Journal of Colloid and Interface Science*, 331(2):251 – 262, 2009. ISSN 0021-9797. doi: http://dx.doi.org/10.1016/j.jcis.2008.12.002. URL http://www.sciencedirect.com/science/article/pii/S0021979708016019. 31

[111] A. M. Schrand, H. Huang, C. Carlson, J. J. Schlager, E. Ōsawa, S. M. Hussain, and L. Dai. Are diamond nanoparticles cytotoxic? *The Journal of Physical Chemistry B*, 111(1):2–7, 2007. doi: 10.1021/jp066387v. URL http://dx.doi.org/10.1021/jp066387v. PMID: 17201422. 31, 35, 51

[112] K. M. Tsoi, Q. Dai, B. A. Alman, and W. C. W. Chan. Are quantum dots toxic? exploring the discrepancy between cell culture and animal studies. *Accounts of Chemical Research*, 46(3):662–671, 2013. doi: 10.1021/ar300040z. URL http://dx.doi.org/10.1021/ar300040z. PMID: 22853558. 31

[113] A. M. Alkilany and C. J. Murphycorresponding. Toxicity and cellular uptake of gold nanoparticles: what we have learned so far? *J Nanopart Res.*, 12(7):2313–2333, 2010. doi: 10.1007/s11051-010-9911-8. 31

[114] O. Shimomura, F. H. Johnson, and Y. Saiga. Extraction, purification and properties of aequorin, a bioluminescent protein from the luminous hydromedusan, aequorea. *Journal of Cellular and Comparative Physiology*, 59(3):223–239, 1962. doi: 10.1002/jcp.1030590302. 33

[115] R. H. Valdivia, A. E. Hromockyj, D. Monack, L. Ramakrishnan, and S. Falkow. Applications for green fluorescent protein (GFP) in the study of hostpathogen interactions. *Gene*, 173(1):47 – 52, 1996. ISSN 0378-1119. doi: http://dx.doi.org/10.1016/0378-1119(95)00706-7. URL http://www.sciencedirect.com/science/article/pii/0378111995007067. Flourescent Proteins and Applications. 33

[116] M. Zimmer. Green fluorescent protein (GFP): Applications, structure, and related photophysical behavior. *Chem. Rev.*, 102(3):759–782, 2002. doi: 10.1021/cr010142r. URL http://dx.doi.org/10.1021/cr010142r. PMID: 11890756. 33

[117] Thermo Fisher Scientific Inc. URL https://www.lifetechnologies.com. (Accessed 08.12.2016). 33, 34

[118] N. E. Conway and L. W. McLaughlin. The covalent attachment of multiple fluorophores to DNA containing phosphorothioate diesters results in highly sensitive detection of single-stranded DNA. *Bioconjug. Chem.*, 2(6):452–457, 1991. doi: 10.1021/bc00012a013. URL http://dx.doi.org/10.1021/bc00012a013. 33

[119] C. I. Stains, J. R. Porter, A. T. Ooi, D. J. Segal, and I. Ghosh. DNA sequence-enabled reassembly of the green fluorescent protein. *J. Am. Chem. Soc.*, 127(31):10782–10783, 2005. doi: 10.1021/ja051969w. URL http://dx.doi.org/10.1021/ja051969w. PMID: 16076155.

[120] R. Wombacher and V. W. Cornish. Chemical tags: Applications in live cell fluorescence imaging. *Journal of Biophotonics*, 4(6):391–402, 2011. ISSN 1864-0648. doi: 10.1002/jbio.201100018. URL http://dx.doi.org/10.1002/jbio.201100018.

[121] B. A. Armitage. Imaging of {RNA} in live cells. *Current Opinion in Chemical Biology*, 15(6):806 – 812, 2011. ISSN 1367-5931. doi: http://dx.doi.org/10.1016/j.cbpa.2011.10.006. URL http://www.sciencedirect.com/science/article/pii/S1367593111001530. Molecular Imaging. 33

[122] H.-A. Wagenknecht. Fluorescent DNA base modifications and substitutes: Multiple fluorophore labeling and the DETEQ concept. *Ann. N. Y. Acad. Sci.*, 1130(1):122–130, 2008. ISSN 1749-6632. doi: 10.1196/annals.1430.001. URL http://dx.doi.org/10.1196/annals.1430.001. 33

[123] Z. Gong, J. He, B. Ju, T.J. Lam, Y. Xu, and T. Yan. Sale of transgenic fish that express gene encoding fluorescent protein, November 16 2010. URL http://www.google.com/patents/US7834239. US Patent 7,834,239. 34

[124] R. Alford, H. M. Simpson, J. Duberman, G. C. Hill, M. Ogawa, C. Regino, H. Kobayashi, and P. L. Choyke. Toxicity of organic

fluorophores used in molecular imaging: Literature review. *Mol. Imaging*, 8(6):341–354, 2009. 34

[125] A. I. Ekimov and A. A. Onushchenko. Quantum size effect in the three dimensional semiconductor microcrystals. *Pisma v JETF*, 34 (6):363–366, 1981. in Russian. 34

[126] N. F. Johnson. Quantum dots: few-body, low-dimensional systems. *J. Phys.: Condens. Matter*, 7(6):965, 1995. URL http://stacks.iop.org/0953-8984/7/i=6/a=005. 34

[127] B. O. Dabbousi, J. Rodriguez-Viejo, F. V. Mikulec, J. R. Heine, H. Mattoussi, R. Ober, K. F. Jensen, and M. G. Bawendi. (CdSe)ZnS core-shell quantum dots: Synthesis and characterization of a size series of highly luminescent nanocrystallites. *The Journal of Physical Chemistry B*, 101(46):9463–9475, 1997. doi: 10.1021/jp971091y. URL http://dx.doi.org/10.1021/jp971091y. 34

[128] W.-S. Chae, T. D. T. Ung, and Q. L. Nguyen. Time-resolved photoluminescence and photostability of single semiconductor quantum dots. *Advances in Natural Sciences: Nanoscience and Nanotechnology*, 4(4):045009, 2013. URL http://stacks.iop.org/2043-6262/4/i=4/a=045009. 34

[129] U. Resch-Genger, M. Grabolle, S. Cavaliere-Jaricot, R. Nitschke, and T. Nann. Quantum dots versus organic dyes as fluorescent labels. *Nat. Methods*, 5:763–775, 2008. doi: 10.1038/nmeth.1248. 34

[130] R. Hardmann. A toxicologic review of quantum dots: Toxicity depends on physicochemical and environmental factors. *Environ Health Perspect.*, 114(2):165–175, 2006. doi: 10.1289/ehp.8284. 35

[131] D. D. Evanoff and G. Chumanov. Synthesis and optical properties of silver nanoparticles and arrays. *ChemPhysChem*, 6(7):1221–1231, 2005. ISSN 1439-7641. doi: 10.1002/cphc.200500113. URL http://dx.doi.org/10.1002/cphc.200500113. 35

[132] J. Turkevich, P. C. Stevenson, and J. Hillier. A study of the nucleation and growth processes in the synthesis of colloidal gold. *Discuss. Faraday Soc.*, 11:55–75, 1951. doi: 10.1039/DF9511100055. URL http://dx.doi.org/10.1039/DF9511100055. 35

[133] X. Huang and M. A. El-Sayed. Gold nanoparticles: Optical properties and implementations in cancer diagnosis and photothermal therapy. *Journal of Advanced Research*, 1(1):13 – 28, 2010. ISSN 2090-1232. doi: http://dx.doi.org/10.1016/j.jare.2010.02.002. URL http://www.sciencedirect.com/science/article/pii/S2090123210000056. 35

[134] S. K. Balasubramanian, L. Yang, L.-Y. L. Yung, C.-N. Ong, W.-Y. Ong, and L. E. Yu. Characterization, purification, and stability of gold nanoparticles. *Biomaterials*, 31(34):9023 – 9030, 2010. ISSN 0142-9612. doi: http://dx.doi.org/10.1016/j.biomaterials.2010.08.012. 35

[135] A. Das, R. Chadha, N. Maiti, and S. Kapoor. Synthesis of pH sensitive gold nanoparticles for potential application in radiosensitization. *Materials Science and Engineering: C*, 55:34 – 41, 2015. ISSN 0928-4931. doi: http://dx.doi.org/10.1016/j.msec.2015.05.048. URL http://www.sciencedirect.com/science/article/pii/S0928493115300990. 35

[136] G. B. Braun, T. Friman, H.-B. Pang, A. Pallaoro, T. H. de Mendoza, A.-M. A. Willmore, an Mann A. P. Kotamraju, V. R., Z.-G. She, K. N. Sugahara, N. O. Reich, T. Teesalu, and E. Ruoslahti. Etchable plasmonic nanoparticle probes to image and quantify cellular internalization. *Nat. Mater.*, 13:904–911, 2014. doi: 10.1038/nmat3982. 35

[137] J. I. Chao, C. C. Chang, and C. L. Cheng. Interaction and toxicity of nanodiamonds in human cells. *The FASEB Journal.*, 20(A75), 2006. 35, 51

[138] H.-D. Wang, C. Hui Niu, Q. Yang, and I. Badea. Study on protein conformation and adsorption behaviors in nanodiamond particleprotein complexes. *Nanotechnology*, 22(14):145703, 2011. URL http://stacks.iop.org/0957-4484/22/i=14/a=145703. 35

[139] O. Faklaris, V. Joshi, T. Irinopoulou, P. Tauc, M. Sennour, H. Girard, C. Gesset, J.-C. Arnault, A. Thorel, J. P. Boudou, P. A. Curmi, and F. Treussart. Photoluminescent diamond nanoparticles for cell labeling: Study of the uptake mechanism in mammalian cells. *ACS Nano*, 3(12):3955–3962, 2009. doi: 10.1021/nn901014j. URL http://dx.doi.org/10.1021/nn901014j. PMID: 19863087. 35, A

[140] L. Kou, J. Sun, Y. Zhai, and Z. He. The endocytosis and intracellular fate of nanomedicines: Implication for rational design. *Asian Journal of Pharmaceutical Sciences*, 8(1):1 – 10, 2013. ISSN 1818-0876. doi: http://dx.doi.org/10.1016/j.ajps.2013.07.001. URL http://www.sciencedirect.com/science/article/pii/S1818087613000020. 35, C

[141] K.-K. Liu, C.-C. Wang, C.-L. Cheng, and J.-I. Chao. Endocytic carboxylated nanodiamond for the labeling and tracking of cell division and differentiation in cancer and stem cells. *Biomaterials*, 30(26):4249 – 4259, 2009. ISSN 0142-9612. doi: http://dx.doi.org/10.1016/j.biomaterials.2009.04.056. URL http://www.sciencedirect.com/science/article/pii/S0142961209004682. 35

[142] E. Perevedentseva, C.-Y. Cheng, P.-H. Chung, J.-S. Tu, Y.-H. Hsieh, and C.-L. Cheng. The interaction of the protein lysozyme with bacteria e. coli observed using nanodiamond labelling. *Nanotechnology*, 18(31):315102, 2007. URL http://stacks.iop.org/0957-4484/18/i=31/a=315102. 35

[143] J. Wehling, R. Dringen, R. N. Zare, M. Maas, and K. Rezwan. Bactericidal activity of partially oxidized nanodiamonds. *ACS Nano*, 8(6):6475–6483, 2014. doi: 10.1021/nn502230m. URL http://dx.doi.org/10.1021/nn502230m. PMID: 24861876. 35

[144] Chi-Cheng Fu, Hsu-Yang Lee, Kowa Chen, Tsong-Shin Lim, Hsiao-Yun Wu, Po-Keng Lin, Pei-Kuen Wei, Pei-Hsi Tsao, Huan-Cheng Chang, and Wunshain Fann. Characterization and application of single fluorescent nanodiamonds as cellular biomarkers. *Proc Natl Acad Sci U S A.*, 104(3):727–759, 2007. 35

[145] K. Solarska-Sciuk, A. Gajewska, S. Glinska, M. Studzian, S. Michlewska, L. Balcerzak, J. Skolimowski, B. Kolago, and G. Bartosz. Intracellular transport of nanodiamond particles in human endothelial and epithelial cells. *Chemico-Biological Interactions*, 219:90 – 100, 2014. ISSN 0009-2797. doi: http://dx.doi.org/10.1016/j.cbi.2014.05.013. URL http://www.sciencedirect.com/science/article/pii/S0009279714001719. 35

[146] N. Mohan, C.-S. Chen, H.-H. Hsieh, Y.-C. Wu, and H.-C. Chang. In vivo imaging and toxicity assessments of fluorescent nanodiamonds in caenorhabditis elegans. *Nano Letters*, 10(9):3692–3699, 2010. doi:

10.1021/nl1021909. URL http://dx.doi.org/10.1021/nl1021909. PMID: 20677785. 35

[147] V. Vaijayanthimala, P.-Y. Cheng, S.-H. Yeh, K.-K. Liu, C.-H. Hsiao, J.-I Chao, and H.-C. Chang. The long-term stability and biocompatibility of fluorescent nanodiamond as an in vivo contrast agent. *Biomaterials*, 33(31):7794 – 7802, 2012. ISSN 0142-9612. doi: http://dx.doi.org/10.1016/j.biomaterials.2012.06.084. URL http://www.sciencedirect.com/science/article/pii/S014296121200748X. 35

[148] M. E. Davis, Z. (G.) Chen, and D. M. Shin. Nanoparticle therapeutics: an emerging treatment modality for cancer. *Nat. Rev. Drug Discovery*, 7:771–782, 2008. 36, 59

[149] L. Zhang, D. Pornpattananangkul, C.-M. J. Hu, and C.-M. Huang. Development of nanoparticles for antimicrobial drug delivery. *Current Medicinal Chemistry*, 17(6):585–594, 2010. doi: 10.2174/092986710790416290.

[150] J. L. Markman, A. Rekechenetskiy, E. Holler, and J. Y. Ljubimova. Nanomedicine therapeutic approaches to overcome cancer drug resistance. *Advanced Drug Delivery Reviews*, 65(1314):1866 – 1879, 2013. ISSN 0169-409X. doi: http://dx.doi.org/10.1016/j.addr.2013.09.019. URL http://www.sciencedirect.com/science/article/pii/S0169409X13002329. Nanotechnology and drug resistance.

[151] T. Sun, Y. Sh. Zhang, B. Pang, D. C. Hyun, M. Yang, and Y. Xia. Engineered nanoparticles for drug delivery in cancer therapy. *Angewandte Chemie International Edition*, 53(46):12320–12364, 2014. ISSN 1521-3773. doi: 10.1002/anie.201403036. URL http://dx.doi.org/10.1002/anie.201403036. 36, 59

[152] T. M. Allen and P. R. Cullis. Liposomal drug delivery systems: From concept to clinical applications. *Advanced Drug Delivery Reviews*, 65(1):36 – 48, 2013. ISSN 0169-409X. doi: http://dx.doi.org/10.1016/j.addr.2012.09.037. URL http://www.sciencedirect.com/science/article/pii/S0169409X12002980. Advanced Drug Delivery: Perspectives and Prospects. 36

[153] T. Minko. Soluble polymer conjugates for drug delivery. *Drug Discovery Today: Technologies*, 2(1):15 – 20, 2005.

ISSN 1740-6749. doi: http://dx.doi.org/10.1016/j.ddtec.2005.05.005. URL http://www.sciencedirect.com/science/article/pii/S1740674905000107. 36

[154] E. Fleige, M. A. Quadir, and R. Haag. Stimuli-responsive polymeric nanocarriers for the controlled transport of active compounds: Concepts and applications. *Advanced Drug Delivery Reviews*, 64(9): 866 – 884, 2012. ISSN 0169-409X. doi: http://dx.doi.org/10.1016/j.addr.2012.01.020. URL http://www.sciencedirect.com/science/article/pii/S0169409X12000257. Approaches to drug delivery based on the principles of supramolecular chemistry. 36, 59

[155] I. F. Tannock and D. Rotin. Acid pH in tumors and its potential for therapeutic exploitation. *Cancer Res.*, 49(16):4373–4384, 1989. 36, 59

[156] R. Arvizo, R. Bhattacharya, and P. Mukherjee. Gold nanoparticles: Opportunities and challenges in nanomedicine. *Expert opinion on drug delivery*, 7(6):753–763, 2010. doi: 10.1517/17425241003777010. 36

[157] C. E. Probst, P. Zrazhevskiy, V. Bagalkot, and X. Gao. Quantum dots as a platform for nanoparticle drug delivery vehicle design. *Advanced Drug Delivery Reviews*, 65(5):703 – 718, 2013. ISSN 0169-409X. doi: http://dx.doi.org/10.1016/j.addr.2012.09.036. URL http://www.sciencedirect.com/science/article/pii/S0169409X12002979. Inorganic nanoparticle platforms. 36

[158] S. Della Penna, C. Del Gratta, C. Granata, A. Pasquarelli, V. Pizzella, R. Rossi, M. Russo, K. Torquati, and S. N. Erne. Biomagnetic system for clinican use. *Philosophical Magazine B*, 80(5): 937–948, 2000. 37

[159] M. S. Grinolds, S. Hong, P. Maletinsky, L. Luan, M. D. Lukin, R. L. Walsworth, and A. Yacoby. Nanoscale magnetic imaging of a single electron spin under ambient conditions. *Nature Physics*, 9:215–219, 2013. doi: 10.1038/NPHYS2543. 37

[160] M. Loretz, T. Rosskopf, J. M. Boss, S. Pezzagna, J. Meijer, and L. D. Degen. Single-proton spin detection by diamond magnetometry. *Science*, 347(6218):139, 2014. doi: 10.1126/science.1259464. 37

[161] L. P. McGuinness, Y. Yan, A. Stacey, D. A. Simpson, L. T. Hall, D. Maclaurin, S. Prawer, P. Mulvaney, J Wrachtrup, F Caruso, R. E. Scholten, and L. C. L. Hollenberg. Quantum measurement and orientation tracking of fluorescent nanodiamonds inside living cells. *Nature Nanotechnology*, 6:358363, 2011. doi: 10.1038/nnano.2011.64. 37

[162] C. Degen. Nanoscale magnetometry: Microscopy with single spins. *Nature Nanotechnology*, 3:643–644, 2008. doi: 10.1038/nnano.2008.328. 38

[163] V. Ivády, T. Simon, J. R. Maze, I. A. Abrikosov, and A. Gali. Pressure and temperature dependence of the zero-field splitting in the ground state of NV centers in diamond: A first-principles study. *Phys. Rev. B*, 90:235205, 2014. doi: 10.1103/PhysRevB.90.235205. URL http://link.aps.org/doi/10.1103/PhysRevB.90.235205. 38

[164] M. Auzinsh, D. Budker, D. F. Kimball, S. M. Rochester, J. E. Stalnaker, A. O. Sushkov, and V. V. Yashchuk. Can a quantum nondemolition measurement improve the sensitivity of an atomic magnetometer? *Phys. Rev. Lett.*, 93:173002, 2004. doi: 10.1103/PhysRevLett.93.173002. URL http://link.aps.org/doi/10.1103/PhysRevLett.93.173002. 39

[165] J. M. Taylor, P. Cappellaro, L. Childress, L. Jiang, D. Budker, P. R. Hemmer, A. Yacoby, R. Walsworth, and M. D. Lukin. High-sensitivity diamond magnetometer with nanoscale resolution. *Nature Physics*, 4:810–816, 2008. doi: 10.1038/nphys1075. 39, 40, 41

[166] L. Childress, M. V. Gurudev Dutt, J. M. Taylor, A. S. Zibrov, F. Jelezko, J. Wrachtrup, P. R. Hemmer, and M. D. Lukin. Coherent dynamics of coupled electron and nuclear spin qubits in diamond. *Science*, 314:281–285, 2006. doi: 10.1126/science.1131871. 40

[167] D. E. Chang, A. S. Sørensen, P. R. Hemmer, and M. D. Lukin. Quantum optics with surface plasmons. *Phys. Rev. Lett.*, 97:053002, 2006. doi: 10.1103/PhysRevLett.97.053002. URL http://link.aps.org/doi/10.1103/PhysRevLett.97.053002. 40

[168] H. Y. Carr and E. M. Purcell. Effects of diffusion on free precession in nuclear magnetic resonance experiments. *Phys. Rev.*, 94:630–638,

1954. doi: 10.1103/PhysRev.94.630. URL http://link.aps.org/doi/10.1103/PhysRev.94.630. 40, 42

[169] S. Meiboom and D. Gill. Modified SpinEcho method for measuring nuclear relaxation times. *Rev. Sci. Instrum.*, 29:688–691, 1958. doi: 10.1063/1.1716296. 40, 42

[170] B. Naydenov, F. Dolde, L. T. Hall, C. Shin, H. Fedder, L. C. L. Hollenberg, F. Jelezko, and J. Wrachtrup. Dynamical decoupling of a single-electron spin at room temperature. *Phys. Rev. B*, 83:081201, 2011. doi: 10.1103/PhysRevB.83.081201. URL http://link.aps.org/doi/10.1103/PhysRevB.83.081201. 42

[171] G. de Lange, D. Ristè, V. V. Dobrovitski, and R. Hanson. Single-spin magnetometry with multipulse sensing sequences. *Phys. Rev. Lett.*, 106:080802, 2011. doi: 10.1103/PhysRevLett.106.080802. URL http://link.aps.org/doi/10.1103/PhysRevLett.106.080802. 42

[172] M. Minsky. Memoir on inventing the confocal scanning microscope. *Scanning*, 10(4):128–138, 1988. ISSN 1932-8745. doi: 10.1002/sca.4950100403. URL http://dx.doi.org/10.1002/sca.4950100403. 43

[173] D. Magde, E. Elson, and W. W. Webb. Thermodynamic fluctuations in a reacting system¯measurement by fluorescence correlation spectroscopy. *Phys. Rev. Lett.*, 29:705–708, 1972. doi: 10.1103/PhysRevLett.29.705. URL http://link.aps.org/doi/10.1103/PhysRevLett.29.705. 45

[174] E. L. Elson and D. Magde. Fluorescence correlation spectroscopy. I. conceptual basis and theory. *Biopolymers*, 13(1):1–27, 1974. ISSN 1097-0282. doi: 10.1002/bip.1974.360130102. URL http://dx.doi.org/10.1002/bip.1974.360130102. 63

[175] D. Magde, E. L. Elson, and W. W. Webb. Fluorescence correlation spectroscopy. II. an experimental realization. *Biopolymers*, 13(1):29–61, 1974. ISSN 1097-0282. doi: 10.1002/bip.1974.360130103. URL http://dx.doi.org/10.1002/bip.1974.360130103. 45, 63

[176] H. J. Carmichael and D. F. Walls. Proposal for the measurement of the resonant Stark effect by photon correlation techniques. *Journal*

of Physics B: Atomic and Molecular Physics, 9(4):L43, 1976. URL http://stacks.iop.org/0022-3700/9/i=4/a=001. 45

[177] H. J. Kimble and L. Mandel. Theory of resonance fluorescence. *Phys. Rev. A*, 13:2123–2144, 1976. doi: 10.1103/PhysRevA.13.2123. URL http://link.aps.org/doi/10.1103/PhysRevA.13.2123. 45

[178] H. J. Kimble, M. Dagenais, and L. Mandel. Photon antibunching in resonance fluorescence. *Phys. Rev. Lett.*, 39:691–695, 1977. doi: 10.1103/PhysRevLett.39.691. URL http://link.aps.org/doi/10.1103/PhysRevLett.39.691. 45

[179] H. J. Kimble, M. Dagenais, and L. Mandel. Multiatom and transit-time effects on photon-correlation measurements in resonance fluorescence. *Phys. Rev. A*, 18:201–207, 1978. doi: 10.1103/PhysRevA.18.201. URL http://link.aps.org/doi/10.1103/PhysRevA.18.201.

[180] E. Jakeman, E. R. Pike, P. N. Pusey, and J. M. Vaughan. The effect of atomic number fluctuations on photon antibunching in resonance fluorescence. *Journal of Physics A: Mathematical and General*, 10 (12):L257, 1977. URL http://stacks.iop.org/0305-4470/10/i=12/a=010.

[181] H. J. Carmichael, P. Drummond, P. Meystre, and D. F. Walls. Intensity correlations in resonance fluorescence with atomic number fluctuations. *Journal of Physics A: Mathematical and General*, 11(5):L121, 1978. URL http://stacks.iop.org/0305-4470/11/i=5/a=007.

[182] D. F. Walls. Evidence for the quantum nature of light. *Nature*, 280: 451–454, 1979. doi: 10.1038/280451a0. 45

[183] M. Koch, C. Sames, M. Balbach, H. Chibani, A. Kubanek, K. Murr, T. Wilk, and G. Rempe. Three-photon correlations in a strongly driven atom-cavity system. *Phys. Rev. Lett.*, 107:023601, Jul 2011. doi: 10.1103/PhysRevLett.107.023601. URL http://link.aps.org/doi/10.1103/PhysRevLett.107.023601. 47

[184] A. Rundquist, M. Bajcsy, A. Majumdar, T. Sarmiento, K. Fischer, K. G. Lagoudakis, S. Buckley, Al. Y. Piggott, and J. Vučković. Nonclassical higher-order photon correlations with a quantum dot strongly coupled to a photonic-crystal nanocavity. *Phys. Rev. A*, 90:023846, 2014. doi: 10.1103/PhysRevA.90.023846. URL http://link.aps.org/doi/10.1103/PhysRevA.90.023846. 47

[185] G. Binnig, H. Rohrer, Ch. Gerber, and E. Weibel. Surface studies by scanning tunneling microscopy. *Phys. Rev. Lett.*, 49:57–61, 1982. doi: 10.1103/PhysRevLett.49.57. URL http://link.aps.org/doi/10.1103/PhysRevLett.49.57. 48

[186] G. Binnig, H. Rohrer, Ch. Gerber, and E. Weibel. Tunneling through a controllable vacuum gap. *Applied Physics Letters*, 40(2):178–180, 1982. doi: http://dx.doi.org/10.1063/1.92999. URL http://scitation.aip.org/content/aip/journal/apl/40/2/10.1063/1.92999. 48

[187] G. Binnig, C. F. Quate, and Ch. Gerber. Atomic force microscope. *Phys. Rev. Lett.*, 56:930–933, 1986. doi: 10.1103/PhysRevLett.56.930. URL http://link.aps.org/doi/10.1103/PhysRevLett.56.930. 48

[188] Y. Seo and W. Jhe. Atomic force microscopy and spectroscopy. *Reports on Progress in Physics*, 71(1):016101, 2008. URL http://stacks.iop.org/0034-4885/71/i=1/a=016101. 48

[189] N. Jalili and K. Laxminarayana. A review of atomic force microscopy imaging systems: application to molecular metrology and biological sciences. *Mechatronics*, 14(8):907 – 945, 2004. ISSN 0957-4158. doi: http://dx.doi.org/10.1016/j.mechatronics.2004.04.005. URL http://www.sciencedirect.com/science/article/pii/S0957415804000455. 48

[190] R. García and R. Pérez. Dynamic atomic force microscopy methods. *Surface Science Reports*, 47(68):197 – 301, 2002. ISSN 0167-5729. doi: http://dx.doi.org/10.1016/S0167-5729(02)00077-8. URL http://www.sciencedirect.com/science/article/pii/S0167572902000778. 50

[191] M. Knoll and E. Ruska. Beitrag zur geometrischen elektronenoptik. i. *Annalen der Physik*, 404(5):607–640, 1932. ISSN 1521-3889. doi: 10.1002/andp.19324040506. URL http://dx.doi.org/10.1002/andp.19324040506. 50

[192] M. Knoll and E. Ruska. Beitrag zur geometrischen elektronenoptik. ii. *Annalen der Physik*, 404(6):641–661, 1932. ISSN 1521-3889. doi: 10.1002/andp.19324040602. URL http://dx.doi.org/10.1002/andp.19324040602. 50

[193] K. D. Vernon-Parry. Scanning electron microscopy: an introduction. *III-Vs Review*, 13(4):40 – 44, 2000. ISSN 0961-1290. doi: http://dx.doi.org/10.1016/S0961-1290(00)80006-X. URL http://www.sciencedirect.com/science/article/pii/S096112900080006X. 50

[194] K. D. Vernon-Parry and A.C. Wright. TEM: An introduction part 2. *III-Vs Review*, 14(1):48 – 51, 2001. ISSN 0961-1290. doi: http://dx.doi.org/10.1016/S0961-1290(01)89008-6. URL http://www.sciencedirect.com/science/article/pii/S0961129001890086. 50

[195] C. Kisielowski, B. Freitag, M. Bischoff, H. van Lin, S. Lazar, G. Knippels, P. Tiemeijer, M. van der Stam, S. von Harrach, M. Stekelenburg, M. Haider, S. Uhlemann, H. Mller, P. Hartel, B. Kabius, D. Miller, I. Petrov, E. A. Olson, T. Donchev, E. A. Kenik, A. R. Lupini, J. Bentley, S. J. Pennycook, I. M. Anderson, A. M. Minor, A. K. Schmid, T. Duden, V. Radmilovic, Q. M. Ramasse, M. Watanabe, R. Erni, E. A. Stach, P. Denes, and U. Dahmen. Detection of single atoms and buried defects in three dimensions by aberration-corrected electron microscope with 0.5- information limit. *Microscopy and Microanalysis*, 14:469–477, 2008. ISSN 1435-8115. doi: 10.1017/S1431927608080902. URL http://journals.cambridge.org/article_S1431927608080902. 50

[196] Kewal K. Jain. *The Handbook of Biomarkers*. Springer, 2010. doi: 10.1007/978-1-60761-685-6. 51

[197] Lauralee Sherwood. *Human Physiology: From Cells to Systems*. Cengage Learning, 9th edition, 2016. ISBN 978-1-285-86693-2. 51

[198] F. Neugart, A. Zappe, F. Jelezko, C. Tietz, J. P. Boudou, A. Krueger, and J. Wrachtrup. Dynamics of diamond nanoparticles in solution and cells. *Nano Letters*, 7(12):3588–3591, 2007. doi: 10.1021/nl0716303. URL http://dx.doi.org/10.1021/nl0716303. PMID: 17975943. 51

[199] L. Shen. Biocompatible polymer/quantum dots hybrid materials: Current status and future developments. *Journal of Functional Biomaterials*, 2(4):355, 2011. ISSN 2079-4983. doi: 10.3390/jfb2040355. URL http://www.mdpi.com/2079-4983/2/4/355. 52

[200] D. Shenoy, W. Fu, J. Li, C. Crasto, G. Jones, C. DiMarzio, S. Sridhar, and M. Amiji. Surface functionalization of gold nanoparticles using hetero-bifunctional poly(ethylene glycol) spacer for intracellular tracking and delivery. *Int J Nanomedicine*, 1:51–57, 2006. 52

[201] T. W. Evans. Review article: albumin as a drugbiological effects of albumin unrelated to oncotic pressure. *Alimentary Pharmacology & Therapeutics*, 16:6–11, 2002. ISSN 1365-2036. doi: 10.1046/j.1365-2036.16.s5.2.x. URL http://dx.doi.org/10.1046/j.1365-2036.16.s5.2.x. 52

[202] B. G. Müller, H. Leuenberger, and T. Kissel. Albumin nanospheres as carriers for passive drug targeting: An optimized manufacturing technique. *Pharm. Res.*, 13(1):32–37, 1996. ISSN 0724-8741. doi: 10.1023/A:1016064930502. 52

[203] Q. Quan, J. Xie, H. Gao, M. Yang, F. Zhang, G. Liu, X. Lin, A. Wang, H. S. Eden, S. Lee, G. Zhang, and X. Chen. HSA coated iron oxide nanoparticles as drug delivery vehicles for cancer therapy. *Molecular Pharmaceutics*, 8(5):1669–1676, 2011. doi: 10.1021/mp200006f. URL http://dx.doi.org/10.1021/mp200006f. PMID: 21838321. 52

[204] Y. Wu, an Eisele K. Pramanik, G., and T. Weil. Convenient approach to polypeptide copolymers derived from native proteins. *Biomacromolecules*, 13(6):1890–1898, 2012. doi: 10.1021/bm300418r. URL http://dx.doi.org/10.1021/bm300418r. PMID: 22559216. 52

[205] S. L. Kuan, Y. Wu, and T. Weil. Precision biopolymers from protein precursors for biomedical applications. *Macromolecular Rapid Communications*, 34(5):380–392, 2013. ISSN 1521-3927. doi: 10.1002/marc.201200662. URL http://dx.doi.org/10.1002/marc.201200662. 52

[206] J. R. Masters. Hela cells 50 years on: the good, the bad and the ugly. *Nature Reviews Cancer*, 2:315–319, 2002. doi: 10.1038/nrc775. 58, 63

[207] H. G. Keizer, H. M. Pinedo, G. J. Schuurhuis, and H. Joenje. Doxorubicin (adriamycin): A critical review of free radical-dependent mechanisms of cytotoxicity. *Pharmacol. Ther.*, 47(2):219 – 231, 1990. ISSN 0163-7258. doi: http://dx.doi.org/10.

1016/0163-7258(90)90088-J. URL http://www.sciencedirect.com/science/article/pii/016372589090088J. 59, 60

[208] K.-I. Kiyomiya, S. Matsuo, and M. Kurebe. Proteasome is a carrier to translocate doxorubicin from cytoplasm into nucleus. *Life Sciences*, 62(20):1853 – 1860, 1998. ISSN 0024-3205. doi: http://dx.doi.org/10.1016/S0024-3205(98)00151-9. URL http://www.sciencedirect.com/science/article/pii/S0024320598001519. 59, 64

[209] V. B. Pai and M. C. Nahata. Cardiotoxicity of chemotherapeutic agents. *Drug Safety*, 22(4):263–302, 2000. ISSN 0114-5916. doi: 10.2165/00002018-200022040-00002. URL http://dx.doi.org/10.2165/00002018-200022040-00002. 59

[210] X. Dai, Z. Yue, M. E. Eccleston, J. Swartling, N. K. H. Slater, and C. F. Kaminski. Fluorescence intensity and lifetime imaging of free and micellar-encapsulated doxorubicin in living cells. *Nanomedicine: Nanotechnology, Biology and Medicine*, 4(1):49 – 56, 2008. ISSN 1549-9634. doi: http://dx.doi.org/10.1016/j.nano.2007.12.002. URL http://www.sciencedirect.com/science/article/pii/S1549963407002547. 59

[211] Y. Wu, S. Ihme, M. Feuring-Buske, S. L. Kuan, K. Eisele, M. Lamla, Y. Wang, C. Buske, and T. Weil. A coreshell albumin copolymer nanotransporter for high capacity loading and two-step release of doxorubicin with enhanced anti-leukemia activity. *Advanced Healthcare Materials*, 2(6):884–894, 2013. ISSN 2192-2659. doi: 10.1002/adhm.201200296. URL http://dx.doi.org/10.1002/adhm.201200296. 60

[212] Siying Qin, Hang Yin, Celi Yang, Yunfeng Dou, Zhongmin Liu, Peng Zhang, He Yu, Yulong Huang, Jing Feng, Junfeng Hao, Jia Hao, Lizong Deng, Xiyun Yan, Xiaoli Dong, Zhongxian Zhao, Taijiao Jiang, Hong-Wei Wang, Shu-Jin Luo, and Can Xie. A magnetic protein biocompass. *Nature Materials*, (1476-4660 UR), 2015. doi: doi:10.1038/nmat4484. 2015/11/16/onlineVL. 77

[213] S. Granick. Ferritin: I. physical and chemical properties of horse spleen ferritin. *J. Biol. Chem.*, 146(2):451–461, 1942. URL http://www.jbc.org/content/146/2/451.short. 77, 78

[214] F. Frolow, A. J. Kalb (Gilboa), and J. Yariv. Structure of a unique twofold symmetric haem-binding site. *Nat. Struct. Biol.*, 1:453 – 460, 1994. doi: doi:10.1038/nsb0794-453. 77

[215] H. U. Ulmer and E. Goepel. Anemia, ferritin and preterm labor. *J. Perinat. Med.*, 16:459–465, 1988. 77

[216] T. D. Johnson-Wimbley and D. Y. Graham. Diagnosis and management of iron deficiency anemia in the 21st century. *Therap. Adv. Gastroenterol.*, 4(3):177–184, 2011. doi: doi:10.1177/1756283X11398736. 77

[217] J. R. Connor, S. L. Menzies, S. M. St. Martin, and E. J. Mufson. A histochemical study of iron, transferrin, and ferritin in Alzheimer's diseased brains. *J. Neurosci. Res.*, 31(1):75–83, 1992. ISSN 1097-4547. doi: 10.1002/jnr.490310111. URL http://dx.doi.org/10.1002/jnr.490310111. 77, 78

[218] P. De Sole, C. Rossi, M. Chiarpotto, G. Ciasca, B. Bocca, A. Alimonti, A. Bizzarro, C. Rossi, and C. Masullo. Possible relationship between al/ferritin complex and alzheimer's disease. *Clin. Biochem.*, 46(12):89 – 93, 2013. ISSN 0009-9120. doi: http://dx.doi.org/10.1016/j.clinbiochem.2012.10.023. URL http://www.sciencedirect.com/science/article/pii/S0009912012005784. 77, 78

[219] P. Riederer, E. Sofic, W.-D. Rausch, B. Schmidt, G. P. Reynolds, and and Youdim M. B. H. Jellinger, K. Transition metals, ferritin, glutathione, and ascorbic acid in parkinsonian brains. *J. Neurochem.*, 52(2):515–520, 1989. ISSN 1471-4159. doi: 10.1111/j.1471-4159.1989.tb09150.x. URL http://dx.doi.org/10.1111/j.1471-4159.1989.tb09150.x. 77, 78

[220] D. T. Dexter, A. Carayon, M. Vidailhet, M. Ruberg, F. Agid, Y. Agid, A. J. Lees, F. R. Wells, P. Jenner, and C. D. Marsden. Decreased ferritin levels in brain in Parkinson's disease. *J. Neurochem.*, 55(1):16–20, 1990. ISSN 1471-4159. doi: 10.1111/j.1471-4159.1990.tb08814.x. URL http://dx.doi.org/10.1111/j.1471-4159.1990.tb08814.x. 77, 78

[221] P. M. Harrison. The structure and function of ferritin. *Biochemical Education*, 14(4):154–162, 1986. ISSN 1879-1468. doi: 10.1016/0307-4412(86)90203-7. URL http://dx.doi.org/10.1016/0307-4412(86)90203-7. 78

[222] E. C. Theil. Ferritin: Structure, gene regulation, and cellular function in animals, plants, and microorganisms. *Annu. Rev. Biochem.*, 56: 289–315, 1987. doi: 10.1146/annurev.bi.56.070187.001445. 78

[223] E. C. Theil. Ferritin: The protein nanocage and iron biomineral in health and in disease. *Inorg. Chem.*, 52(21):12223–12233, 2013. doi: 10.1021/ic400484n. URL http://dx.doi.org/10.1021/ic400484n. PMID: 24102308. 78

[224] A. Luzzago, P. Arosio, C. Iacobello, G. Ruggeri, L. Capucci, E. Brocchi, F. De Simone, D. Gamba, E. Gabri, S. Levi, and A. Albertini. Immunochemical characterization of human liver and heart ferritins with monoclonal antibodies. *Biochimica et Biophysica Acta (BBA) - Protein Structure and Molecular Enzymology*, 872 (12):61 – 71, 1986. ISSN 0167-4838. doi: http://dx.doi.org/10.1016/0167-4838(86)90147-0. URL http://www.sciencedirect.com/science/article/pii/0167483886901470. 78

[225] P. Rucker, F. M. Torti, and S. V. Torti. Role of h and l subunits in mouse ferritin. *J. Biol. Chem.*, 271(52):33352–33357, 1996. doi: 10.1074/jbc.271.52.33352. URL http://www.jbc.org/content/271/52/33352.abstract.

[226] M. C. Sammarco, S. Ditch, A. Banerjee, and E. Grabczyk. Ferritin L and H subunits are differentially regulated on a post-transcriptional level. *Journal of Biological Chemistry*, 283(8):4578–4587, 2008. doi: 10.1074/jbc.M703456200. URL http://www.jbc.org/content/283/8/4578.abstract. 78

[227] P. M. Harrison and P. Arosio. The ferritins: molecular properties, iron storage function and cellular regulation. *Biochimica et Biophysica Acta (BBA) - Bioenergetics*, 1275(3):161 – 203, 1996. ISSN 0005-2728. doi: http://dx.doi.org/10.1016/0005-2728(96)00022-9. URL http://www.sciencedirect.com/science/article/pii/0005272896000229. 78, 79

[228] U. Voskoboynik. Anomalous field dependence of blocking temperature of natural horse-spleen ferritin. *Acta Phys. Pol. A*, 92 (Supplement, S-43), 1997. 78

[229] Y. L Raikher, Stolyar S.B. Ladigina V. P. Stepanov, V. I., D. A. Balaev, and Balashoyu M. Ischenko, L. A. Magnetic properties of

biomineral nanoparticles produced by bacteriums klebsiell oxytoca. *Fizika tverdogo tela*, 52(2):277–284, 2010. (in russian). 78

[230] S. K. H. Lam, J. R. Clem, and W. Yang. A nanoscale SQUID operating at high magnetic fields. *Nanotechnology*, 22(45):455501, 2011. URL http://stacks.iop.org/0957-4484/22/i=45/a=455501. 78

[231] S. H. Kilcoyne and R. Cywinski. Ferritin: a model superparamagnet. *Journal of Magnetism and Magnetic Materials*, 140144, Part 2:1466 – 1467, 1995. ISSN 0304-8853. doi: http://dx.doi.org/10.1016/0304-8853(94)00626-1. URL http://www.sciencedirect.com/science/article/pii/0304885394006261. International Conference on Magnetism. 78

[232] R. P. Guertin, N. Harrison, Z. X. Zhou, S. McCall, and F. Drymiotis. Very high field magnetization and AC susceptibility of native horse spleen ferritin. *Journal of Magnetism and Magnetic Materials*, 308(1):97 – 100, 2007. ISSN 0304-8853. doi: http://dx.doi.org/10.1016/j.jmmm.2006.05.010. URL http://www.sciencedirect.com/science/article/pii/S0304885306007931. 78

[233] Y.-R. Chang, H.-Y Lee, K. Chen, C.-C. Chang, D.-S. Tsai, C.-C. Fu, S.-S. Lim, Y.-K. Tzeng, C.-Y. Fang, C.-C. Han, H.-C. Chang, and W. Fann. Mass production and dynamic imaging of fluorescent nanodiamonds. *Nature Nanotechnology*, 3:284–288, 2008. doi: 10.1038/nnano.2008.99. 79

[234] P.A. Glossop and C.A.L. Lane. Novel compounds active as muscarinic receptor antagonists, January 21 2010. URL http://www.google.co.in/patents/WO2010007561A1?cl=und. WO Patent App. PCT/IB2009/052,984. 79

[235] N. Xia, Y. Xing, G. Wang, Q. Feng, Q. Chen, H. Feng, X. Sun, and L. Liu. Probing of EDC/NHSS-mediated covalent coupling reaction by the immobilization of electrochemically active biomolecules. *Int. J. Electrochem. Sci.*, 8:2459–2467, 2013. 79

[236] E. Wajnberg, L. J. El-Jaick, M. P. Linhares, and D. M. S. Esquivel. Ferromagnetic resonance of horse spleen ferritin: Core blocking and surface ordering temperatures. *Journal of Magnetic Resonance*, 153 (1):69 – 74, 2001. ISSN 1090-7807. doi: http://dx.doi.org/10.1006/jmre.2001.2430. URL http://www.sciencedirect.com/science/article/pii/S1090780701924309. 86

[237] Ł. Cywiński, R. M. Lutchyn, C. P. Nave, and S. Das Sarma. How to enhance dephasing time in superconducting qubits. *Phys. Rev. B*, 77:174509, 2008. doi: 10.1103/PhysRevB.77.174509. URL http://link.aps.org/doi/10.1103/PhysRevB.77.174509. 86

[238] P. Maletinsky, S. Hong, M. S. Grinolds, B. Hausmann, M. D. Lukin, R. L. Walsworth, M. Loncar, and A. Yacoby. A robust scanning diamond sensor for nanoscale imaging with single nitrogen-vacancy centres. *NATURE NANOTECHNOLOGY*, 7:320–324, 2012. doi: 10.1038/NNANO.2012.50. 88

[239] M. S. Grinolds, P. Maletinsky, S. Hong, M. D. Lukin, R. L. Walsworth, and A. Yacoby. Quantum control of proximal spins using nanoscale magnetic resonance imaging. *Nature Physics*, 9:215–219, 2011. doi: 10.1038/nphys2543. 88

[240] S. Hong, S. M. Grinolds, P. Maletinsky, R. L. Walsworth, M. D. Lukin, and A. Yacoby. Coherent, mechanical control of a single electronic spin. *Nano Letters*, 12(8):3920–3924, 2012. doi: 10.1021/nl300775c. URL http://dx.doi.org/10.1021/nl300775c. PMID: 22800099. 88

[241] D. Kim, N.-K. Chung, S. Allen, S. J. B. Tendler, and J. W. Park. Ferritin-based new magnetic force microscopic probe detecting 10 nm sized magnetic nanoparticles. *ACS Nano*, 6(1):241–248, 2012. doi: 10.1021/nn203464g. URL http://dx.doi.org/10.1021/nn203464g. PMID: 22148318. 92

[242] S. J. Singer and G. L. Nicolson. The fluid mosaic model of the structure of cell membranes. *Science*, 175(4023):720–731, 1972. URL http://www.jstor.org/stable/1733071. A

List of Figures

2.1. Diamond and graphit equlibrium 6
2.2. NV center in diamond lattice 9
2.3. Electron levels of NV center. Spectra of NV centers. 12
2.4. Optically detected magnetic resonance 16
2.5. Spin states at the Bloch sphere. 18
2.6. Rabi oscillation 19
2.7. Sequence for measurement and the result of T_1 time 22
2.8. Sequence for measurement and the result of T_2 time 24
2.9. Electron levels of NV center close to the diamond surface. 26
2.10. SiV center in diamond lattice. Spectra of SiV center. . . . 27
2.11. Detonation nanodiamonds. 29
2.12. Treatment of nanodiamonds surface. 31

3.1. Organic fluorescent particles 34
3.2. Drug delivery systems 36
3.3. Different magnetic sensors 38
3.4. ODMR of NV center with different external magnetic field 39
3.5. Detection of the magnetic field 41

4.1. Principles of confocal microscope 44
4.2. Antibunching correlation function 46
4.3. Example of the autocorrelation function for the diffusion measurement 48
4.4. Modes of AFM 49

5.1. Protein modification 53
5.2. TEM of uncoated and coated nanodiamonds 54
5.3. Stability of coating at the different pH 56
5.4. Colocalization of proteins and nanodiamonds 58
5.5. Doxorubicin molecule 60
5.6. Doxorubicin release 61
5.7. Doxorubicin release in buffers 62
5.8. Nanodiamonds and Doxorubicin in HeLa cells 65
5.9. Spectra of Nanodiamonds and Doxorubicin in HeLa cells . 66

5.10. Clinical test of drug release 68
5.11. Size measurements of nanodiamonds with two color center 70
5.12. Fluorescence measurements of nanodiamonds with two color center 72

6.1. The structure of ferritin molecule 79
6.2. EDC coupling for the attachment of ferritin to the nanodiamond 80
6.3. Nanodiamonds with attached ferritin molecules 81
6.4. Position of NV center inside nanodiamond 83
6.5. Data of the coherence time T_1 for nanodiamond with and without ferritin molecules 84
6.6. Data of the coherence time T_2 for nanodiamond with and without ferritin molecules 85
6.7. Numerical simulation for relaxation times 87
6.8. AFM tip (silica particle) with ferritin molecules 90
6.9. Photocounts for different T_2 91
6.10. Photocounts for same T_2 with different contrasts 92

A.1. Cell membrane structure . . . . . B
A.2. Passive membrane transport . . . . . B
A.3. Active membrane transport C

Acknowledgement

The PhD is the best time in the life of any scientist. It is a superposition of interesting research and communication and freedom of duty to search for grants. Now, when I am finishing I have dual feeling. I am sad that happy and carefree time is over. On the other hand I am able to go to the adult scientific life. During my PhD I was lucky to work together with many good and interesting people, to whom I would like to express my deep gratitude.

- ✯ First of all, I would like to thank ***Professor Fedor Jelezko*** for the great opportunity to work in his group and for invaluable experience. He was always very happy to help with experiments in the lab and answer attentively to any questions. The discussions with him helped not only to clarify the physics behind the problem, but also develop scientific intuition.

- ✯ The profound gratitude I would like to express to ***Boris Naydenov***, who supported me during my PhD in all research problems as well as in bureaucratic questions. I always knew that he can find time for the discussion in any case. He kindly consented to be a second reader of my thesis. His help in the correction of my thesis is inestimable.

- ✯ I would also like to thank ***Professor Alexander Kubanek*** for finding the time to be part of the examination committee for my PhD defence and for careful reading this dissertation.

- ✯ For experimental physicist it is very hard to work in the lab alone, and I am happy that ***Andrea Kurz*** worked with me. It was a good time of mutual understanding and support. All German words in my thesis would not exist without her.

- ✯ When I started my PhD I did not know, that I would have to work so close to the field of chemistry. In the beginning I was a bit scared whether I come smoothly into it or not. Fortunately, it was not so hard, thanks to ***Professor Tanja Weil*** and her group, who opened for me interesting world of organic chemistry. She was always

very kind and well-disposed to me, and I knew that at any time I can come and ask for help. Also, I would like to show gratitude to ***Yuzhou Wu*** and ***Goutam Pramanik***, who spent a lot of time in deep explanation of chemical techniques, which were used for sample preparation.

✯ The experimental result are not completed until they are represented by theoretical model. I would like to thank ***Professor Martin Plenio*** and his group, especially ***Jianming Cai***. They found exhaustive explanation for all our problems and gave hints about future experiments.

✯ Also I express gratitude to ***Professor Ute Kaiser*** and ***Professor Paul Walther*** and their groups to permit us to look into the world of nano-objects and single atoms by electron microscopy.

✯ The life in new country gives many unexpected challenges, which I would not be able to solve so fast without the support of ***Maria Heuschmid***. She was always open and very friendly. She was able to create the family feeling in the institute.

✯ My first visit to Germany became possible because of ***Professor Jörg Wrachtrup***. I am very very much obliged to him for this, especially because in his institute I have met my future husband.

✯ Of course I would like to thank my parents ***Larisa Ermakova*** and ***Vatily Ermakov*** for their support and understanding in all my life.

✯ Many thanks I would like to say to my husband ***Petr Siyushev*** for his love, care, and making my life interesting. It is so important to have a person in your life, who completely understands you and thinks with you on the same wavelength.

Curriculum Vitae

Personal Details

Name	Anna Vitalyevna Ermakova
Date of Birth	05. October, 1988
Place of Birth	Novopolotsk, Belarus
email	annermakova@gmail.com

Education

2011-2016	PhD, Institute for Quantum Optics, University of Ulm, Ulm, Germany
2010-2011	Master student (Physics), Belarusian State University, Minsk, Belarus
2005-2010	Diploma student (Physics), Belarusian State University, Minsk, Belarus
2003-2005	Attended the Lyceum of Rostov State Transport University, Rostov-on-Don, Russia
1995-2003	Attended the Suvorov's Lyceum, Rostov-on-Don, Russia

Experience

Languages	Russian (native), Belarusian (native), English (fluent), German (pre-intermediate)
Programs	MatLab, Mathematica, Origin, SRIM, Blender 3D Modeling, MS Office, Inkscape, LaTeX, LabView, Delphi

December 8, 2016

List of publications

Parts of this dissertation have already been published in the journal articles 1, 3 and 4.

1 *Programmable Biopolymers for Advancing Biomedical Applications of Fluorescent Nanodiamonds*
Y. Wu, A. Ermakova, W. Liu, G. Pramanik, M. Vu, A. Kurz, L. McGuinness, B. Naydenov, S. Hafner, R. Reuter, J. Wrachtrup, J. Isoya, T. Simmet, F. Jelezko, & T. Weil
Advanced Functional Materials **25**, 6576-6585 (2015). doi: 10.1002/adfm.201502704

2 *Spectral control of nanodiamond using dressed photon-phonon etching*
R. Nagumo, F. Brandenburg, A. Ermakova, F. Jelezko, & T. Yatsui
Applied Physics A **121**, 1335-1339 (2015). doi: 10.1007/s00339-015-9400-0

3 *Size-dependent luminescence of color centers in composite nanodiamonds*
V.A. Shershulin, V.S. Sedov, A. Ermakova, U. Jantzen, L. Rogers, A.A. Huhlina, E.G. Teverovskaya, V.G. Ralchenko, F. Jelezko, & I.I. Vlasov
Physica Status Solidi A **212**, 2600-2605 (2015). doi: 10.1002/pssa.201532204

4 *Detection of a few metallo-protein molecules using color centers in nanodiamonds*
A. Ermakova, G. Pramanik, J.-M. Cai, G. Algara-Siller, U. Kaiser, T. Weil, Y.-K. Tzeng, H.C. Chang, L.P. McGuinness, M.B. Plenio, B. Naydenov, & F. Jelezko
Nano Letters **13**, 33053309 (2013). doi: 10.1021/nl4015233

Erklärung

Ich versichere hiermit, dass ich die vorliegende Arbeit selbständig angefertigt habe und keine anderen als die angegebenen Quellen und Hilfsmittel benutzt, sowie die wörtlich und inhaltlich übernommenen Stellen als solche kenntlich gemacht habe.

Weiterhin erkläre ich, dass die vorliegende Arbeit weder vollständig noch in Auszügen einer anderen Fakultät mit dem Ziel einen akademischen Titel zu erwerben vorgelegt worden ist. Ich bewerbe mich hiermit erstmalig um den Doktorgrad der Naturwissenschaften der Universität Ulm

Ulm, den 28. Juni 2016

Anna Ermakova